

Alma Mater Studiorum – Università di Bologna

DOTTORATO DI RICERCA IN  
\_\_INGEGNERIA ELETTRONICA\_\_

Ciclo \_\_23\_\_

Settore/i scientifico-disciplinare/i di afferenza: \_\_\_\_ING – IND / 33\_\_\_\_

TITOLO TESI

PHYSICAL MODEL OF PD BEHAVIOR AND  
RELEVANT DAMAGE GROWTH FROM  
MICRO-CAVITIES IN POLYETHYLENE-BASED  
MATERIAL UNDER AC VOLTAGE

Presentata da: \_\_\_\_\_WANG LE\_\_\_\_\_

**Coordinatore Dottorato**

**Relatore**

\_\_Prof. Domenico Casadei\_\_

\_\_Prof. Gian Carlo Montanari\_\_

**Esame finale anno 2011**

# Index

<b>Preface of the thesis</b>	<b>1</b>
<b>Chapter 1. Introduction</b>	<b>3</b>
1.1. General concepts of ageing	3
1.2. Review of the life models	4
1.2.1. Phenomenological models	4
1.2.2. Physical ageing models	5
1.2.2.1 Field limited space charge (FLSC) model	5
1.2.2.2 Percolation model	6
1.2.2.3 Space charge DMM model	7
1.2.2.4 Ageing models based on the electro-dynamic stress	8
<b>Chapter 2. Theoretical Background</b>	<b>9</b>
2.1. PD-induced ageing model under DC field	10
2.1.1. Presence of the free electrons in the cavity	10
2.1.2. Electron avalanche generation	13
2.1.3. Damage accumulation at the cavity surface	15
2.2. Differences between modeling under DC and AC field	17
2.3. PD model under AC field	18
2.3.1. Electric field in the cavity under AC field	18
2.3.2. PD inception	19
2.3.3. Discharge at electric field polarity inversion time	20
2.3.4. Discharge magnitude	23
2.4. Interaction between PD and the surrounding dielectrics	23
<b>Chapter 3. Time Behavior of the PD Activity</b>	<b>25</b>
3.1. Specimens and experimental setup	25
3.2. Time behavior of PD in the cavity under AC field	26
3.2.1. Time evolution of PD at 10kV	26
3.2.2. Time evolution of PD at 12.5kV	29
3.3 Evolution of PD-induced damage growth rage	31
3.4 Time evolution of the PD inception voltage	33
3.5 Summary	34
Appendix 1	36
<b>Chapter 4. Gas Pressure in the Cavity</b>	<b>43</b>
4.1. Calculation of gas pressure evolution through PDIV	43
4.2. Measurement of gas pressure in the cavity	44
4.2.1. PD activity under CGP condition	45
4.2.2. PD activity under CGV condition	46
4.2.3. Time evolution of gas pressure in small cavities	48
4.3. Correlation between PD and gas in the cavity	49
4.4. Summary	51
Appendix 2	52
<b>Chapter 5. Modification of the Dielectric/Cavity Interface</b>	<b>55</b>
5.1 Test object and experimental procedure	55
5.2 Morphology and composition of the PD byproduct	55
5.2.1 Morphology of the PD byproduct	55
5.2.2 Composition of the PD byproduct	58

5.3	Degradation of the polymer surface	59
5.4	Correlation between PD patterns and interface conditions	62
5.5	Summary	63
<b>Chapter 6. Numerical Simulation of the PD Patterns</b>		<b>64</b>
6.1	Algorithm of the simulation	64
6.1.1	PD inception probability	64
6.1.2	Discharge amplitude	66
6.2	Evolution of the injection parameters	66
6.3	Summary	71
<b>Conclusions</b>		<b>72</b>
<b>References</b>		<b>73</b>

# PREFACE

The increasing need of electrical energy, the progressive ageing of most electrical infrastructures and the reduction of redundancy capability of most electrical networks are emphasizing the critical role of insulation failure in electrical apparatus. Despite of major improvements in manufacturing technologies, it can be speculated that one of the main causes of the failures of the insulating materials under normal working conditions is the unavoidable presence of microscopic defects in the insulation, such as micro-cavities, protrusions and contaminants. Partial discharges (PD) occurring at cavities in the insulating material are believed to be one of the most important causes of polymeric insulation breakdown under AC voltage. On the basis of this background, significant research has been carried out in the last two decades in order to understand PD phenomenology in micro-cavities embedded in polymer matrix.

The ultimate objective of our work in this thesis is to obtain and verify a model based on physical laws and measurable physical parameters, which is able to describe both failure time and main characteristics of PD activity, such as phase resolved PD (PRPD) patterns, PD repetition rate and amplitude. For this purpose, we observed the time behavior of PD activity in artificial cavities in PE-layered artificial specimens under different values of AC voltage. In order to outline regularities in PD behavior during the degradation processes, a quasi-deterministic series of ageing stages were extracted from the time behavior curves of PD repetition rate and amplitude.

The time evolution of the PD patterns and parameters (i.e. PD repetition rate and amplitude) is largely affected by the physical, chemical and electrical conditions of the dielectric/cavity interface, as well as the conditions of the gas filling the cavity. Therefore, the correlation between PD and the gas pressure in the cavity, as well as the evolution of the dielectric/cavity interface morphology, were studied in this thesis. The content of each chapter is reported briefly in the following.

In Chapter 1, the general concept of ageing of the insulating material subjected to thermo-electrical stresses is introduced. The main phenomenological and physical models formulated up to now are briefly described and commented.

In Chapter 2, the previously developed models of damage inception and growth from micro-cavities in polymeric insulating materials under both DC and AC fields are described. The differences between modelling under DC and AC fields are outlined. The interaction between PD and the surrounding dielectrics during the ageing process is introduced briefly.

In Chapter 3, life and ageing tests results on PE-based three-layer specimens having artificial cylindrical micro-cavities are reported. The typical time behavior curves of the PD parameters (i.e. PD repetition rate and amplitude) are extracted from the experimental results. A quasi-deterministic series of ageing stages was extracted from the curves. The product of the PD repetition rate and amplitude is proposed as a parameter that can evaluate the PD-induced damage growth rate. The time evolution of the PD inception voltage (PDIV) is studied and reported.

In Chapter 4, the typical time behavior curve of the gas pressure in the micro-cavities is obtained and reported. The PD behavior in the cavities under

constant gas volume condition and under constant gas pressure condition is compared. The influence of the gas pressure on the PD is discussed.

In Chapter 5, the modification of the dielectric/cavity interface morphology is investigated using optic microscope, SEM (scanning electron microscope) and AFM (atomic force microscope). The PD byproducts on the cavity surface are analyzed using EDAX (energy-dispersive X-ray spectroscopy) and confocal Raman microprobe spectroscopy.

In Chapter 6, typical PRPD patterns at each ageing stage are fitted to numerical simulations based on the physical model described in Chapter 2. The fitting parameters provide insight into the time evolution of the PRPD patterns and PD statistical parameters.

# CHAPTER 1

## INTRODUCTION

### 1.1 General Concept of Ageing

According to IEC and IEEE standards, ageing is defined as occurrence of irreversible, deleterious changes in insulating materials or systems which affect their serviceability, i.e. their ability to satisfy requested performances [1]. When the changes of the chemical composition and physical properties reach a critical entity, the insulation is not reliable and, thus, maintenance or replacement of the insulation system would be required. The causes of ageing are applied stresses and factors of influence. The former are primary causes. The factors of influence, which are able to affect the ageing rate only when stresses are applied, are secondary causes. A consistent definition of ageing influence factor is ‘factors imposed by operation environment, technology, or test that influence the performance of an insulation system or electrical equipment subjected to stresses’ [2].

The concept of ageing can be translated into mathematical language for insulating materials, as follows. Referring to applied stresses,  $S_1, S_2, \dots, S_N$ , as the primary causes of ageing, the dependence of ageing,  $A$ , on the property,  $p$ , selected to evaluated ageing can be written as [2]

$$A = F(p) \quad (1-1)$$

where  $p = P/P_0$  is the observed (diagnostic) property in relative terms (property  $P$  relative to the initial value,  $P_0$ , for the unaged insulation).  $A$  is a dimensionless quantity. Failure occurs when  $p$  reaches a limiting value  $p_L$ . The ageing rate is given by

$$R_A = dA/dt \quad (1-2)$$

in which  $R_A$  is assumed to be dependent on only on stresses, not on ageing time,  $t$ . In particular,  $R_A$  can be described by an additive relationship when stresses are applied in sequence and mutual interactions are not expected, while more complex expressions (multiplicative, mixed) should be used for simultaneous stresses, depending on the intensity of interaction.

A simple solution for the integral of equation (1-2) is achieved under the assumption of constant amplitude of applied stresses with time, that is

$$A = R_A(S_1, S_2, \dots, S_N)t \quad (1-3)$$

When  $p$  decays to a limiting value  $p_L$  below which the insulation is unable to maintain service ability, it is assumed that failure occurs. At that moment, the aging time becomes lifetime  $L$ , and equation (1-3) becomes

$$A_L = F(P_L) = R_A(S_1, S_2, \dots, S_N)L \quad (1-4)$$

where  $A_L$  is the aging limit or aging at failure. Equations (1-3) and (1-4) can be called the general aging equation and the general life equation, respectively.

## 1.2 Review of the life Models

Life models that can provide usable life expressions for thermal, electrical and mechanical stresses have been available for many years. Different approaches have been followed to achieve these models. The approaches mainly fall in two categories: the macroscopic and the microscopic. The macroscopic model, also called phenomenological model, is based on fitting lifetimes versus applied stress. The microscopic model, also called physical ageing model, is based on the assumption that the prevailing cause of electrical and mechanical ageing is accelerated by localized degradation triggered by micro-defects in practical insulation system. These two kinds of models are summarized in the following subsections.

### 1.2.1 Phenomenological models

Phenomenological models were the first to appear in literature. They are used as phenomenological tools fitting life data coming from accelerated electrical, thermal, and mechanical life tests. They can provide an estimate of insulation lifetime as a function of applied stress. These models contain a relatively small number of parameters. Although the model equations are usually simple, it may take a long time to estimate these parameters by accelerated life tests, because the main ageing mechanism is often unknown and the extrapolation of the experimental results is uncertain. Besides, the number of parameters increases with the superposition of different kinds of stresses.

Significant phenomenological models are: Dakin model for electrical aging, inverse power and exponential models. These models have been widely used up to now, and will likely be used also in the future for the design of insulation systems subjected to a level of electrical stress able to age insulation. Besides, the chemical reaction rate model (Arrhenius model) for thermal ageing, as well as Eyring models for electrical and mechanical ageing were also reported and discussed in literature [3-9]. Just to recall, the well-known models are reported, respectively, below:

$$\text{Dakin: } L = C_E \exp(-nE) / (E - E_{cr}) \quad (1-5)$$

$$\text{Inverse Power Model: } L = C_E E^{-n} \quad (1-6)$$

$$\text{Exponential Model: } L = L_0 \exp[-n'(E - E_{cr})] \quad (1-7)$$

$$\text{Arrhenius: } L = L' \exp\left[\frac{\Delta\Phi}{k} \left(\frac{1}{T} - \frac{1}{T_0}\right)\right] \quad (1-8)$$

$$\text{Eyring: } L = C_E \frac{h}{kT} \exp\left(\frac{\Delta G}{kT}\right) \quad (1-9)$$

where  $L$  is the lifetime (i.e. time to failure) of the insulation system,  $E$  is the electric field,  $E_{cr}$  is the threshold field above which electric ageing occurs (there is no ageing at fields below  $E_{cr}$ , thus infinite electrical life),  $L_0$  is the life for  $E = E_{cr}$ ,  $\Delta\Phi$  is the activation energy of the degradation process,  $k$  is the Boltzmann constant,  $T$  is the absolute temperature,  $L'$  is the life for  $T = T_0$ ,  $h$  is the Planck constants and  $\Delta G$  is the Gibbs (free) energy of the electro-thermal degradation process.  $C_E$ ,  $n$  and  $n'$  are the model parameters, which depend on material, electric field ( $E$ ) and temperature ( $T$ ).  $n$  and  $n'$  are called voltage endurance coefficients for the inverse power and exponential models, respectively.

The Eyring model was modified by Endicott *et al* [9] to produce a life expression that included explicitly electrical and thermal stresses:

$$L = C_E T^{-w} \exp\left(\frac{-\Delta G}{kT}\right) \exp[-(k_1 + k_2 / T)E] \quad (1-10)$$

with  $w$ ,  $k_1$  and  $k_2$  being further coefficients (more details about such coefficients can be found in [10]).

## 1.2.2 Physical ageing models

Physical models are designed to provide a physical explanation of the aging processes. Hence, it seems to constitute an advance with respect to the phenomenological models. Physical models of ageing are mostly based on the consideration that life is conditioned by the unavoidable presence of micro or macro defects in insulation systems. Therefore, they are meant to describe the evolution of damage from insulation defects, such as cavities, conducting particles and protrusions. They provide expressions for the damage growth process that will eventually cause failure to the insulation system. Some physical ageing models are introduced below.

### 1.2.2.1 Field limited space charge (FLSC) model

The Field Limited Space Charge (FLSC) Model is based on the injection of charge from electrodes into the insulation bulk, which takes place at very high electric field values (e.g. larger than 100 kV/mm). The conductivity of insulating materials can be enhanced by several orders of magnitude at high field, due to the dependence of the activation energy on electric field. This could increase the locally current density and

cause the formation and growth of local conductive paths, leading to breakdown after they reach a critical length [11-12].

The FLSC Model uses the so-called Field-Limited Space-charge Current theory as a background. According to this theory, there is a threshold field,  $E_c$ , below which injected charges have a low mobility, so that it takes a long time to reach the equilibrium situation predicted by the Space Charge Limited Current (SCLC) model. Above  $E_c$  the strongly non-linear dependence of charge mobility on electric field causes the rapid penetration of space charge clouds (or packets [13]) into the insulation bulk, reducing the electric field at the interface between dielectric and electrode/defect in a very short time. The field-limited space charge current may cause dielectric heating (under AC voltage) as well as Maxwell stresses, which might initiate local damage events. The failure criterion of this model is the formation of a fast degradation process (e.g. the electrical tree). A life model can be extracted from this physical description of the damage process:

$$L \propto 1/[r^2 \cdot E_l \cdot \left(\frac{E}{E_c} - 1\right)^2] \quad (1-11)$$

where  $L$  is the time to failure,  $E_l$  is the Laplacian field,  $E$  is the local (Poissonian) field,  $E_c$  is the Poissonian threshold field for the onset of the field-limited space charge current and  $r$  is the radius of the charge injection tip. Equation (1-11) holds for  $E > E_c$ , while life becomes infinite for  $E \leq E_c$ .

### 1.2.2.2 Percolation model

The Percolation Model [14] considers ageing as the generation and extension of conducting regions that cause failure either via a conducting channel crossing through the insulation or via the triggering of a rapid degradation mechanism (e.g. electrical tree). This model starts with the premise that charges are present in the polymer in traps with a variable range of trap depths. It is shown that the energy barriers between pairs of traps for charge transit can be reduced to zero at a specific value of local electric field depending on the inter-trap separation, the shape of the trap potential surface and the respective trap depths. By considering the trap sites to be uniformly distributed in space with a range of trap depths randomly distributed over a given interval, a critical field can be deduced above which the barriers between traps are reduced to zero for a set of sites forming a 3D percolation cluster. At these fields the charges exist in extended states with the structure of the percolation cluster, and consequently possess a high mobility with a large collision path length. In this case, impact excitation and impact ionization become possible. The ionization process can be regarded as a charge de-trapping process from the charged traps, rather than ionization of the polymer molecule. Chemical modifications and damage will take place on the filamentary paths that form the structure of the percolation cluster.

The Percolation Model relates to the elimination of trap-to-trap barriers in a local electric field and the formation of local conducting paths in which a small number of

electrons can gain sufficient energy to cause local damage, rather than a gain in the kinetic energy of electrons sufficient to cause a large scale catastrophic increase in current and thermal damage.

### 1.2.2.3 Space charge DMM model

The DMM (Dissado-Mazzanti-Montanari) Model is based on a thermodynamic approach to the degradation rate of insulation subjected to electrical and thermal stress. Within this thermodynamic framework, space charge accumulated within the polymer under an applied voltage is a cause of ageing due to the relevant local stress enhancement. The model was initially developed for the DC voltage regime [15], and then extended to AC regime [16].

In the DC DMM Model, the insulation is considered as a system that made of chemical species, or moieties (i.e. the micro-structural units of the polymer that undergo damage), in thermodynamic equilibrium between the initial state of reactant state (state 1) and the final state of product (state 2). The ageing process is described in terms of a “forward” reaction (state 1 to state 2) and a countering “backwards” reaction. These alternative states can be transformed into one another by passing through an intermediate transition state at a higher free energy. They are therefore connected by a free energy barrier,  $\Delta G$ , and both forward and reverse reactions are allowed, with rates depending on the relevant concentrations of moieties in the two states and the appropriate magnitude of the barrier. In the presence of an electric field, the system is in a global non-equilibrium state and is driven to change in time until it either reaches a thermodynamic equilibrium or an amount of local modification sufficient to initiate a more rapid failure mechanism. The time-to-failure derived in this way is the time taken for the system to reach the critical level of modification required to ‘switch-on’ the rapid failure process.

The failure criterion in this model is set by assuming that the fraction of degraded moieties,  $M_d$ , exceeds locally a critical fraction,  $M_d^*$ , which corresponds to the formation of a cavity large enough for the occurrence of partial discharge. Therefore, the DMM Model provides the time to formation of critical voids, rather than time-to-breakdown. According to the DC DMM Model, the life of the insulation system,  $L$ , can be expressed as:

$$L(E,T) = \frac{h}{2kT} \exp\left(\frac{\frac{\Delta_H - C'E^{2b}}{k} - \frac{\Delta_S}{k}}{T}\right) \ln\left[\frac{M_{eq}(E)}{M_{eq}(E) - M_d^*}\right] \left[\cosh\left(\frac{\frac{\Delta}{k} - C'E^{2b}}{2T}\right)\right]^{-1} \quad (1-12)$$

$$M_{eq}(E) = \left[1 + \exp\left(\frac{\frac{\Delta}{k} - C'E^{2b}}{T}\right)\right]^{-1} \quad (1-13)$$

where  $M_{eq}(E)$  is the value of  $M_d$  at the equilibrium between forward and backward reactions;  $T$  is the absolute temperature,  $\Delta_H$  and  $\Delta_S$  are the activation enthalpy and entropy per moiety respectively;  $\Delta$  is free energy difference between reactant and product state.  $E$  is the external applied (Laplacian) field;  $C'$  is a constant depending essentially on material properties;  $b$  is a constant that enters the above expression through the relationship between stored charge per charge-center and applied electric field.

A proposal was made to extend the DC DMM model to AC voltages by accounting for the role of electrical fatigue in the presence of a sinusoidal electric field. The final expression was presented in [16], together with details of its deviation. The determination of model parameters for both the DC DMM model and the AC DMM model was discussed and shown to be feasible in [17]. A further refinement of the model, emphasizing the role played by local elemental strain, is described in [18, 19].

#### 1.2.2.4 Ageing models based on the electro-dynamic stress

In the previously described models, the main cause of the insulation degradation is assumed to be the space charge. Other authors (e.g. Lewis [20] and Crine [21]) consider the cause of the electrical ageing to be the electro-dynamic stresses produced by the electric field. The physical basis of these models is the assumption that the ageing is a thermally-activated process that requires the system to be activated over a free energy barrier. In presence of electric field, the energy barrier is reduced by a square-field term, which takes into account the electro-dynamic effect of the field.

In the model from Lewis, attention is focused on the electro-mechanical stress that tends to expend the structure of the polymer against cohesive forces. When the electro-mechanic energy overcomes the free energy barrier, a loss of cohesion takes place between two adjacent zones of the polymer. The end point of the model is the condition in which the orthogonal stress enlarges the cavity up to the formation of cracks in the insulation and a faster degradation process is triggered, such as partial discharges. The numerical model of ageing was formulated by considerations on the partially reversible reaction of expansion of the polymer and on the reduction of the activation barrier  $\Delta G$ , due to the electric field. The life expression provided by this model under DC field is

$$L = \frac{h}{2kT} \cdot \exp\left(\frac{\Delta G}{kT}\right) \cdot \operatorname{csch}\left(\frac{\varepsilon \cdot \Delta V \cdot E^2}{2kT}\right) \quad (1-14)$$

where  $\Delta V$  is the activation volume,  $\varepsilon$  is the permittivity of the dielectric. A similar equation was proposed for AC fields, in which the AC frequency is substituted for  $(kT/h)$  as the denominator of the pre-exponential. In the framework of this model, the increase of the accumulated space charge with the ageing is a consequence of the growth of the nano-cavities.

## CHAPTER 2

### THEORETICAL BACKGROUND

In this Chapter, physical ageing models of partial discharge (PD) behavior and relevant damage inception from micro-cavities in dielectric material under DC and AC voltage are presented. The physics and chemistry of PD in cavities embedded in dielectrics are briefly introduced.

The considered system for the ageing modeling, sketched in Figure 2.1, consists of a polyethylene (PE) slab of thickness  $D$ , enclosed between plane parallel metallic electrodes, with an embedded cylindrical micro-cavity filled with air at atmospheric pressure. The dimensions of the cavity are height  $d$  (along the field direction) and circular basis  $S$  (of radius  $R$ ). This system simulates typical micro-cavities which can be found in PE-based power cable insulation after extrusion.

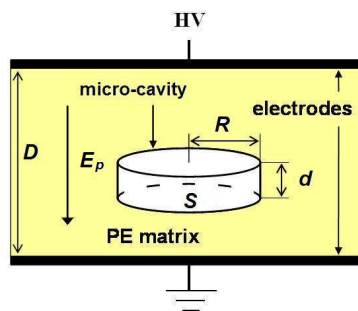


**Figure 2.1:** Sketch of the system considered for the proposed aging and life model: a PE matrix with an embedded cylindrical cavity (cavity dimensions are emphasized)

In the ageing models under both DC and AC field, we assume the main degradation process to be a bond-breaking process within a PE slab at the dielectric/cavity interface, caused by the bombardment of avalanche electrons generated in the PD process. The degradation involves a subsequent formation of free radicals and chemically reactive species in the slab that is severely and irreversibly damaged. The insulation system is considered to fail as soon as the extension of the damaged zone along the electric field is large enough for starting a rapid failure mechanism, e.g. electrical tree.

In Section 2.1, the physical ageing model under DC field is introduced, following [1-4]. Analytical expressions for electron injection rate, damage growth rate and time-to-failure are derived as a function of material properties, cavity size, applied electric field and temperature. In Section 2.2, the main differences between the ageing modeling under DC and AC fields are discussed. In Section 2.3, the physical model of PD activity under AC field is reported. In Section 2.4, the interaction between PD behavior and the surrounding dielectrics (i.e. the gas filling the cavity and the

dielectric/cavity interface) is briefly discussed.

## 2.1 PD-induced Ageing Model under DC Field

The general process of damage inception and growth from cavities embedded in dielectrics has common features under DC and AC field. Three steps can be singled out in the process:

1. presence of the free electrons in the cavity, available for PD inception;
2. electron avalanche generation and hot-electron production in the cavity;
3. damage accumulation of the polymer surface due to hot-electron impinging the dielectric/cavity interface.

The details of each step under DC field are described in the following subsections.

### 2.1.1 Presence of the free electrons in the cavity

The production of free electrons in the cavities can be attributed to two terms: the background radiation and the field-assisted injection of electrons from the dielectric/cavity interface. It is claimed that the background radiation, particularly high energy photons, can play a role, ionizing the gas molecules in the cavity and/or extracting the electrons from the cavity walls. However, in practical insulation system (e.g. power cables) and for realistic size of cavities, the background radiation effect is negligible [5, 6]. Therefore, the predominant mechanism is the field-assisted charge injection from the dielectric/cavity interface. The presence of free electrons in the cavity is closely related to the electric field.

If a constant DC voltage is applied, the poling field,  $E_p$ , is built in the polymer matrix far away from the cavity (see Figure 2.1). The electric field,  $E_i$ , is built in the cavity.  $E_i$  can be considered to be made of two contributions:

$$E_i = E_0 + E_q \quad (2-1)$$

where  $E_0$  is the background field in the cavity (i.e. the electric field in absence of discharges, including the field contribution due to the polarization),  $E_q$  is the electric field generated by the space charge,  $q_{SC}$ , deployed at the dielectric/cavity interface by the previous PD.  $E_i$ ,  $E_0$  and  $E_q$  are function of time. Under the hypothesis of linearity,  $E_0$  is related to the poling field,  $E_p$ , through a suitable constant  $f_b$ :

$$E_0 = f_b \cdot E_p \quad (2-2)$$

in which  $E_p$  is the field that would exist at the cavity location in the absence of the cavity itself,  $f_b$  is a constant parameter that accounts for the field enhancement due to the different permittivity of the gas.  $f_b$  depends on the geometry of the cavity ( $d$  and  $R$ ) and on the dielectric relative permittivity,  $\epsilon_r$ , of the dielectric.  $E_q$  depends on the distribution of space charge,  $q_{SC}$ . In a first approximation, such dependence can be

assumed as linear and accounted by a constant factor  $f_c$ , as follows:

$$E_q = f_c \cdot q_{SC} \quad (2-3)$$

$f_c$  also depends on the cavity geometry.  $q_{SC}$  decays through processes such as neutralization due to conductivity on cavity surface and diffusion into the dielectric bulk. The decay process can be approximated by

$$q_{SC} = q_{SC0} \cdot e^{-\Delta t/\tau} \quad (2-4)$$

where  $q_{SC}$  is the remaining space charge value after  $\Delta t$  ( $\Delta t = 0$  immediately after the previous PD),  $q_{SC0}$  is the amount of charge at the cavity surface after the previous PD took place,  $\tau$  is the time constant of the charge relaxation process.

Once the electric field is built in the system, the electrons, injected from the electrodes or already present in the PE matrix, travel through the PE matrix due to thermally-activated hopping conduction mechanism [7] and reach the dielectric/cavity interface. There, they get trapped, because of the negative electron affinity of PE, leading to storage of space charge at the dielectric/cavity interface [8, 9]. Subsequently, some electrons have a chance of being emitted into the cavity through the Schottky effect, thanks to the fact that the activation energy for electron detrapping,  $\phi$ , can become lower than the actual charge trap depth (work function),  $U_0$ , due to both the Laplacian and the Poissonian fields, as well as the Coulombic repulsion between stored charges on the surface. The number of electrons,  $n(t)$ , accumulated on the cavity surface at a given time  $t$  depends on a balance between the incoming flux of electrons due to conduction in PE and the outgoing flux related to Schottky emission. The balance is accounted for by the following system of equations:

$$\frac{dn(r,t)}{dt} = \frac{JS}{q_e} (1 - e^{-\phi(r,t)/kT}) \quad (2-5)$$

$$\phi(r,t) = U_0 - q_e \left( \frac{q_e f_a E_p}{4\pi\epsilon_0} \right)^{\frac{1}{2}} - \frac{q_e}{4\pi\epsilon_0} \int_S \frac{\sigma(r',t)}{|r-r'|} dr' \quad (2-6)$$

where  $J$  is the conduction current density,  $q_e$  is electron charge,  $t$  is time,  $k$  is Boltzmann constant,  $T$  is absolute temperature,  $r$  is radial coordinate of circular surface  $S$  (ranging from 0 to  $R$ ),  $\phi(r,t)$  is activation energy for electron detrapping,  $\sigma(r', t)$  is electron surface density,  $U_0$  is the work function of the dielectric/cavity interface,  $\epsilon_0$  is the permittivity of the cavity gas (air),  $E_p$  is electric field in the polymer

matrix,  $f_a$  is a factor used to include the enhancement of the field in the cavity. In the absence of significant space charge accumulation at the dielectric/cavity interface, the field in the cavity  $E_i$  can be described by  $E_i = f_a E_p$ . In the case that  $d \leq 0.2R$  (see Figure 2.1),  $f_a = \epsilon_r$ , in which  $\epsilon_r$  is relative permittivity of the polymer.

The first term of equation (2-5),  $JS/q_e$ , is the incoming flux electrons, while the second term,  $\frac{JS}{q_e} \cdot e^{-\phi(r,t)/kT}$ , is the outgoing flux due to detrapping and emission.

Equation (2-6) accounts for the decrease in the value of  $\phi$  with respect to  $U_0$ , caused

by electric field,  $q_e \left( \frac{q_e f_a E_p}{4\pi\epsilon_0} \right)^{\frac{1}{2}}$ , and to the Coulombic repulsion of the accumulated

of electrons on the cavity surface,  $\frac{q_e}{4\pi\epsilon_0} \int_s \frac{\sigma(r',t)}{|r-r'|} dr'$ .

In order to solve equations (2-5) and (2-6), the following hypotheses are made:

1. all electrons arriving at the surface get trapped;
2. at time  $t$ , electrons on the surface are uniformly distributed with a charge density  $\sigma(r',t) = JSt/\pi R^2$ ;
3. detrapping rates are much slower than trapping ones;
4. emission times of electrons are much longer than drift (travel) times across the cavity;
5. chemical traps at the interface are neglected.

Under these assumptions the problem becomes linear, and the Hartree term,

$\frac{q_e}{4\pi\epsilon_0} \int_s \frac{\sigma(r',t)}{|r-r'|} dr'$ , is simplified as  $\frac{JStq_e}{2\pi R\epsilon_0}$ . Equation (2-5) can be recast as:

$$\frac{dn(t)}{dt} = \frac{JS}{q_e} \left\{ 1 - \exp \left[ - \frac{U_0 - q_e \left( \frac{q_e f_a E_p}{4\pi\epsilon_0} \right)^{\frac{1}{2}} - \frac{q_e JSt}{2\pi\epsilon_0 R}}{kT} \right] \right\} \quad (2-7)$$

By solving equation (2-7) for  $n(t)$ , we get the number of injected electrons at time  $t$ :

$$n_{inj}(t) = JSt/q_e - n(t) \quad (2-8)$$

The time to injection of the first electron,  $t_{inj}$  can be obtained by solving the following integral equation:

$$\int_0^{t_{inj}} \frac{dn_{inj}(t)}{dt} dt = 1 \quad (2-9)$$

By solving equation (2-9), we obtain the first electron injection rate,  $R_{inj}=1/t_{inj}$ :

$$R_{inj} = \frac{q_e JS}{2\pi kT \varepsilon_0 R} \ln \left\{ 1 + \frac{q_e^2}{2\pi \varepsilon_0 R kT} \exp \left[ \frac{U_0 - q_e \left( \frac{q_e f_a E_p}{4\pi \varepsilon_0} \right)^{\frac{1}{2}}}{kT} \right] \right\}^{-1} \quad (2-10)$$

$R_{inj}$  in equation (2-10) is assumed as an average value for the injection of all the electrons injected in the cavity after the first one.

### 2.1.2 Electron avalanche generation

Once the electrons are injected in the cavity, they are accelerated by the electric field. If the field in the cavity,  $E_i$ , exceeds the PD inception field, the electronic avalanche process takes place, multiplying the starting electron by impact ionization of gas molecules. This process results in an exponential growth of the electrons inside the cavity. The quantitative description of this process is based on the classic theory of discharges in air at atmospheric pressure over small distances and, thus, on the 1<sup>st</sup> and 2<sup>nd</sup> Townsend coefficients.

When the electron avalanche impinges on the PE surface, the electrons interface with the PE matrix in different ways. Below a critical energy, electrons are not able to modify the matrix. An electric energy of no less than 8 eV is needed for causing Dissociative Electron Attachment (DEA) process that will break C-H bonds and alter the PE surface in a permanent way (creating also chemically aggressive free radicals). Only electrons having energy in excess of such value are able to cause the damage. Therefore, they are referred to as “hot-electrons” in the following text.

In order to evaluate the damage introduced by the electron avalanche, the fraction of hot-electrons,  $F_{hot}$ , has to be considered [1, 2, 4]. It has to be derived from the energy distribution of electrons colliding with the dielectric/cavity interface. The time evolution of electron energy distribution depends on the energy,  $w$ , electric field in the cavity,  $E_i$ , and time,  $t$ . Hence, it can be denoted as  $n(w, E_i, t)$ . In practice, the electron energy distributions come to an equilibrium value,  $n(w, E_i, 0)$ , in a very short time. Then the energy spectrum of electrons remains steady, while their total number increases exponentially. Therefore,  $n(w, E_i, t)$  can be written as [3, 10]:

$$n(w, E_i, t) = n(w, E_i, 0) \cdot e^{\beta(E_i)t} \quad (2-11)$$

where  $e^{\beta(E_i)t}$  is the field-dependent multiplication rate factor. By assuming that all the avalanche electrons impact the surface at the same time,  $t_A$ , equation (2-11) at  $t_A$  can be recast as:

$$n(w, E_i, t_A) = n(w, E_i, 0) \cdot e^{\beta(E_i)t_A} = n(w, E_i, 0) \cdot e^{\beta(E_i)d/v_A} \quad (2-12)$$

in which  $d$  is the cavity height,  $v_A$  is electron mean velocity. By setting  $\alpha(E_i) = \beta(E_i) \cdot d/v_A$ , equation (2-12) can be rewritten as

$$n(w, E_i, d/v_A) = n(w, E_i, 0) \cdot e^{\alpha(E_i)d} \quad (2-13)$$

By normalizing the steady-state part of the distribution to one (i.e.  $\int_0^\infty n(w, E_i, 0)dw = 1$ ), the total number of electrons arriving at the polymer surface starting from one single injected electron,  $N_{el}$ , can be derived from equation (2-13):

$$N_{el} = \int_0^\infty n(w, E_i, 0) e^{\alpha(E_i)d} dw = e^{\alpha(E_i)d} \quad (2-14)$$

By considering the electron attachment to electronegative molecules present in the air, the attachment coefficient  $\eta(E_i)$  has to be subtracted to  $\alpha(E_i)$ . Hence,  $N_{el}$  becomes:

$$N_{el} = e^{[\alpha(E_i) - \eta(E_i)]d} = e^{\alpha_{eff}(E_i)d} \quad (2-15)$$

where  $\alpha_{eff}(E_i) = \alpha(E_i) - \eta(E_i)$  is the effective ionization coefficient. In the following discussion, the electron attachment process (i.e.  $\eta(E_i)$ ) is not considered.

In Section 2.1.1, we obtained the average rate of electron injection in the cavity,  $R_{inj}$ , as shown in equation (2-10). In Section 2.1.2, equation (2-14) shows the electron avalanche multiplication factor,  $N_{el}$ . The product of these two parameters,  $R_{inj} \cdot N_{el}$ , provides the electron impinging rate on the dielectric/cavity interface,  $R_{el}$ , as follows:

$$\begin{aligned}
R_{el} &= R_{inj} N_{el} = \\
&= \frac{q_e JS}{2\pi\epsilon_0 RkT} \cdot \frac{e^{\alpha(f_a E_p)d}}{\ln \left[ 1 + \frac{q_e^2}{2\pi\epsilon_0 RkT} \cdot \exp \left( \frac{U_0 - q_e \left( \frac{q_e f_a E_p}{4\pi\epsilon_0} \right)^{\frac{1}{2}}}{kT} \right) \right]}
\end{aligned} \tag{2-16}$$

$R_{el}$ , is a variable that depends on  $E_p$ ,  $T$ ,  $J$ ,  $R$ ,  $d$  and material properties. It plays an important role in calculating the damage growth rate from the interface, as will be discussed in subsection 2.1.3.

### 2.1.3 Damage accumulation at the cavity surface

Depending on cavity size and electric field, hot-electrons can be produced in the electron multiplication process [10-13]. They collide with the dielectric/cavity interface, causing irreversible degradation to the polymer matrix.

The time-to-failure (or lifetime),  $L$ , of the insulation system is defined as the time to the formation of a damaged zone of critical size  $d_c$ , made of contiguous damaged slabs of thickness  $D_{dis}$  [14]. The critical size is regarded as an extension of the damaged zone in the direction of the applied field that is large enough for starting a fast failure mechanism [15-19], e.g. electrical tree induced by injection of hot-electrons into the polymer matrix by the tip of the defect. Under this assumption, a preliminary expression of an ageing model for the system shown in Figure 2.1 can be derived, as shown in equation (2-17).

$$R_{dis} = D_{dis} / t_{dis} \tag{2-17}$$

where  $t_{dis}$  is the time-to-disruption (i.e. the time to severe and irreversible chemical degradation) of the slab having thickness  $D_{dis}$ . It provides the damage growth rate,  $R_{dis}$ , associated with chemical bond-breaking processes due to hot-electron bombardment. The disruption of successive damaged slabs is assumed to proceed with time and, essentially, with the same mechanism. After the damaged zone reaches the critical thickness  $d_c$ , the electrical tree occurs. This model considers the failure time as the time to form a damaged zone having critical size rather than actual time-to-breakdown.  $d_c$  is called the failure criterion, since tree propagation is generally much shorter than the time needed to incept the tree itself.

Based on the above discussion,  $L$  can be estimated as follows:

$$L = d_c / R_{dis} \quad (2-18)$$

From Equations (2-17) and (2-18),  $L$  can be recast as a linear function of  $t_{dis}$ , namely:

$$L = d_c \cdot \frac{t_{dis}}{D_{dis}} \quad (2-19)$$

An expression of  $t_{dis}$  as a function of the cavity size (height  $d$  and surface radius  $R$ ), electric field in the polymer matrix  $E_p$ , temperature  $T$  and material properties can be written as follows [2]:

$$t_{dis} = \frac{N_{CH}}{2R_{el}F_{hot}F_{eff}} \quad (2-20)$$

where  $N_{CH}$  is the number of C-H bonds in the volume of a slab having thickness  $D_{dis}$ ,  $R_{el}$  is the rate of electrons colliding with the polymer surface after being injected into the cavity and multiplied in the avalanche,  $F_{hot}$  is the fraction of hot-electrons (see [2]),  $F_{eff}$  is the fraction of hot-electrons that are effective in causing chemical damage through DEA, the factor 2 at the denominator comes from the assumption that the slab is considered to be irreversibly damaged when half of C-H bonds are broken. Since the volume of the disrupting slab can be calculated as the product of slab thickness,  $D_{dis}$ , by cavity surface,  $S$ , equation (2-20) can be rewritten as:

$$t_{dis} = \frac{\rho_{CH}D_{dis}S}{2R_{el}F_{hot}F_{eff}} \quad (2-21)$$

where  $\rho_{CH}$  is the volume density of C-H bonds in the polymer, that depends also on its crystallinity.

Resorting to equations (2-18) to (2-21), the damage growth rate  $R_{dis}$  can be evaluated. First of all, the disruption time,  $t_{dis}$ , can be expressed as:

$$t_{dis} = \frac{\rho_{CH}D_{dis}\pi\varepsilon_0RkT}{F_{hot}F_{eff}Jq_e} \left\{ \ln \left[ 1 + \frac{q_e^2}{2\pi\varepsilon_0RkT} \exp \left( \frac{U_0 - q_e \left( \frac{q_e f_a E_p}{4\pi\varepsilon_0} \right)^{\frac{1}{2}}}{kT} \right) \right] \right\} e^{-\alpha(f_a E_p)d} \quad (2-22)$$

Then, by inserting the expression of  $t_{dis}$  into equation (2-17), the analytical expression of damage growth rate as a function of  $E_p$ ,  $T$ ,  $d$ ,  $R$ ,  $J$  and material properties (i.e.  $\rho_{CH}$ ,  $U_0$ ) can be determined, as show below:

$$R_{dis} = \frac{F_{hot} F_{eff} J q_e}{\rho_{CH} \pi \epsilon_0 R k T} \cdot \frac{e^{\alpha (f_a E_p) d}}{\ln \left[ 1 + \frac{q_e^2}{2 \pi \epsilon_0 R k T} \exp \left( \frac{U_0 - q_e \left( \frac{q_e f_a E_p}{4 \pi \epsilon_0} \right)^{\frac{1}{2}}}{k T} \right) \right]} \quad (2-23)$$

Therefore, according to equations (2-18) and (2-23), time-to-failure,  $L$ , can be derived, being inversely proportional to  $R_{dis}$ .

## 2.2 Differences between Modeling under DC and AC Field

The differences between the DC and AC ageing models lie in two fundamental aspects, which are (a) the availability of electrons that can start an avalanche and (b) the influence of space charge induced by the previous discharges.

Under DC field, PD generally have low repetition rate (e.g. few discharges per minute [10], depending on the electric field). The electrons emitted into the cavity are provided by the electric conduction process. There is a balance between time for electrons to reach the dielectric/cavity interface (through injection from electrodes and conduction in the polymer) and time for electrons deployed by a PD to decay (through neutralization and diffusion). Generally, in a good insulation the first term (electron transportation in the polymer bulk) predominates in the balance. Thus, the PD repetition rate is governed by bulk conductivity.

Under sinusoidal voltage at 50Hz, the repetition rate of the PD is high, ranging from tens to more than one thousand PD per second (depending on the electric field, the cavity size and the energy trap depth on the cavity surface). The period of the applied field can be comparable to the decay time of the space charge deposited at the dielectric/cavity interface (milliseconds), so that the contribution of space charge decay must be taken into account [10, 12, 15]. Indeed, after the first PD occurs under AC field, the main source of the electrons available for injection is provided by the space charges at the dielectric/cavity interface, which are generated by previous PD. These space charges could modify the electric field in the cavity and change the injection probability of electrons. Therefore, the effect of the space charge generated by the previous PD must be considered.

Furthermore, the electron injection in the cavity under AC field is a random process. Therefore, the modeling of the PD phenomenon under AC field must be approached on a stochastic base. The model should be able to describe injection rate, discharge amplitude and the effect of space charge deployed on the dielectric/cavity interface by the previous PD.

## 2.3 PD Model under AC Field

In this section, the main features of PD phenomena are introduced in a gas-filled cavity under AC field. The algorithm is based on an existing model [20, 21], obtained by considering the phenomenological and physical mechanisms governing the PD in dielectric-bonded cavities. The approach is aimed at obtaining a model of the PD phenomenon based on physical-chemical properties of the insulation system and the geometry of the micro-cavity [10, 12].

### 2.3.1 Electric field in the cavity under AC field

Under AC field, electric field in the cavity,  $E_i$ , can also be considered to be made of two contributions,  $E_i = E_0 + E_q$ . If sinusoidal voltage is applied to the system, the background field in the cavity,  $E_0$ , can be expressed as:

$$E_0 = E_{peak} \cdot \sin(\omega t) \quad (2-24)$$

where  $E_{peak}$  is the peak value of  $E_0$ ,  $\omega$  is the angular frequency of the sinusoidal voltage applied to the system. The space charge generated field,  $E_q$ , can be expressed by equation (2-3).

After a discharge completely extinguished, an equal amount of positive (ions) and negative charges (electrons) will be deployed on the cavity surfaces near the electrodes having opposite polarity to the charges, as shown in Figure 2.2.

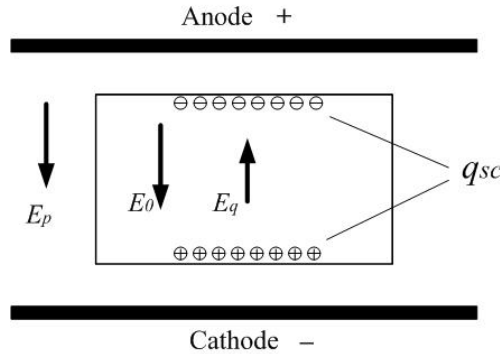


**Figure 2.2** Contribution of the space charge distribution to the electric field in the cavity.  $E_0$  - background field in the cavity,  $E_q$  - space charge generated electric field,  $E_p$  - electric field in the polymer matrix.

These charges cumulate with the charge previously deployed, increasing or decreasing the net charge on the surface,  $q_{SC}$ , according to:

$$q_{SC}(t_{PD}^+) = q_{SC}(t_{PD}^-) + q_{PD}(t_{PD}) \quad (2-25)$$

where the charge  $q_{PD}(t_{PD})$  is the charge deployed by a discharge occurring at the time

$t_{PD}$ ,  $q_{SC}(t_{PD}^-)$  is the charge deployed at the cavity surface before the discharge.  $q_{PD}(t_{PD})$  adds algebraically to  $q_{SC}(t_{PD}^-)$ , giving place to the new amount of charge,  $q_{SC}(t_{PD}^+)$ , which generates  $E_q$ . Meanwhile, space charge decays during the time interval between discharges, which can be described by equation (2-4).

Figure 2.3 reports the time evolution of  $E_0$  (black curve),  $E_q$  (red curve) and  $E_i$  (blue curve), assuming the discharge takes place at the first maximum of the  $E_0$ . The space charge generated field largely affects the field in the cavity and, thus, the PD activity (particularly the discharge amplitude [22]).

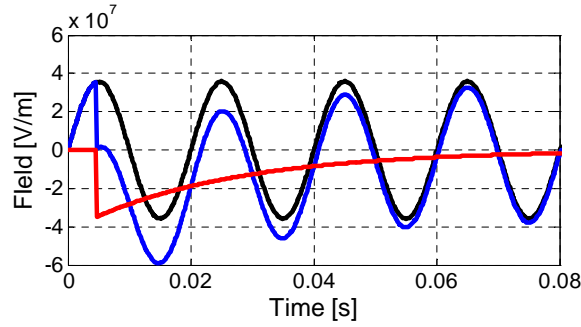


**Figure 2.3** Time evolution of  $E_0$  (black curve),  $E_q$  (red curve) and  $E_i$  (blue curve).

### 2.3.2 PD inception

In order to start a partial discharge in the cavity, the following two conditions have to be satisfied simultaneously:

1. a starting electron appears in the cavity;
2. the electric field in the cavity,  $E_i$ , is high enough to turn the starting electrons into the avalanche.

As regards the second condition, the PD inception field,  $E_{inc}$ , (considering streamer discharges) is governed by a critical avalanche criterion [21]:

$$E_{inc} = P \cdot \left( \frac{E_p}{P} \right)_{cr} \cdot \left[ 1 + \frac{B}{(2PR)^n} \right] \quad (2-26)$$

where  $P$  is the gas pressure in the cavity,  $R$  is the radius of the cavity,  $(E/P)_{cr}$ ,  $B$  and  $n$  characterize the ionization process in the gas inside the cavity. In the case the gas is air,  $(E_p/p)_{cr} = 24.2 \text{ VPa}^{-1}\text{m}^{-1}$ ,  $B = 8.6 \text{ ml}^{1/2}\text{Pa}^{1/2}$  and  $n = 0.5$ . After the inception criterion is fulfilled, an injection electron is additionally required to trigger the ionization process in the cavity. The electron injection rate is the main focus of this section.

As stated in section 2.2, a stochastic approach must be introduced in the PD modeling under AC voltage. The production of starting electrons needs to be dealt

with by a stochastic method. The probability,  $p$ , for the occurrence of an initiatory electron during a time interval  $dt$  is evaluated by the cumulative probability function associated with the hazard  $h$  of having a initiatory electron, as defined in [22], by:

$$p = 1 - e^{-h \cdot dt} \quad (2-27)$$

where  $h$  is the hazard of having a starting electron. It is assumed to consist of two terms:

$$h = h_{bg} + \lambda \quad (2-28)$$

where  $h_{bg}$  accounts for all the contributions to the starting electron availability that do not depend on the discharge activity (e.g. conduction in the polymer),  $\lambda$  is the detrapping rate of the charge carriers deployed at the cavity surface by the previous PD. If the Richardson-Schottky detrapping mechanism is considered,  $\lambda$  can be written as [8, 10]:

$$\lambda = \frac{dN_{dt}}{dt} = N_{dt} \cdot v_0 \cdot e^{-\frac{\left( U_0 - \sqrt{\frac{q_e^3 \cdot K \cdot E_i}{4\pi\epsilon_0}} \right)}{kT}} \quad (2-29)$$

where  $N_{dt}$  is the number of electrons on the cavity surface available for injection,  $v_0$  is the fundamental phonon frequency (about  $10^{14}$  Hz for polyethylene),  $U_0$  is charge trap depth,  $q_e$  is the electron charge value,  $E_i$  is the electric field in the cavity,  $\epsilon_0$  is the permittivity of the cavity gas (air),  $k$  is the Boltzmann constant and  $T$  is the absolute temperature. The coefficient  $K$  is introduced to take into account the local field enhancement caused by the charge carriers deployed at the dielectric/cavity interface. Its value and physical meaning are discussed in the following subsection.

### 2.3.3 Discharge at electric field polarity inversion time

The inception delay time is defined as the time interval from the moment the electric field in the cavity exceeds the PD inception field to the moment the starting electrons are available. Under sinusoidal voltage, discharges that occur at the polarity inversion (i.e. the moment at which the polarity of  $E_i$  changes sign) is usually characterized by an inception delay that is statistically longer than the subsequent PD of the same half voltage cycle. The polarity inversion generally takes place at the moment when the background field ( $E_0$ ) has the largest variation rate (with  $\omega t$  close to  $0^\circ$  and to  $180^\circ$ ). A longer inception delay corresponds to a larger variation of the electric field during the delay time and, thus, to a higher electric field which gives place to the discharge. Therefore, the first discharge occurring after the polarity inversion has higher amplitude than the subsequent PD.

After the first PD occurs under AC field, the main source of the electrons available for injection is provided by the charges at the cavity surface. In order to have a PD after the inversion of the polarity of the electric field in the cavity, an electron must be extracted from a negatively charged surface. Therefore, the dynamics of the space charge deployed at the cavity surface by the previous PD could be the key factor to explain the formation of the special shape of the patterns of PD in the PE embedded cavities, which is known as the “rabbit-like” pattern (see Figure 2.4). In [10, 12], an approach is proposed to explain the formation of the “rabbit-like” pattern based on the considerations about the electrostatic effect of the space charge deployed by the PD [12, 23, 24]. The physical consideration of this hypothesis is introduced below.

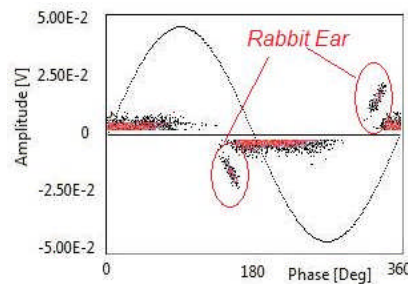


**Figure 2.4** “Rabbit-like” shape pattern of the PD in PE embedded cavities

At the time period between polarity inversion and the occurrence of the first PD, the electrons, generated by discharges in the previous half voltage cycle, accumulate on the cavity surface close to the cathode, as shown in Figure 2.5. In order to have the first PD in the half voltage cycle, a starting electron must be extracted from the negatively charged surface. The hazard of having the starting electron for the avalanche can be calculated according to equations (2-27) to (2-29).

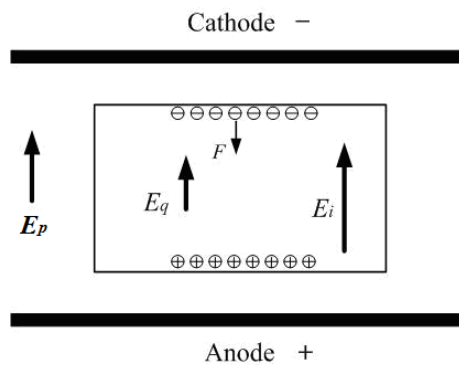


**Figure 2.5** Extraction of the electron from a negatively charged surface after the polarity inversion.  $F$  is the extraction force acting on the electrons.

The first PD after polarity inversion deposits positive charges on the cavity surface near the cathode (referred to as cathode surface in the following) and deposits negative charges on the one near the anode (referred to as anode surface in the following), changing the original charge polarity on the surfaces, as presented in Figure 2.6. Hence, after the first PD takes place, the net charge deployed on the cathode surface is positive and the charge on the anode surface is negative, as shown

in Figure 2.7. The inversion of the polarity of  $E_q$  can also be observed in Figure 2.7.

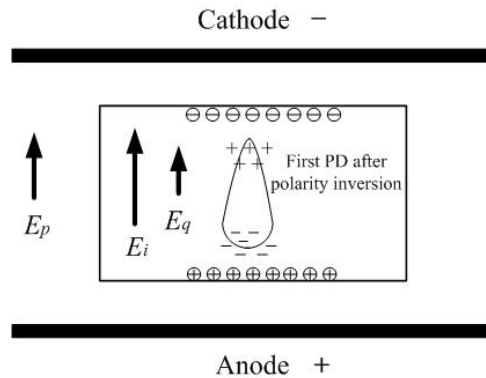


**Figure 2.6** First PD after polarity inversion

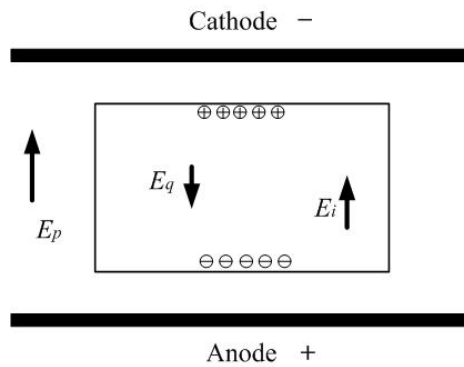


**Figure 2.7** Space charge distribution and electric field in the cavity after the first PD occurs

The net charge deployed on the cathode surface is positive and it is given by a layer of positive ions. The effect of the space charge in this condition is to reduce the electric field in the central part of the cavity. However, locally near the cathode surface, the electric field which extracts the electrons is enhanced by the presence of the layer of positive ions, as it happens in solid polymeric insulators where the accumulation hetero-charge near the electrode enhances the charge injection from it [25]. Thus, after the first discharge takes place, the electron injection probability is enhanced. Therefore, the coefficient  $K$  is defined as follows:

$$K \begin{cases} =1, & \text{if } E_q \cdot E_i > 0; \text{ (for the first PD after the polarity inversion)} \\ >1, & \text{if } E_q \cdot E_i < 0; \text{ (for the subsequent PD of the same half-cycle)} \end{cases}$$

Before the first PD occurs after polarity inversion,  $E_q$  has the same direction as  $E_i$  (see Figure 2.5). The probability of having a starting electron is small for starting the first PD in the half voltage cycle. Therefore, a small  $K$  value ( $K = 1$ ) is defined. The space charge deployed by the first PD varies the electric field in the cavity and near the cavity surface, resulting in a larger probability of electron injection. Thus a large  $K$  value is defined ( $1 < K < 10$ ) for the subsequent PD.

### 2.3.4 Discharge magnitude

Discharge magnitude is related to the amount of charges generated by the PD in the avalanche. The knowledge of the number of generated charge carriers and their energy distribution, particularly at the moment they impact on the dielectric/cavity surface, are fundamental to the evaluation of damage growth rate,  $R_{dis}$ . In [10], a novel method is proposed to simulate the discharge process by taking into account only the main phenomena involved in the process, i.e. the avalanche electron multiplication and the space charge generated electric field. The avalanche multiplication is accounted for by the Townsend law, using the electric field dependant first Townsend coefficient,  $\alpha(E_i)$ .

In the numerical simulation, the amount of charges generated by the PD is evaluated on the basis of electric field in the cavity by a cubic spline data interpolation,  $q_{PD} = f(E_i)$ . The function  $f(E_i)$ , in general, depends on the cavity height,  $d$ , first Townsend coefficient  $\alpha$  and the effect of the electric field generated by the space charge on the cavity surface,  $E_q$ . It is obtained using simulations where the effective ionization coefficient was adjusted by trial and error [10].

## 2.4 Interaction between PD and the Surrounding Dielectrics

The research the PD phenomenon starts from the 1960's. Significant progress has been made on the research of PD-induced ageing of solid dielectrics. Researchers now agree on the main mechanisms pertaining to the PD-induced degradation of the dielectric, which can be attributed to two processes: physical attack by bombardment of high energy particles and chemical degradation. The PD induced ageing process is now generally accepted to proceed along the following line, as described by Figure 2.8:

1. The cavity surface conductivity increases due to the deposition of acid byproducts due to the interaction of the avalanches with the polymer. Many authors [26, 27] have detected an increase of the surface conductivity not long after the PD process was initiated, both on the cavity surface in PE and epoxy. According to the research of Hudon [27], the degradation products on an epoxy surface can raise the surface conductivity by six orders of magnitude.
2. The roughness of the cavity surface increases due to charge carrier bombardment and chemical erosion by PD by-products.
3. After a certain ageing period, the solid byproducts (e.g. crystals as reported in [26, 28]) starts to accumulate on the cavity surface.
4. Field enhancement at crystal tips leads to a further intensification and localization of the PD process and pit can be formed. As a consequence, electrical tree growth is initiated.
5. Eventually, breakdown occurs due to the growth of electrical tree.

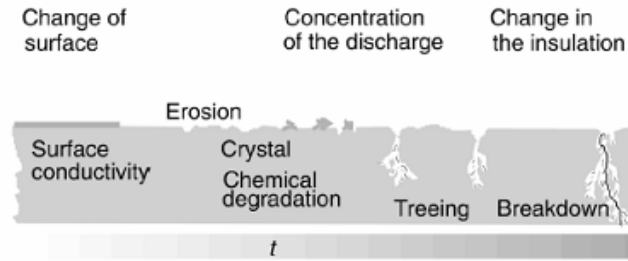


**Figure 2.8** Ageing process of the PD induced damage, after Temmen [29]

The chemical reactions that accompany the interaction between PD and the dielectric/cavity interface have been extensively studied. These reactions result in gaseous, liquid and solid byproducts. A large amount of carbon monoxide (CO) and carbon dioxide (CO<sub>2</sub>) was found in cavities embedded in both LDPE and XLPE exposed to PD [30, 31]. Liquid byproducts were found to be a mixture of simple organic compounds, like formic, acetic and carboxylic acids [32]. After a long period of ageing (e.g. some hundreds of hours), the solid PD byproduct could be found in the form of crystals, which have been positively identified as hydrated oxalic acid (C<sub>2</sub>H<sub>2</sub>O<sub>4</sub>·2H<sub>2</sub>O) by Hundon *et al* [33]. Carbonyl compounds (C=O) were found on the surface of the cavity in both PE and epoxy material, which can be considered as a clear sign of oxidative degradation caused by the PD activity.

Although the degradation of polymer materials due to discharges has received much attention in the past, the influence of the degradation and the byproducts on the nature of the discharge itself has not been fully recognized and understood. Some researchers worked on this subject and obtained some preliminary results. For example, Hudon *et al* [34] found that the byproducts deposited on the surface may change the discharge mechanism. Sekii *et al* [35] reported that the chemically active species produced by the PD in oxygen containing gas atmosphere can lead to the decrease of discharge magnitude.

According to the discussion in section 2.1 and section 2.3, the variation in the physical-chemical and electrical properties of the gas in the cavity and the cavity surface has significant influence on the PD activity in the cavity. In particular, the variation of the gas quality (e.g. density and composition) can affect the 1<sup>st</sup> Townsend coefficient and, thus, affects the electron avalanche in the cavity. The changes in the cavity surface roughness and conductivity can lead to the variation of the charge injection rate and space charge generated electric field, through affecting the work function,  $U_0$ , and space charge relaxation time constant,  $\tau$ .

Therefore, in order to develop the PD induced ageing model under AC field, the time behavior of the PD activity in the cavity and the physical-chemical and electrical properties of the surrounding dielectrics at different ageing periods must be investigated, outlining common features of PD degradation processes.

## CHAPTER 3

### TIME BEHAVIOR OF THE PD ACTIVITY

The considered system, sketched in Figure 2.1, was realized with specimens made of three layers of PE sheets having a cylindrical artificial cavity in the center of the middle layer. Life tests and PD measurements were performed on the specimens under AC voltage. The PD activity taking place in the artificial cavities was monitored continuously by the PD detector in the entire ageing process. Typical characteristics of the PD parameters, i.e. discharge repetition rate and discharge magnitude, are extracted from the behavior curves of these parameters and reported in this chapter.

#### 3.1 Specimens and Experimental Setup

The test object simulating a dielectric embedded cavity (Figure 2.1) was made of two layers of cross-linked polyethylene XLPE and one layer of low-density polyethylene (LDPE) with a micro-cavity punched in the center, as illustrated in Figure 3.1. The thickness of the top and bottom XLPE layers is 0.15mm and the thickness of the middle LDPE layer is 0.1mm. The PE sheets were cut to square pieces having area  $80 \times 80 \text{ mm}^2$ . The diameter of the cavity circular basis is 0.4 mm. In order to obtain repeatable results, the specimens were manufactured carefully following a strict procedure. In particular, the PE layers were cured at  $80 \text{ }^\circ\text{C}$  for 72 h to expel cross-linking byproducts and humidity. The layers were soldered together at  $100 \text{ }^\circ\text{C}$  under vacuum condition.

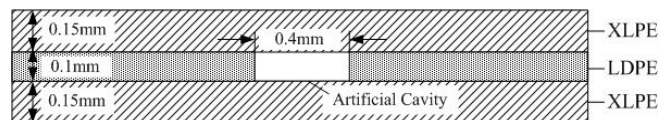


**Figure 3.1** Structure and dimension of the PE layered specimen

Top and bottom XLPE layer thickness = 0.15mm, Middle LDPE layer thickness = 0.1mm,  
Cavity basis diameter = 0.4mm, Cavity height = 0.1mm

Figure 3.2 sketches the measurement system for studying the time behavior of PD in the three-layer specimens. The high voltage electrode was a stainless steel one, with Rogowsky profile. The ground electrode was a stainless steel plane. The electrodes and the specimen were all immersed in insulating oil to avoid surface discharges and flashover. The PD current taking place in the cavity was coupled by a high frequency current transformer (HFCT) connected to the ground lead. The coupled signal was then processed and recorded using a commercial PD detector, PDCheck (bandwidth 40 MHz, sampling rate 100 MS/s).

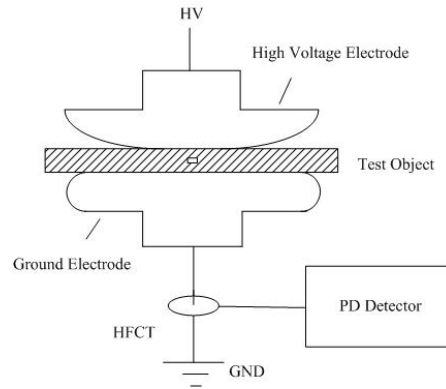


**Figure 3.2** A sketch of the experimental system

### 3.2 Time Behavior of PD in the Cavity under AC Field

#### 3.2.1 Time evolution of PD at 10 kV

Life tests and PD measurements were performed at room temperature on fifteen specimens at 10 kV, corresponding to an average background electric field ( $E_0$ ) in the cavity 43.5 kV/mm. The average PD inception voltage of the unaged specimens is 2.1 kV ( $E_0 = 9.1$  kV/mm). All the voltage and electric field values reported in this thesis are RMS values. Among the fifteen specimens, eleven broke down within less than 200 h. The other four specimens did not reach breakdown after a relatively long time, because the PD activity in the cavities stopped at certain times (recorded as ageing times). They were removed from life testing after PD extinction. Their ageing times were considered as censored data in the statistical processing of the results. The PD inception voltage (PDIV), average PD inception field in the cavity and failure times or ageing times of the fifteen specimens are reported in Table A1.1 in Appendix 1. The Weibull plot of the whole set of data (censored testing) is shown in Figure 3.3, with confidence intervals at probability 95%. The Weibull scale ( $\alpha$ ) and shape ( $\beta$ ) parameters are 178 h and 0.8, respectively.

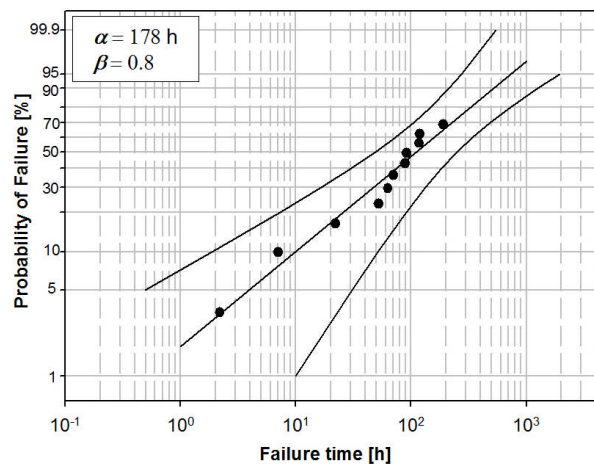


**Figure 3.3** Weibull plot of failure times of PD tests at 10 kV (11 failed, 4 censored). Confidence intervals at probability 95%.

Among the fifteen specimens tested at 10 kV, ten were continuously monitored by the PD detector during the entire ageing process. The phase resolved PD (PRPD) patterns, repetition rates,  $N_w$  (i.e. the number of PD pulses per voltage period) and the scale parameters of the Weibull distribution fitting the discharge amplitude values,  $Q_{alfa}$ , were recorded for both positive and negative discharges every 30 minutes. The time behavior curves of  $N_w$  and  $Q_{alfa}$  are reported in Table A1.2 in Appendix 1. As can be seen, most of the specimens show similar characteristics in the  $N_w$  and  $Q_{alfa}$  curves. The mean values of  $N_w$  and  $Q_{alfa}$  at different ageing period were extracted and shown as a function of normalized time (100% corresponds to failure time) in Figure 3.4 and Figure 3.5. According to the trend of  $N_w$  and  $Q_{alfa}$ , the ageing process can be divided into four stages. The boundaries between them are marked by the dashed lines in the figures. 90% probability confidence intervals are reported for the  $N_w$  and  $Q_{alfa}$  values and also for the stage boundaries.

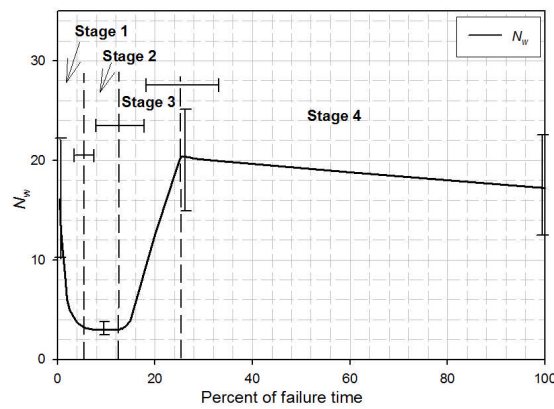


**Figure 3.4** Typical behavior curve of  $N_w$ . Confidence intervals at probability 90%.

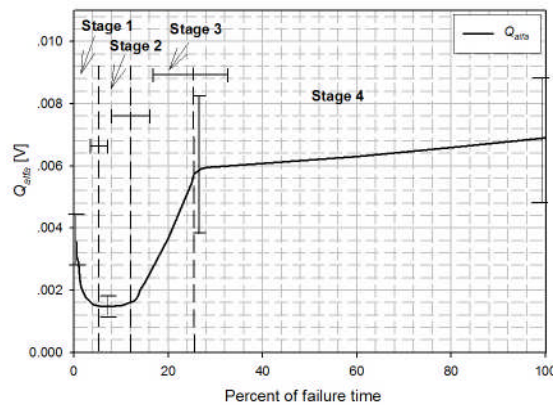


**Figure 3.5** Typical time behavior curve  $Q_{alfa}$ . Confidence interval at probability 90%.

The changing characteristics of  $N_w$  and  $Q_{alfa}$  at each ageing stage are:

**Stage 1** (from voltage application to 6% of failure time): both  $N_w$  and  $Q_{alfa}$  decrease steeply with ageing time. At the beginning of voltage application,  $N_w$  and  $Q_{alfa}$  values are 16.1 and 3.5 mV, respectively. At the end of stage 1, they decrease to 3.0 and 1.5mV.

**Stage 2** (from 6% to 13% of failure time):  $N_w$  and  $Q_{alfa}$  keep almost constant values ( $N_w = 3.0$ ,  $Q_{alfa} = 1.5$  mV).

**Stage 3** (from 13% to 25 % of failure time):  $N_w$  and  $Q_{alfa}$  increase rapidly and linearly.

At the end of Stage 3,  $N_w$  and  $Q_{alfa}$  reach relatively large values, 20.4 and 5.8 mV, respectively.

**Stage 4** (from 25% to breakdown):  $N_w$  decreases linearly and  $Q_{alfa}$  increases linearly in this stage. At 100% of failure time,  $N_w$  and  $Q_{alfa}$  values are 17.4 and 8.1mV, respectively.

Examples of the recorded PRPD patterns are presented in Figure 3.6 and Figure 3.7. In the first three ageing stages, all the specimens show the typical “rabbit-like” shape patterns, as shown in Figure 3.6. However, two different types of pattern shape can be observed in stage 4. Hence, the ten specimens under monitoring can be divided into two groups based on the pattern shape in stage 4. The first group consists of specimens having failure times less than 150 h. Their patterns exhibit the typical “rabbit-like” shape in the entire stage, as shown in Figure 3.7a and 3.7b. The second group consists of specimens G1-NO.3, G3-NO.1 and G4-NO.4 (see Table A1.2), having ageing times 235 h, 190 h and 276 h, respectively. Their patterns change into the “turtle-like” shape, as highlighted in Figure 3.7c and 3.7d. The pattern transformation times distribute randomly between 26 h and 200 h, as marked by the red lines of the  $N_w$  and  $Q_{alfa}$  curves in Table A1.2. Among the second group of specimens, G3-NO.1 reached breakdown at 190h. Specimens G1-NO.3 and G4-NO.4 did not reach breakdown and PD stopped at 235 h and 276 h, respectively. As a reference, the PD patterns and parameters (i.e.  $N_w$  and  $Q_{alfa}$ ) at various ageing times are reported in Tables A1.3 and A1.4 in Appendix 1 for specimens G4-NO.3 (from the first group, failure time = 119.5 h) and G4-NO.4 (from the second group, ageing time = 276 h), respectively.

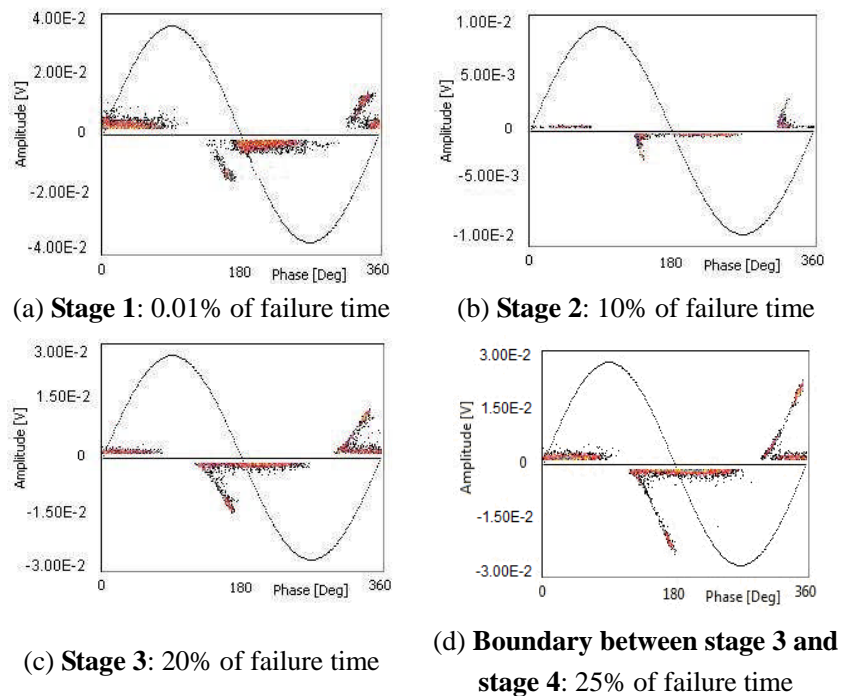


**Figure 3.6** Example of PD patterns in the first three aging stages (see Figure 3.4 and Figure 3.5).

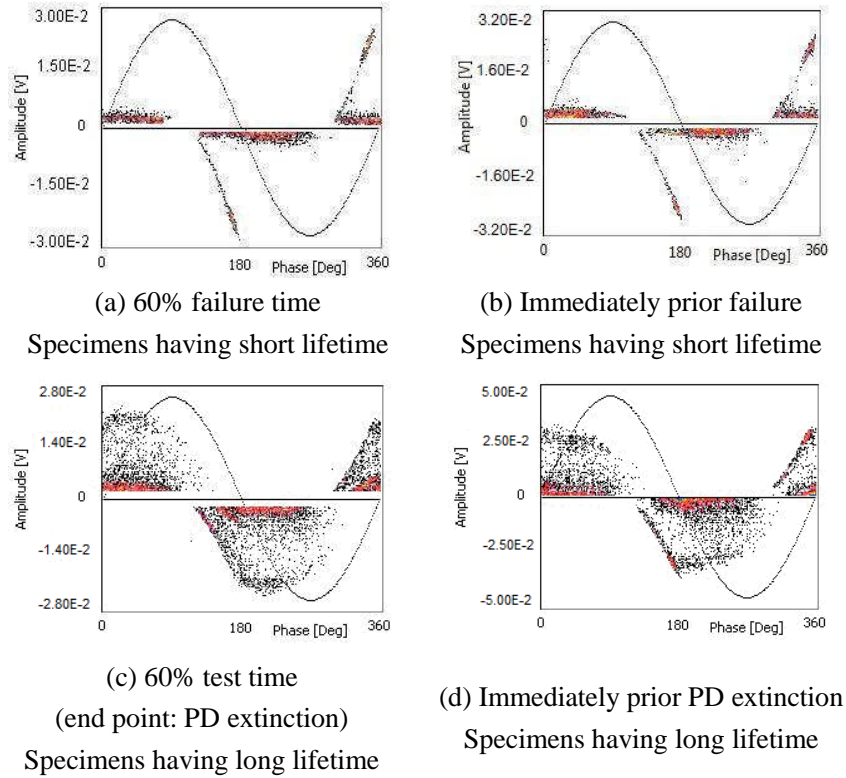


**Figure 3.7** Example of PD patterns in stage 4 (see Figure 3.4 and Figure 3.5).

### 3.2.2 Time evolution of the PD activity at 12.5 kV

Life tests and PD measurements were performed on fourteen specimens at 12.5 kV at room temperature. All the specimens broke down within 50 h. The PDIV, average PD inception field and failure times of these specimens are reported in Table A1.5 in Appendix 1. Weibull distribution plots of lifetime are shown in Figure 3.8 with confidence interval of probability 95%. The Weibull scale ( $\alpha$ ) and shape ( $\beta$ ) parameters are 15.7 h and 1.1 respectively, as reported in the figure.

PD were monitored continuously for six specimens during the ageing at 12.5 kV. Time behavior curves of  $N_w$  and  $Q_{alfa}$  of these specimens are shown in Table A1.6 in Appendix 1. The mean of  $N_w$  and  $Q_{alfa}$  at 12.5 kV were extracted and shown as a function of normalized time (100% corresponds to failure time) in Figure 3.9 and Figure 3.10, respectively. As can be seen, the ageing process at 12.5 kV can also be divided into four ageing stages. The stage boundaries, as well as 90% probability confidence intervals for the  $N_w$  and  $Q_{alfa}$  values and for the boundaries, are reported in Figure 3.9 and Figure 3.10.  $N_w$  and  $Q_{alfa}$  curves at 12.5 kV show similar characteristics to the curves at 10 kV, which suggests that the time behavior of  $N_w$  and  $Q_{alfa}$  are independent of the ageing voltage.

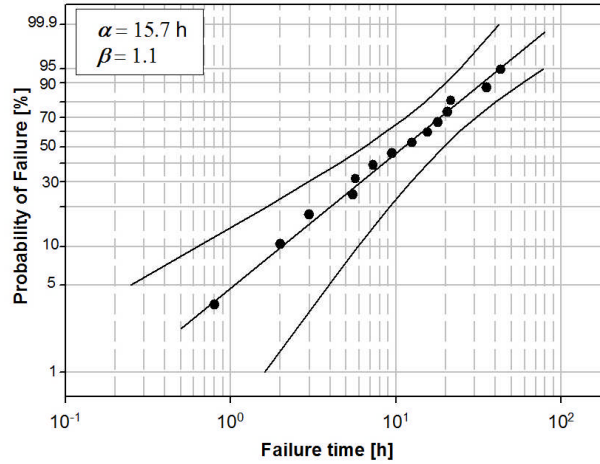


**Figure 3.8** Weibull plot of failure times of PD tests at 12.5 kV. Confidence intervals at probability 95%.

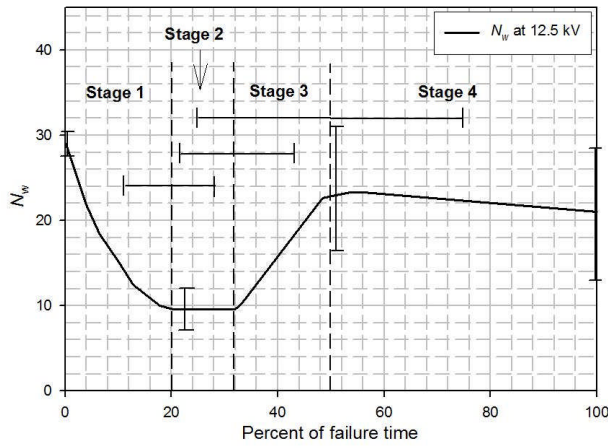


**Figure 3.9** Typical time behavior curve of  $N_w$  at 12.5 kV. Confidence interval at probability 90%.

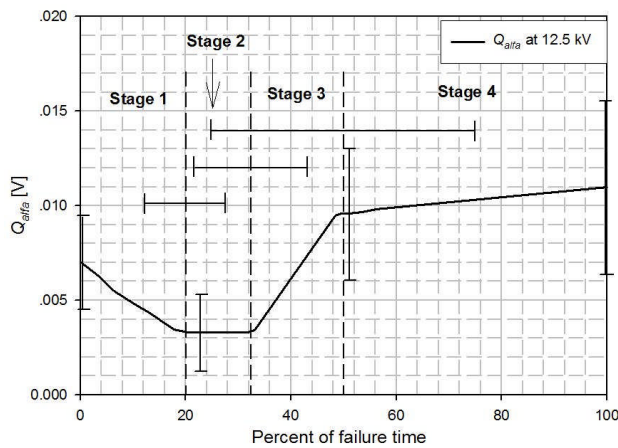


**Figure 3.10** Typical time behavior curve of  $Q_{alfa}$  at 12.5 kV. Confidence interval at probability 90%.

The PRPD patterns at 12.5 kV show the typical “rabbit-like” shape characteristic at each ageing stage. Examples of the patterns are displayed in Figure 3.11.

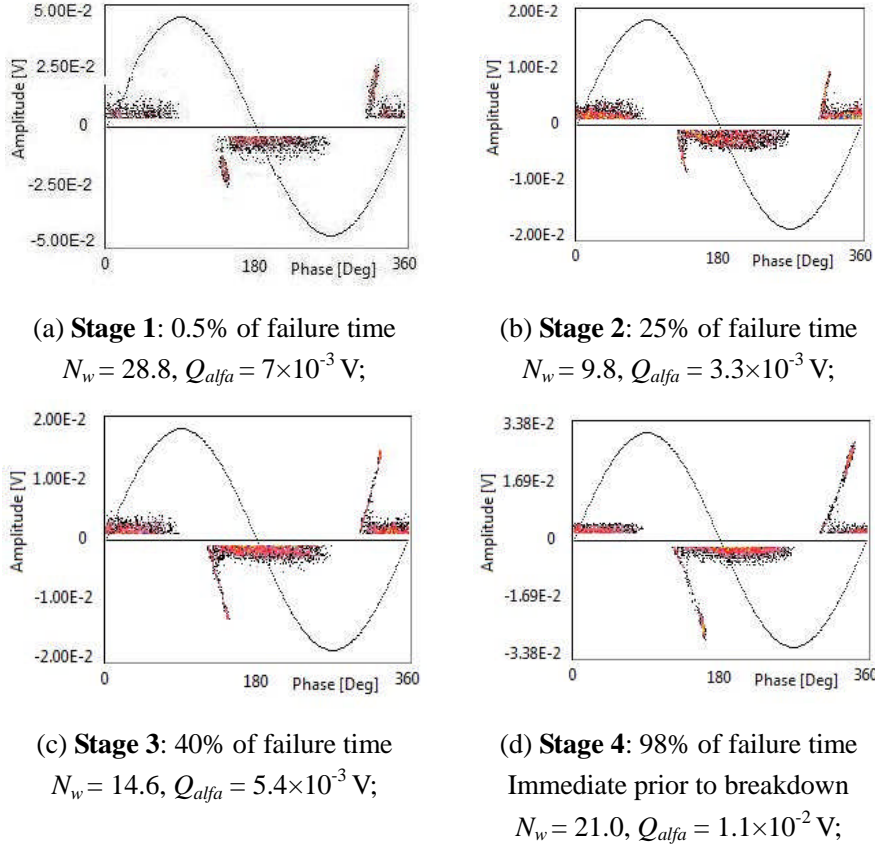


**Figure 3.11** Examples of PD patterns at every ageing stage at 12.5 kV

### 3.3 Evaluation of PD-induced Damage Growth Rate

PD activity generally undergoes fluctuation, as reported in subsections 3.2.1 and 3.2.2. The fluctuation of PD repetition rate and magnitude affect damage growth rate on the dielectric/cavity interface. In Chapter 2, an expression for the life,  $L$ , of the insulation system is obtained by assuming that time-to-failure is the time to the formation of a damaged zone of critical size  $d_c$ , with a damage growth rate,  $R_{dis}$  (see equation (2-18)). In the attempt of evaluating the damage growth rate,  $R_{dis}$ , an approach based on simple statistics was followed, as discussed in the following.

$N_w$  is the number of discharges taking place in a voltage cycle and  $Q_{alfa}$  is the 63.2% percentile of the discharge amplitude distribution of one acquisition. The product  $N_w \cdot Q_{alfa}$  can provide an indication of the average number of electrons impacting on the polymer surface during each voltage cycle and, thus reflects the amount of energy released by the discharges during each voltage cycle (indeed, a correct estimate would require the knowledge of energy distribution of the electrons in each avalanche as a function of the overvoltage at which the PD occurs, which can be done through the model described in [1]). More C-H bonds could be broken rising the discharge energy, which will cause more damage to the polymer. Therefore, larger  $N_w \cdot Q_{alfa}$  value corresponds to higher damage growth rate and, consequently, to shorter failure time. Hence,  $N_w \cdot Q_{alfa}$  can be used as a parameter that evaluates  $R_{dis}$ . The average values of  $N_w \cdot Q_{alfa}$  over the entire lifetime of one specimen,  $\overline{N_w \cdot Q_{alfa}}$ , could be used to indicate the average damage growth rate in the entire ageing process. The

calculation of  $\overline{N_w \cdot Q_{alfa}}$  is briefly introduced below.

During the ageing process, the PD detector acquires  $N_w$  and  $Q_{alfa}$  values every 30 minutes and records them as the elements of two vectors,  $[N_{w0}, N_{w1}, N_{w2} \dots N_{wn}]$  and  $[Q_{alfa0}, Q_{alfa1}, Q_{alfa2} \dots Q_{alfan}]$ .  $N_{wi}$  and  $Q_{alfai}$  ( $i = 0, 1, 2 \dots n$ ) correspond to  $N_w$  and  $Q_{alfa}$  values after  $i/2$  hours of the voltage application.  $\overline{N_w \cdot Q_{alfa}}$  is calculated by the following equation:

$$\overline{N_w \cdot Q_{alfa}} = \frac{1}{n+1} \sum_{i=0}^n (N_{wi} \cdot Q_{alfai}) \quad (3-1)$$

The  $\overline{N_w \cdot Q_{alfa}}$  values are reported in Figure 3.12 as a function of failure times of specimens tested at 10 kV and 12.5 kV. As can be seen, in general,  $\overline{N_w \cdot Q_{alfa}}$  decreases as the failure time increases. Some deviations can be found (see the plots marked by the rectangle in Figure 3.12), most likely due to the randomness of cavity surface morphology and specimen manufacturing. Specimens may attain longer failure times even if the discharge energy released in a voltage cycle (i.e. the value of  $N_w \cdot Q_{alfa}$ ) is comparable or larger than that of the other specimens. The general time behavior of  $\overline{N_w \cdot Q_{alfa}}$  supports the hypothesis that  $\overline{N_w \cdot Q_{alfa}}$  can evaluate the damage growth rate as a function of ageing time.

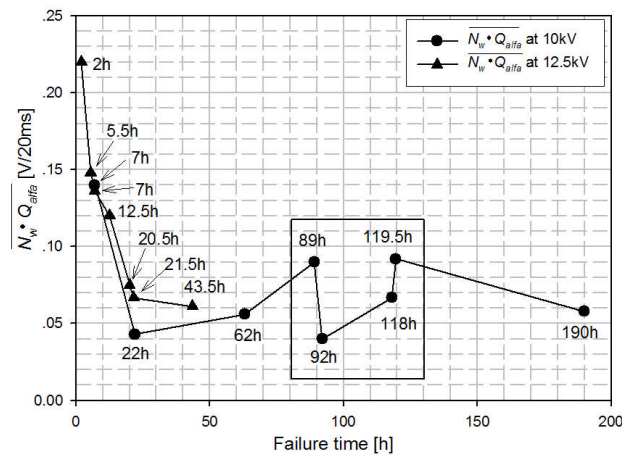


**Figure 3.12**  $\overline{N_w \cdot Q_{alfa}}$  values as a function of failure time of the specimens tested at 10 kV and 12.5 kV

The time behavior curves of  $N_w \cdot Q_{alfa}$  at 10 kV and 12.5 kV are reported in Figure 3.13 and Figure 3.14, respectively. 90% of confidence intervals for the  $N_w \cdot Q_{alfa}$  values and the stage boundaries are reported in the figures.

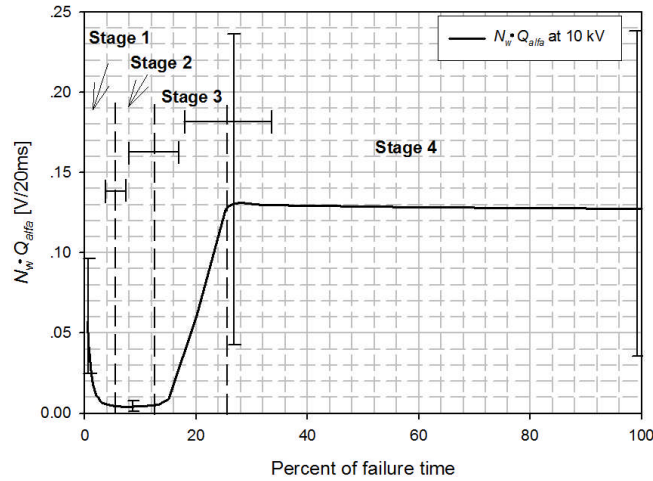


**Figure 3.13** Typical time behavior of  $N_w \cdot Q_{alfa}$  at 10 kV. Confidence interval of probability 90%.

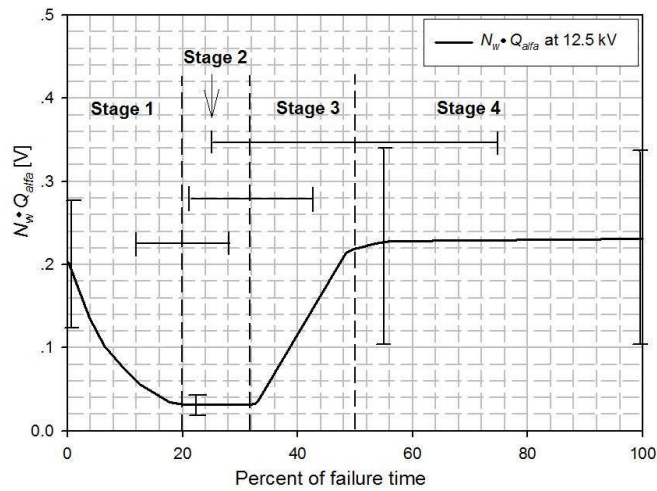


**Figure 3.14** Typical time behavior of  $N_w \cdot Q_{alfa}$  at 12.5 kV. Confidence interval of probability 90%.

The time behavior curve of  $N_w \cdot Q_{alfa}$  is similar to the curves of  $N_w$  and  $Q_{alfa}$  in the first three ageing stages, whereas it keeps almost constant value in stage 4, with larger values than in the other stages. Stage 4 takes about 75% of the entire ageing process at 10 kV and about 50% at 12.5 kV. Larger  $N_w \cdot Q_{alfa}$  values and longer time suggest that most damage on the cavity surface is caused in the fourth ageing stage and, therefore, stage 4 accounts for the main contribution to lifetime.

### 3.4 Time Evolution of the PD Inception Voltage

The evolution of the PD inception voltage (PDIV) was observed on five specimens (#1 - #5) having the same geometry as that shown in Figure 3.1. These specimens were aged at 10 kV. During the ageing process, the ageing voltage was shortly removed and the PDIV was measured at various times. Figure 3.15 shows the measurement results for each specimen. Figure 3.16 shows the average PDIV values of the five specimens as a function of ageing times in log-log coordinates. Confidence intervals at probability 90% of the PDIV values are reported. It is interesting to observe that the average PDIV

values increases steadily with ageing time following the power law. The slope rate of the fitting line in Figure 3.16 is 0.2, as reported in the figure.

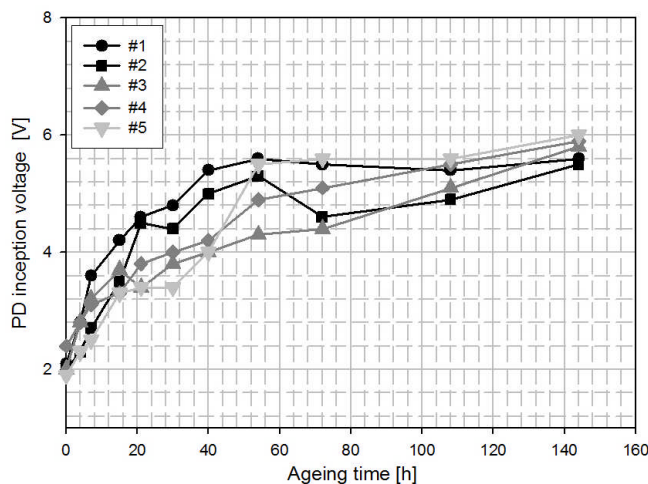


**Figure 3.15** PDIV values of specimens #1 to #5

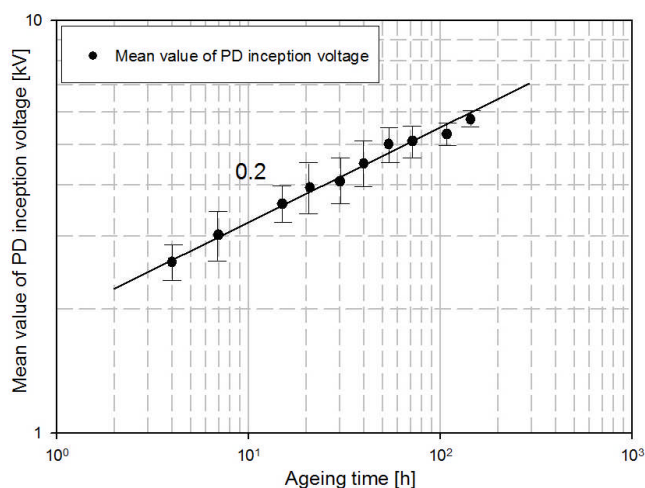


**Figure 3.16** Average PDIV values at different ageing times. Confidence intervals at probability 90%.

As can be seen in Figure 3.15 and Figure 3.16, the average PDIV value for the unaged specimens is 2.1 kV, corresponding to the background electric field in the cavity ( $E_0$ ) 9.1 kV/mm. After ageing 140 h at 10 kV, it increases to 5.8 kV, corresponding to  $E_0 = 25.2$  kV/mm.

### 3.5 Summary

In this chapter, we studied the behavior of the PD activity in artificial cylindrical cavities embedded in three-layer PE-based specimens under AC field. Four ageing stages could be singled out according to the characteristics of PD statistical parameters, i.e. discharge repetition rate,  $N_w$ , and amplitude,  $Q_{alfa}$ . Two different types of pattern shape (i.e. “rabbit-like” and “turtle-like”) could be observed in the last ageing stage for specimens having long and short failure times, respectively. The product  $N_w \cdot Q_{alfa}$  can be used to evaluate the PD-induced damage growth rate at the dielectric/cavity interface in each ageing stage. The time behavior of  $N_w \cdot Q_{alfa}$  suggests that the last

ageing stage contributes mostly to the failure of the specimen. The evolution of PD inception voltage at different ageing times was studied. Results show that the PDIV increases with the ageing time following the power law.

## Appendix 1

Ageing tests and PD measurements were performed on fifteen specimens with artificial cavities at 10kV (background electric field in the cavity 43.5kV/mm). Their PDIV, average PD inception field in the cavity and failure times (or ageing times) are reported in Table A1.1.

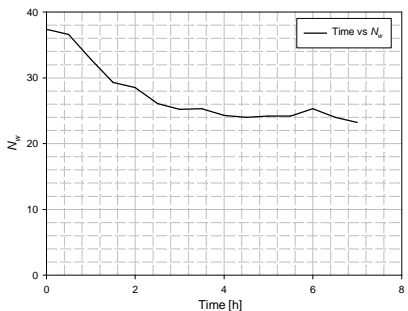
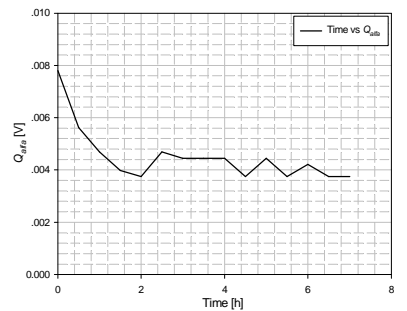
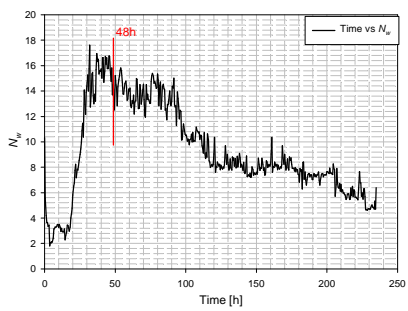
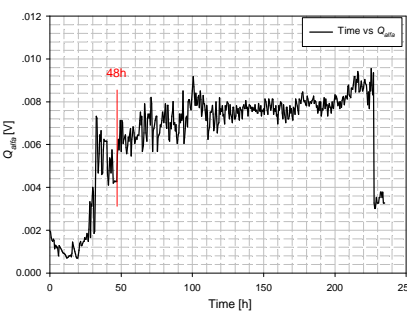
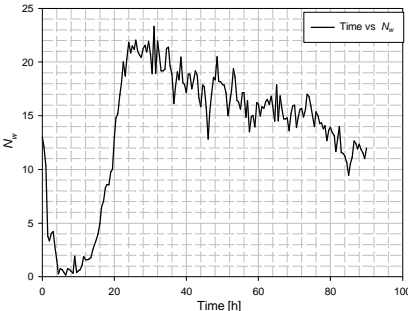
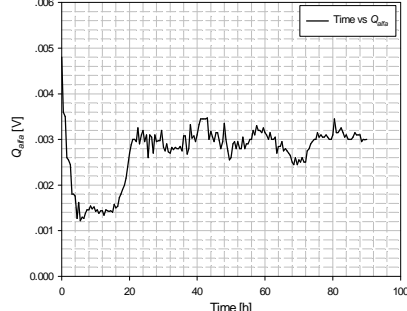
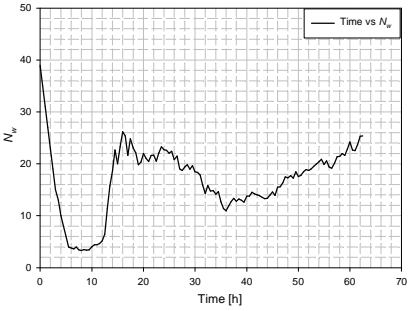
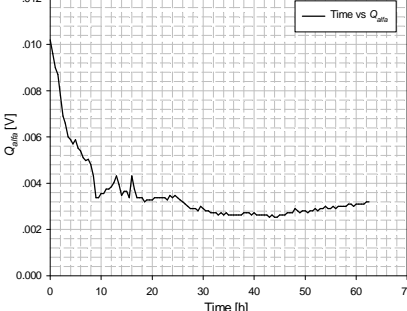
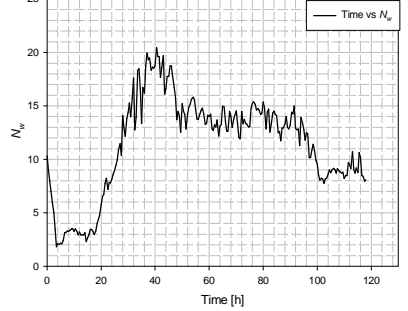
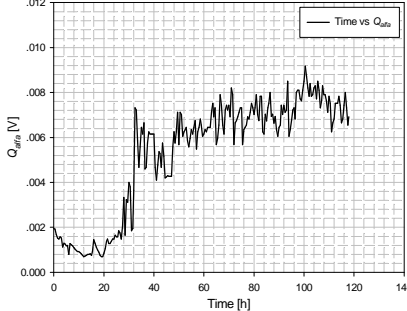
Among the fifteen specimens, ten of them were monitored by the PD detector during the entire ageing process. The time behavior curves of  $N_w$  and  $Q_{alfa}$  of the ten specimens are reported in Table A1.2 as a function of the ageing time.

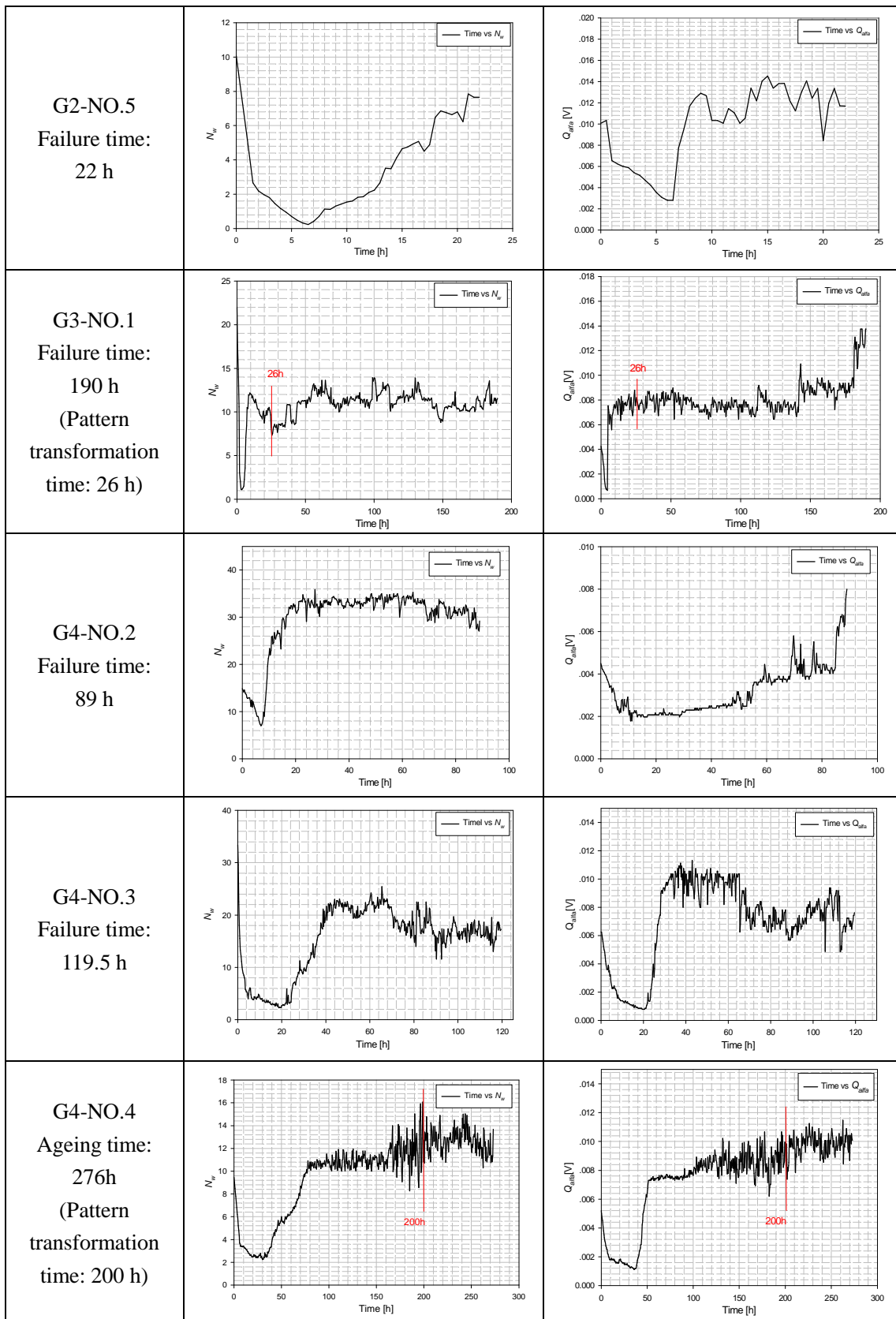
PRPD patterns of specimens G4-NO.3 (from the first group) and G4-NO.4 (from the second group) are reported in Tables A1.3 and A1.4, respectively.

**Table A1.1** Failure times or ageing times of the specimens tested at 10kV

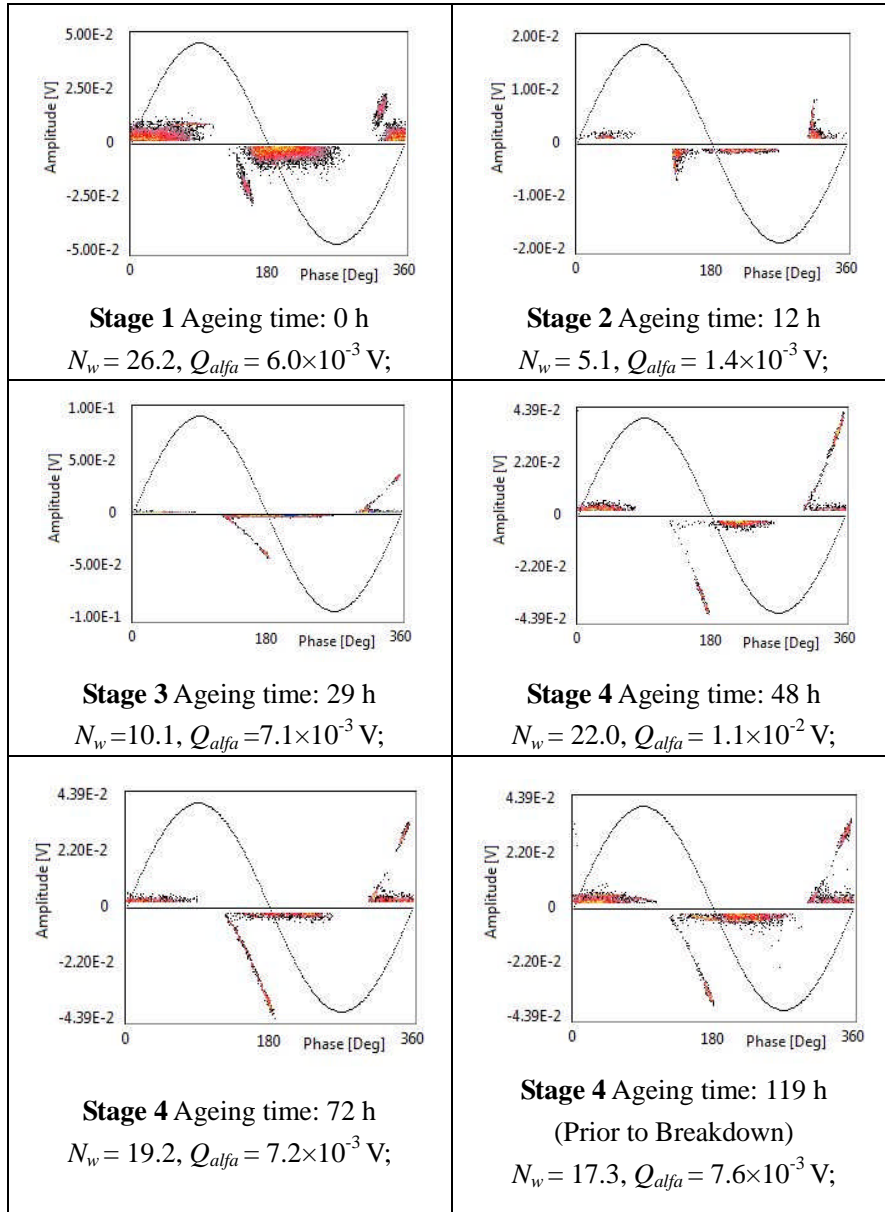
Specimen	PD inception voltage (kV)	Average PD inception Field in the cavity (kV/mm)	Failure time or Ageing time (h)
G1-NO.1	2.5	10.9	Failure time 7 h
G1-NO.2	2.0	8.7	Ageing time 490 h
G1-NO.3	2.0	8.7	Ageing time 235 h
G1-NO.4	2.0	8.7	Failure time 92 h
G1-NO.5	2.5	10.9	Ageing time 440 h
G1-NO.6	2.0	8.7	Failure time 63 h
G2-NO.2	2.3	10.0	Failure time 118 h
G2-NO.5	2.0	8.7	Failure time 22 h
G2-NO.6	2.0	8.7	Failure time 70 h
G2-NO.7	2.3	10.0	Failure time 52.2 h
G2-NO.8	2.0	8.7	Failure time 2.2 h
G3-NO.1	2.1	9.2	Failure time 190 h
G4-NO.2	2.0	8.7	Failure time 89 h
G4-NO.3	2.2	9.6	Failure time 119.5 h
G4-NO.4	2.0	8.7	Ageing time 276 h
Average Value	2.1	9.2	Weibull scale parameter $\alpha = 178$ h

**Table A1.2** Time behavior curves of  $N_w$  and  $Q_{alfa}$

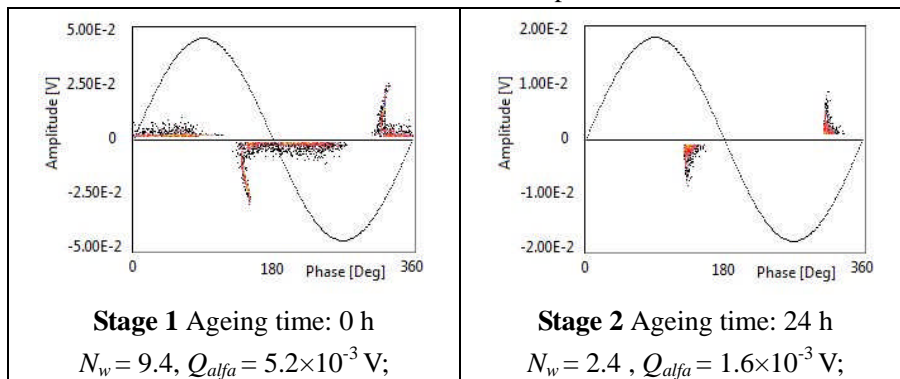
Specimen	Time behavior curve of $N_w$	Time behavior curve of $Q_{alfa}$
<p>G1-NO.1 Failure time: 7 h</p>		
<p>G1-NO.3 Ageing time: 235 h (Pattern transformation time: 48 h)</p>		
<p>G1-NO.4 Failure time: 92 h</p>		
<p>G1-NO.6 Failure time: 63 h</p>		
<p>G2-NO.2 Failure time: 118 h</p>		

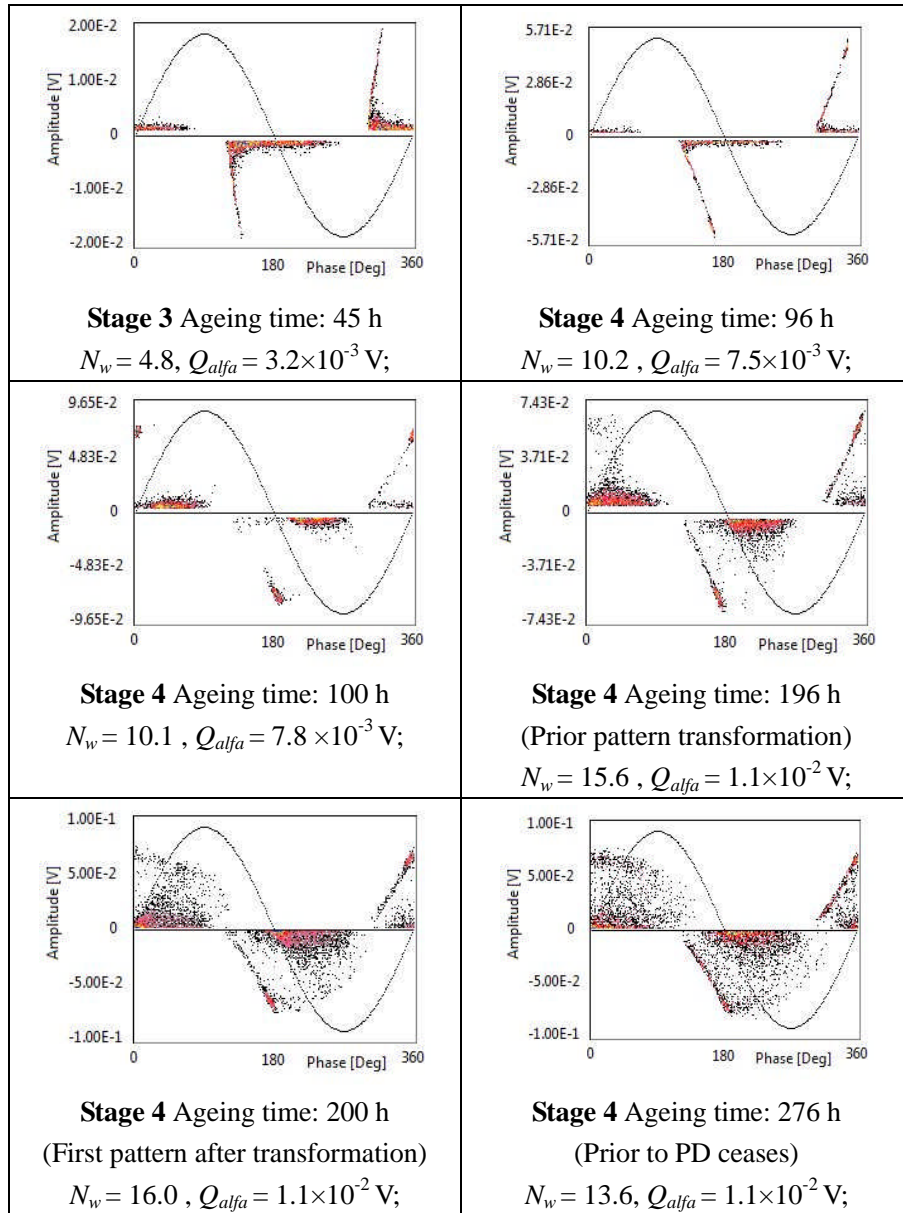


**Table A1.3** Evolution of the PD patterns of G4-NO.3



**Table A1.4** Evolution of the PD patterns of G4-NO.4





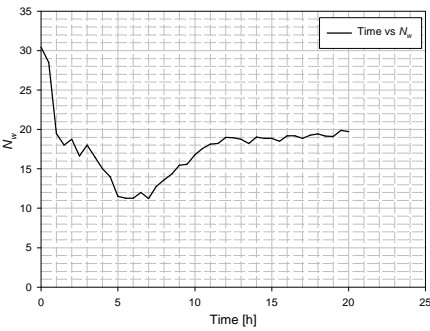
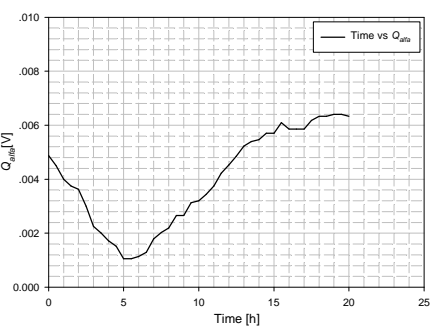
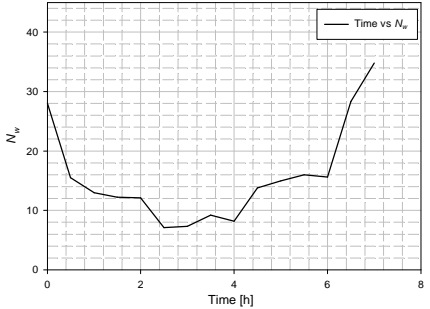
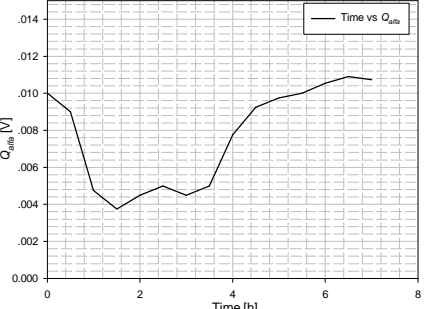
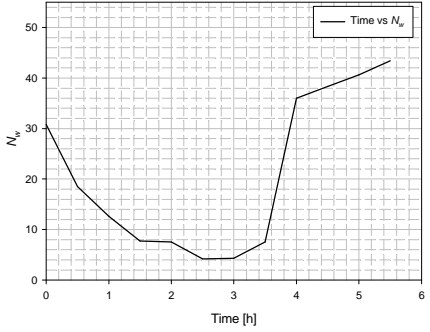
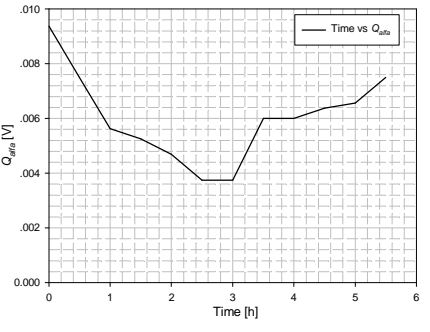
Ageing tests and PD measurements were performed on fourteen specimens at 12.5kV. Table A1.5 shows the PDIV, average PD inception field in the cavity and failure times of these specimens. Six of them were monitored by the PD detector. The time behavior curves of  $N_w$  and  $Q_{alfa}$  at 12.5 kV are reported in Table A1.6.

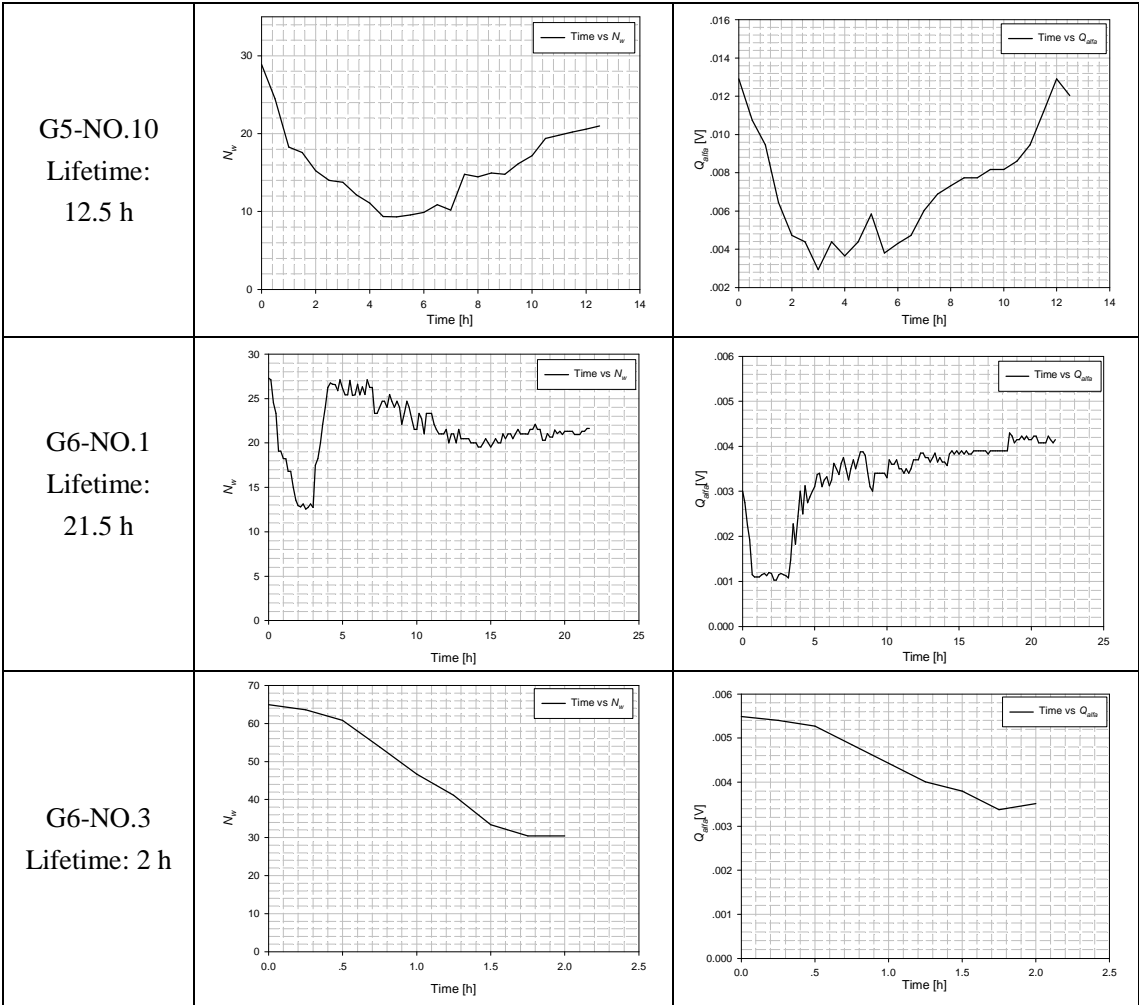
**Table A1.5** Life test results at 12.5 kV

Specimen	PD inception voltage (PDIV) (kV)	Average PD inception Field in the cavity (kV/mm)	Failure time (h)
G1-NO.1	2.5	10.9	35.5
G1-NO.3	2.0	8.7	9.5
G1-NO.6	2.0	8.7	15.5
G2-NO.3	2.0	8.7	0.8
G2-NO.4	2.5	10.9	20.5

G2-NO.6	2.0	8.7	7.3
G2-NO.8	2.3	10.0	5.5
G2-NO.10	2.2	8.7	12.5
G3-NO.1	2.0	8.7	43.0
G3-NO.2	2.6	10.0	18.0
G3-NO.3	2.0	8.7	3.0
G4-NO.1	2.1	9.2	21.5
G4-NO.3	1.8	8.7	2.0
G4-NO.5	2.0	9.6	5.7
Average Value	2.1	9.2	Mean value of lifetime=14.3h; Weibull scale parameter $\alpha=15.7h$

**Table A1.6.** Time behavior of  $N_w$  and  $Q_{alfa}$  at 12.5kV

Specimen	Time behavior of $N_w$	Time behavior of $Q_{alfa}$
G5-NO.4 Lifetime: 20 h		
G5-NO.6 Lifetime: 7 h		
G5-NO.8 Lifetime: 5.5 h		



# CHAPTER 4

## GAS PRESSURE IN THE CAVITY

The variation of the PD patterns and parameters reported in Chapter 3 can be attributed to the changes of the dielectric/cavity interface and of the quality of the gas filling the cavity (i.e. gas pressure and composition). Regarding the gas quality, the interaction between PD and gas pressure was studied extensively [1-5]. In particular, the gas pressure was suggested as a new physical parameter of the ageing process in [1]. In this chapter, the evolution of the gas pressure in PE-embedded cavities was studied and its effect on PD activity was discussed.

### 4.1 Calculation of Gas Pressure Evolution through PDIV

The inception of the self-sustained discharge in the cavity largely depends on the gas pressure. Gutfleish and Niemeyer discussed the relationship between the streamer inception field and the gas pressure in [6]. Considering the streamer discharge in the cavity filled with air, the average PD inception field,  $E_{inc}$ , can be expressed as follows:

$$E_{inc} = \left( \frac{E}{P} \right)_{cr} \cdot P \cdot \left[ 1 + \frac{B}{(P \cdot d)^n} \right] \quad (4-1)$$

where  $P$  is the gas pressure;  $d$  is the cavity height;  $(E/P)_{cr}$ ,  $B$  and  $n$  characterize the ionization processes in the gas inside the cavity. In the case that the gas is air,  $(E/P)_{cr} = 24.2 \text{ V} \cdot \text{Pa}^{-1} \cdot \text{m}^{-1}$ ,  $B = 8.6 \text{ Pa}^{0.5} \cdot \text{m}^{0.5}$ ,  $n = 0.5$ .

The PD inception field,  $E_{inc}$ , at different ageing times at 10 kV can be obtained from the average PDIV values reported in Figure 3.16. According to equation (4-1), the evolution of the gas pressure can be calculated, as shown in Figure 4.1.

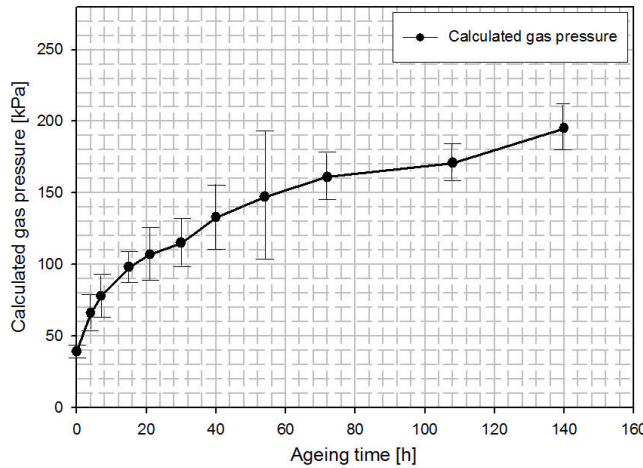


**Figure 4.1** Cavity gas pressure values calculated from the PE inception

According to the calculation results, the gas pressure is 40 kPa an unaged specimens. It increases monotonously during the ageing and reaches almost 200 kPa at 140 h. This behavior suggests that PD in an occluded cavity produce more gaseous molecules than it consumes in the entire ageing process, which seems to be unbelievable. Furthermore, the behavior conflicts with that reported in literature [2-4], i.e. the cavity gas pressure exhibits a short fluctuation in the initial ageing period and then a continuous decrease. The deviation could be explained by the two premises of equation (4-1): 1) the cavity gas should always be air (about 78% nitrogen and 21% oxygen); 2) uniform electric field. In fact, during the ageing process, PD activity can change the gas composition and modify the cavity surface, possibly creating solid pits (e.g. crystals [7]) at which the electric field can be largely enhanced. Since both conditions are likely violated, equation (4-1) can be unable in our case to provide realistic results. Indeed, a pressure of 150 to 200 kPa in the cavity at the end of the ageing does not appear to be plausible.

## 4.2 Measurement of Gas Pressure in the Cavity

In order to infer the evolution of gas pressure and its effect on PD activity, we studied PD behavior under constant gas pressure (CGP) and constant gas volume (CGV) conditions. The test object under CGV was made of three layers of XLPE with an artificial cavity punched in the center of the middle layer, as shown in Figure 4.2. Under CGP, a capillary (external diameter 1.2mm; internal diameter 0.3mm; length 125mm) was inserted into the middle XLPE layer and connected with the cavity, as shown in Figure 4.3. A silicon oil plug was introduced in the capillary as a marker. The gap between the capillary and the XLPE was sealed by silicone grease to prevent air from flowing in (or out) of the cavity. The electrodes and the specimen were immersed in insulating oil to avoid surface discharges or flashover.

The aging tests under CGP were stopped for a few seconds at regular times in order to record the position of the silicon oil plug, thus evaluating the evolution of the gas volume in the cavity. Under both CGP and CGV conditions, the PD signal was recorded and processed by the PD detector. Experimental results under CGP and CGV are reported in the following two subsections, respectively.

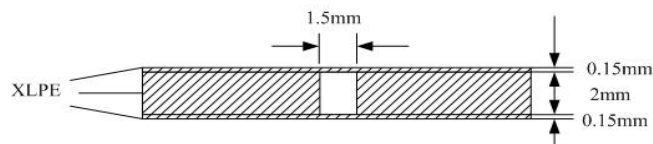


**Figure 4.2** Structure and dimensions of the three-layer XLPE specimen (for ageing tests under CGV). Top and bottom layer thickness = 0.15 mm, middle layer thickness = 2 mm, cavity diameter = 1.5 mm.

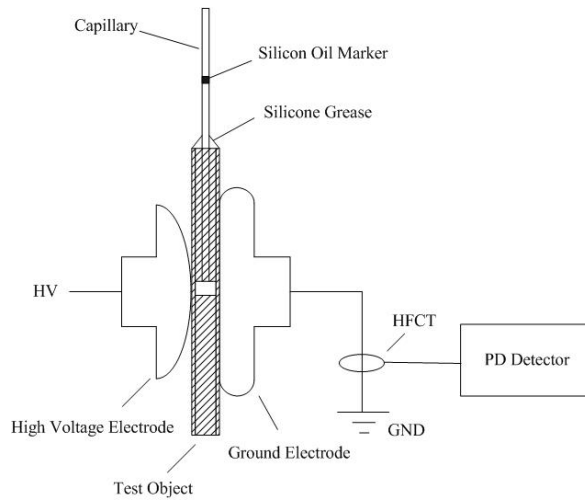


**Figure 4.3** Sketch of the experimental setup for tests under CGP, see also Figure 4.2.

### 4.2.1 PD activity under CGP condition

Under CGP, ageing tests were performed at 8 and 9 kV, corresponding to average background electric field in the cavity ( $E_0$ ) of 3.8 and 3.9 kV/mm, respectively. Three specimens were tested at each voltage level. The time behavior of the gas volume and the ageing time (or failure time) of each specimen are reported in Figure 4.4. The gas volume values are reported in percentage of the value measured before voltage application. As can be seen, the gas volume of the six specimens shows similar behavior: it decreases steeply to about 75% in the first 10 minutes, it increases linearly to about 82% from 10 to 30 minutes and then it decreases again almost linearly.

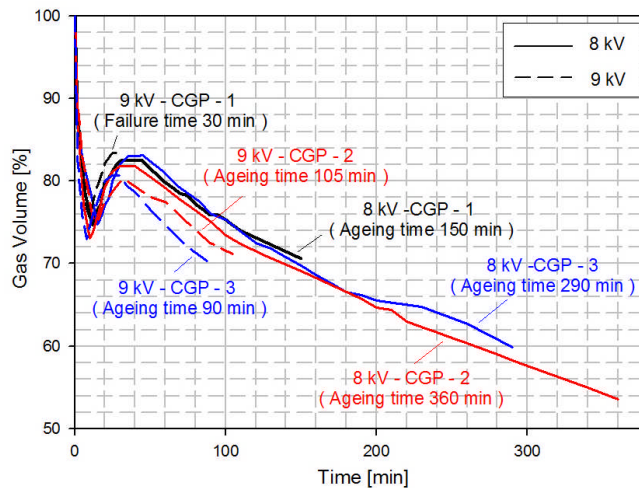


**Figure 4.4** Time behavior curves of the gas volume at 8 kV and 9 kV during ageing tests under CGP for specimens CGP-1, CGP-2 and CGP-3 at each voltage level

Figure 4.5 reports examples of the time behavior of  $N_w \cdot Q_{alfa}$  at 8 and 9 kV, plotted together with the gas volume curves for specimens 8kV-CGP-1 and 9kV-CGP-3. In the first 30 minutes,  $N_w \cdot Q_{alfa}$  and the gas volume have similar trend: they both decrease rapidly in the first 10 minutes and, then, increase steeply in the following 20

minutes. However, after 30 minutes,  $N_w \cdot Q_{alfa}$  fluctuates in a small range, whereas the gas volume shows linear reduction. It is noteworthy that the gas volume and  $N_w \cdot Q_{alfa}$  reach a minimum exactly at the same time (e.g. at 8 min for specimen 9kV-CGP-3 and at 12 min for specimen 8kV-CGP-1, see Figure 4.5). Similar behavior of gas volume and  $N_w \cdot Q_{alfa}$  were observed in other specimens.

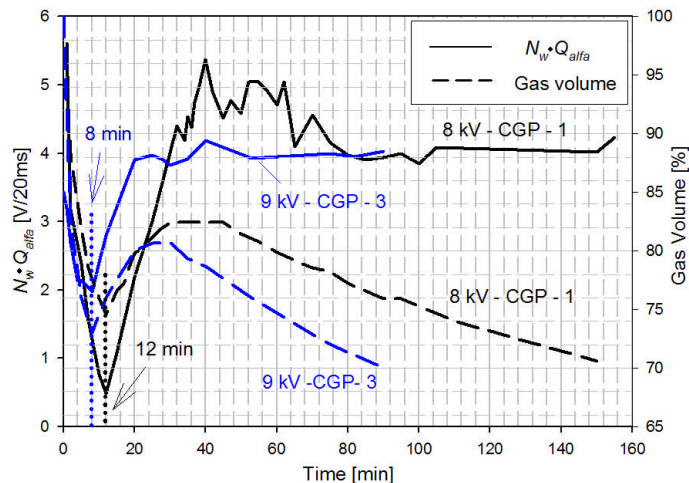
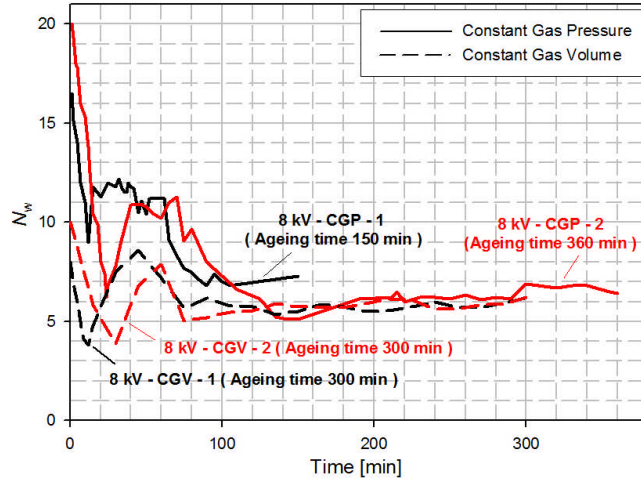


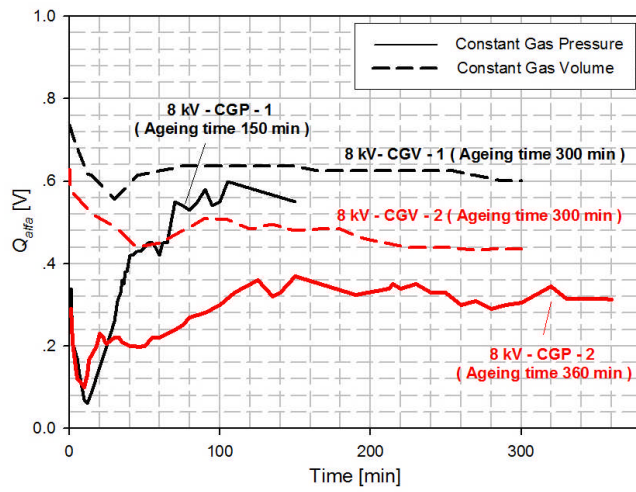
**Figure 4.5** Examples of behavior curves of  $N_w \cdot Q_{alfa}$  and gas volume under CGP during ageing test for specimens 8kV-CGP-1 and 9kV-CGP-3.

#### 4.2.2 PD activity under CGV condition

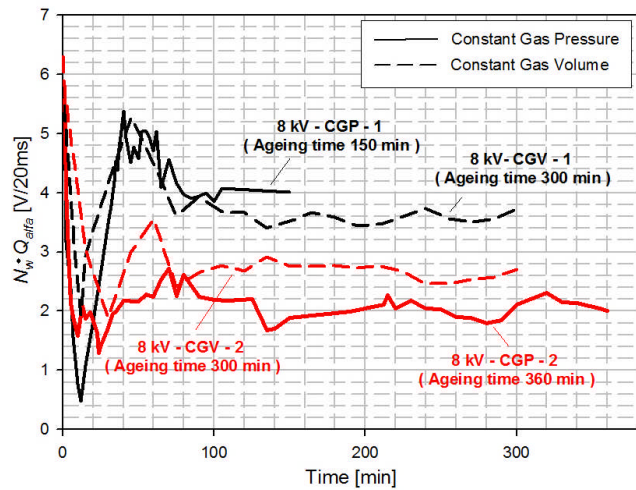
The PD measurements under CGV were performed at 8 kV on two specimens (i.e. 8kV-CGV-1 and 8kV-CGV-2) having the same geometry to that shown in Figure 4.2, without the capillary connected to the cavity. The time behavior curves of  $N_w$ ,  $Q_{alfa}$  and  $N_w \cdot Q_{alfa}$  for specimens tested at 8 kV under CGV (dashed lines) and CGP (solid lines) conditions are displayed in Figure 4.6a, 4.6b and 4.6c. The ageing times of the specimens are reported in the figures. As can be seen,  $N_w$  and  $Q_{alfa}$  curves under CGV show similar changing characteristics to those under CGP. On average,  $N_w$  shows smaller values and  $Q_{alfa}$  shows larger values under CGV in the first 100 minutes (see Figure 4.6a and 4.6b). However,  $N_w \cdot Q_{alfa}$  shows very close values during the entire ageing process under CGP and CGV (see Figure 4.6c). The PRPD patterns at different ageing times for the four specimens are displayed in Appendix 2. The slight difference in  $N_w$  and  $Q_{alfa}$  values can be attributed to the differences in the gas density and composition (e.g. the ratio  $O_2/N_2$  [8]). The similar behavior and close value of the PD parameters ( $N_w$ ,  $Q_{alfa}$  and  $N_w \cdot Q_{alfa}$ ) under CGV and CGP suggest that PD activity in the cavity is not significantly influenced by gas pressure changes.



(a)  $N_w$  curves



(b)  $Q_{alfa}$  curves



(c)  $N_w \cdot Q_{alfa}$  curves

**Figure 4.6** Time behavior curves of  $N_w$  (a),  $Q_{alfa}$  (b) and  $N_w \cdot Q_{alfa}$  (c) as a function of ageing time at 8 kV for specimens CGP-1 and CGP-2 under CGP, and for specimens CGV-1 and CGV-2 under CGV.

If we assume that the ideal gas law is applicable under both CGP and CGV, some

considerations about the state of the gas can be drawn. Under CGP, the gas volume decreases with time. According to the ideal gas law,

$$P \cdot V = n \cdot R \cdot T \quad (4-2)$$

where  $P$  being the gas pressure (Pa),  $V$  the gas volume ( $\text{m}^3$ ),  $n$  the number of gas moles (mol),  $R$  the gas constant ( $8.31 \text{ J} \cdot \text{K}^{-1} \cdot \text{mol}^{-1}$ ) and  $T$  the absolute temperature of the gas (K), the number of gas molecules (i.e.  $n$ ) must decrease in the cavity as well. If the time evolution of  $n$  is the same under CGP and CGV, gas pressure in the occluded cavity under CGV should have similar time behavior with the gas volume under CGP. Therefore, based on Figure 4.4, we can estimate the time evolution of the gas pressure in the cavity under CGV, as reported in Figure 4.7 (where  $t_1$  and  $t_2$  indicate the transition time of the curve).

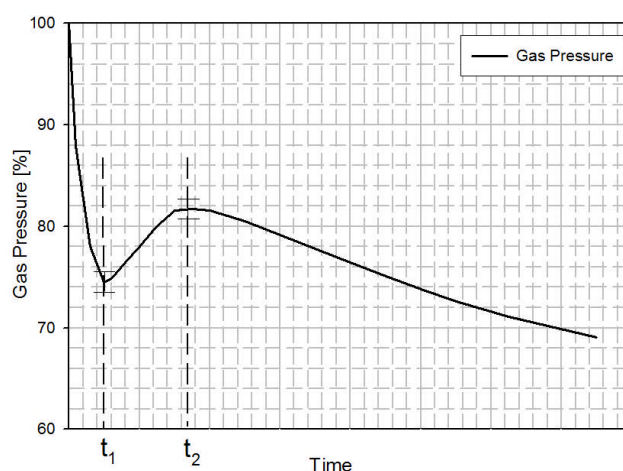


**Figure 4.7** Time behavior curve of cavity gas pressure under CGV, estimated applying equation (4-2) to the data of Figure 4.4.

From the voltage application to  $t_1$ , the gas pressure decreases steeply to about 75% of the original value. From  $t_1$  to  $t_2$ , it experiences an increase and reaches a level of about 82%. After  $t_2$ , it decreases continuously and linearly. The transition times  $t_1$  and  $t_2$  can be obtained from the time behavior of  $N_w \cdot Q_{alfa}$  (see Figure 4.5):  $t_1$  is the time at which  $N_w \cdot Q_{alfa}$  decreases to the minimum value and starts to increase;  $t_2$  is the time when  $N_w \cdot Q_{alfa}$  reaches a relatively stable value.

### 4.2.3 Time evolution of gas pressure in small cavities

It is evident that the test objects used for ageing tests (see Figure 3.1) have different cavity sizes with respect to those used to infer gas pressure trends (see Figure 4.2). It could be speculated, therefore, that the latter could be not representative of what happens in the former. Indeed, a careful comparison of Figures 3.4, 3.5, and 4.6 shows that the trends of  $N_w$  and  $Q_{alfa}$  in small and large cavities are similar, thus suggesting that the trend curve reported in Figure 4.7 can be generalized for cavities embedded in dielectric materials. Furthermore, similar gas pressure behavior was obtained by Gjaerde [2, 3] in flat cylindrical cavities (basis diameter 40 mm; height 0.125 mm)

using the CIGRE method II system, also implying that the pressure evolution could be similar for various cavity shapes and sizes. Mizutani et al [4] reported analogous gas volume behavior curve under CGP to those shown in Figure 4.4. They attributed the decrease of gas volume at the beginning to the consumption of oxygen molecules by the oxidation reaction at the dielectric/cavity interface and production of byproducts such as CO<sub>2</sub> and H<sub>2</sub>O. This deduction was verified by Sekii by analyzing the gas composition and cavity surface of the aged specimens using Gas Chromatography-Mass Spectroscopy (GC-MS) and Fourier Transform Infrared Spectroscopy (FTIR) [9-11].

On the basis of Figure 4.7, it is possible to infer the gas pressure evolution in small cylindrical cavities in each ageing stage (see Figures 3.4 and 3.5), as reported in Figure 4.8. In stage 1, the gas pressure decrease rapidly and reaches the minimum (about 75% of the original value) in stage 2. Subsequently, in stage 3, it experiences an almost linear increase and reaches 82%. In stage 4, the gas pressure keeps decreasing until breakdown.

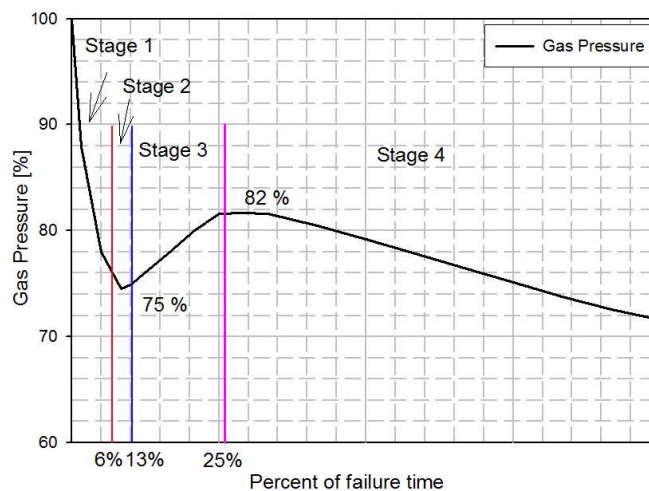
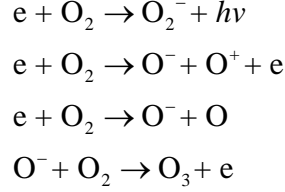


**Figure 4.8** Time evolution of gas pressure in small cavities in each ageing stage

### 4.3 Correlation between PD and Gas in the Cavity

The discharge repetition rate and amplitude show similar behavior and close values under CGV and CGP conditions (see Figure 4.6), which suggests that the variation of gas pressure is not sufficient by itself to fully explain the evolution of PD in the cavity (see Figures 3.4 and 3.5). In addition to that, the behavior of PDIV, shown in Figures 3.15 and 3.16, clearly does not match the time evolution of gas pressure (see Figure 4.8). Hence, the contributions of the variation of the gas composition and the dielectric/cavity interface must be considered. Based on the time behavior of the PD statistical parameters and gas pressure, it is possible to discuss the correlation between PD activity and the physical/chemical conditions of the gas filling the cavity. The interaction between PD avalanches and gas molecules can give rise to reactive species through [12]:



The reactive species, mainly ozone, oxygen ions and oxygen atoms, can readily react with the PE surface. Oxygen in the cavity may be gradually consumed in the oxidative reaction. An oxidized layer containing carbonyl radicals (C=O) was found, indeed, on the cavity surface [9, 13]. The oxygen consumption process decreases the cavity gas pressure. At the same time, gaseous byproducts like CO<sub>2</sub> and CO may be generated from the cavity surface and diffuse into the cavity [9, 10], which tends to increase the gas pressure.

According to these considerations, what observed during ageing can be described through the following sequence of events. During stage 1, the oxygen consumption rate might be higher than the generation rate of the gaseous byproduct. Thus, the gas pressure decreases. The reduction of  $N_w$  and  $Q_{alfa}$  during this period can be attributed more to the composition of the gas in the cavity than to the variation of the gas density. The amount of oxygen molecules gradually decreases in the cavity. Thus, the ratio O<sub>2</sub>/N<sub>2</sub> becomes low, which can cause the decrease of  $Q_{alfa}$  [8]. In addition, the lower gas density will reduce the effective ionization coefficients and, therefore, decrease  $N_w$  and  $Q_{alfa}$ .

Stage 2 begins when pressure reaches the minimum values and starts to increase. This can be due to that production rate of the decomposition byproducts exceeds gas consumption rate. Sekii et al [9] reported that the amount of CO<sub>2</sub> generated by the PD increases with ageing time, supporting this deduction. Meanwhile, CO and CO<sub>2</sub> can be dissociated by the PD, releasing oxygen [3]. The regeneration of O<sub>2</sub> can lead to the increase of  $Q_{alfa}$  in stage 3. The increase of  $N_w$  could also be related to the variation of the gas density and quality.

In stage 4, the gas consumption rate exceeds the regeneration rate again. Thus, the cavity gas pressure and the ratio O<sub>2</sub>/N<sub>2</sub> decrease with a rate that depends on the temperature and the background electric field [2].

## 4.4 Summary

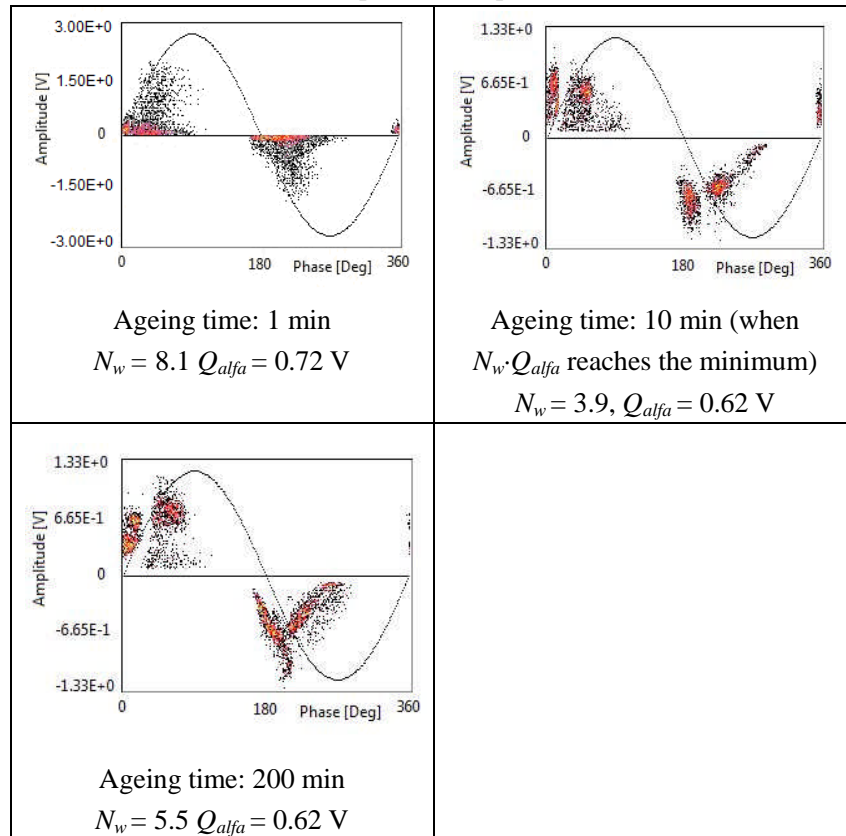
In this chapter, PD behavior in PE-embedded cavities is studied and compared under CGP and CGV conditions. Time evolution of the gas volume in the cavity is obtained under CGP. The behavior of gas pressure under CGV is inferred according to the ideal gas law and the gas volume evolution. PD measurement results show that  $N_w$  and  $Q_{alfa}$  have similar changing trends and close values under CGP and CGV, suggesting that the gas pressure has very slight influence on the PD activity. It can be speculated that the variation of gas composition can largely affect the PD evolution.

However, the evolution of the PD phenomenology, as reported in Chapter 3, cannot be explained thoroughly only considering the changes of the gas filling the cavity. The condition of the dielectric/cavity interface must also play a fundamental role in PD evolution. Cavity surface roughness and surface conductivity can change during the PD ageing, due to at least three effects: hot electron bombardment, chemical radical erosion and byproduct deposition. Liquid and solid PD byproducts (mainly organic acid) may accumulate on the cavity surface during the early ageing period (i.e. following the oxygen consumption in stage 1), which may increase surface conductivity [7, 14, 15]. Both electron bombardment and chemical attack can modify the surface of the polymer matrix. Generally, it has been observed an increase of the surface roughness [13], which can be due to crystal formation (induced by the weak acids deposited on the surface) and/or “etching” of the polymer matrix, due to electronic bombardment or chemical attack.

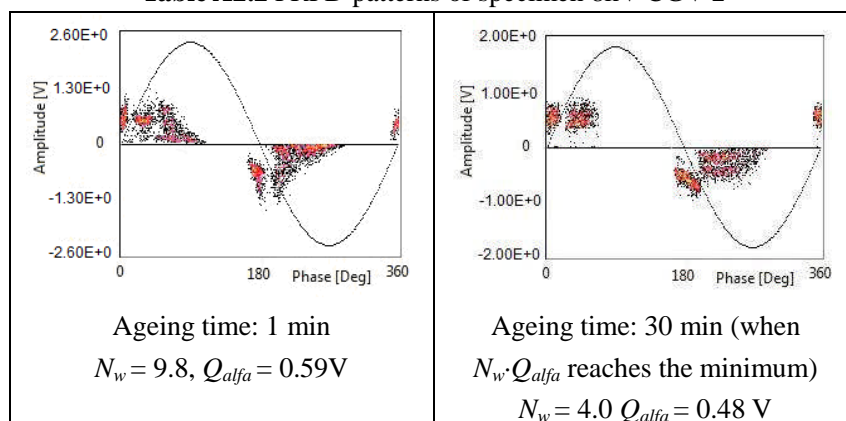
## Appendix 2

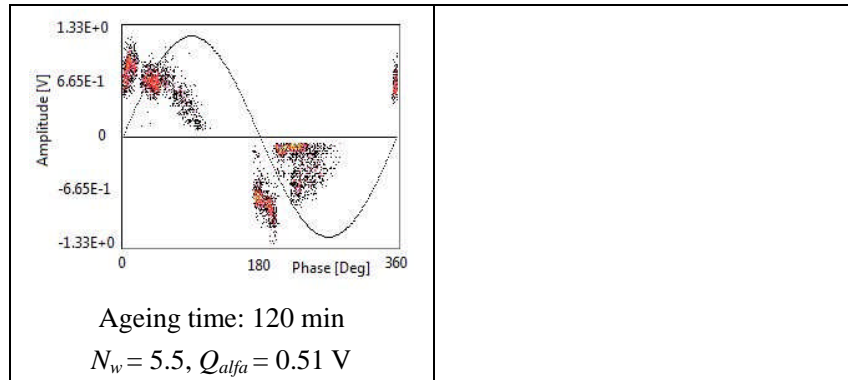
PRPD patterns of specimens 8kV-CGV-1, 8kV-CGV-2, 8kV-CGP-1 and 8kV-CGP-2 at various ageing times are shown in Tables A2.1, A2.2, A2.3 and A2.4, respectively.

**Table A2.1** PRPD patterns of specimen 8kV-CGV-1

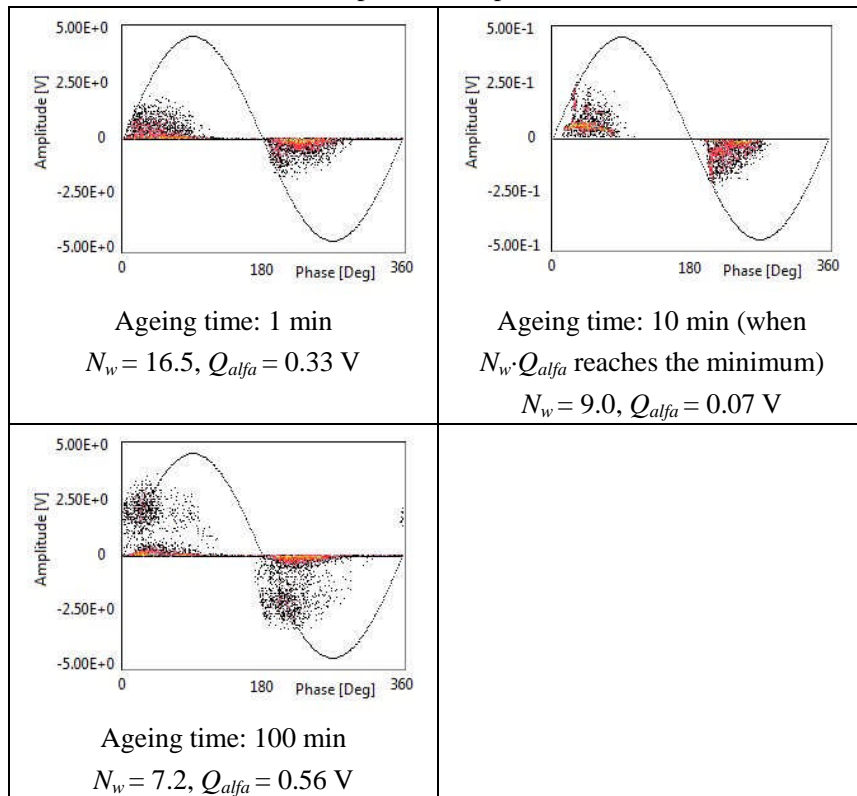


**Table A2.2** PRPD patterns of specimen 8kV-CGV-2

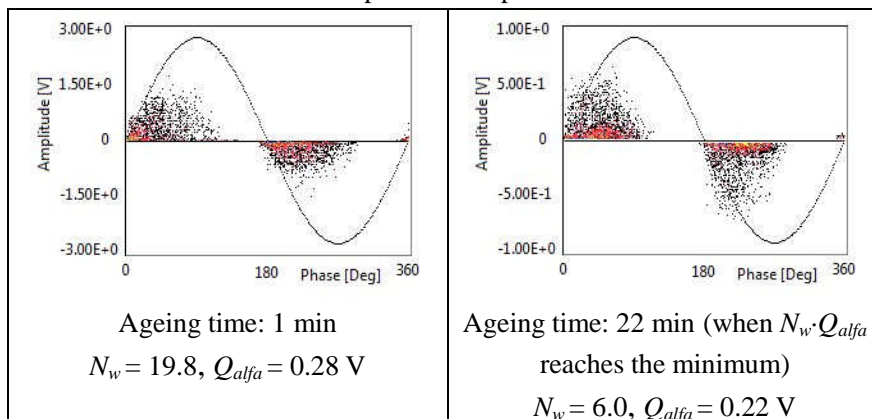


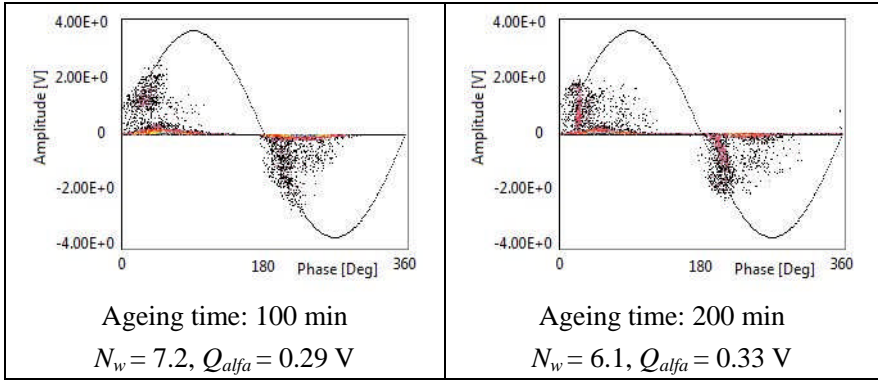


**Table A2.3** PRPD patterns of specimen 8kV-CGP-1



**Table A2.4** PRPD patterns of specimen 8kV-CGP-2





# CHAPTER 5

## MODIFICATION OF THE DIELECTRIC/CAVITY INTERFACE

### INTERFACE

The physical/chemical conditions of the dielectric/cavity interface have significant influence on the PD activity (see Section 2.4). In order to study the modification of the interface morphology during the PD-induced ageing, we performed microscope observation on specimens having various ageing times. Microscopic photos of the dielectric/cavity interface at different ageing stages are reported in this chapter. The correlation between PD and the interface conditions is inferred.

### 5.1 Test Object and Experimental Procedure

The specimens used for microscopy observation have the same structure and dimension to those used for the ageing tests (see Chapter 3), as shown in Figure 5.1. Five specimens, labeled from NO.1 to NO.5, were aged at 10kV (background electric field in the cavity  $E_0 = 43.5$  kV/mm) using the system sketched in Figure 3.2. These specimens were removed from ageing before failure. Their ageing times are 40 h, 70 h, 90 h, 100 h, and 120 h, respectively. Discharge repetition rate ( $N_w$ ), amplitude ( $Q_{alfa}$ ) and PRPD patterns were recorded by the PD detector at the time they were removed from ageing.

After ageing, the layers of the specimens were separated and the dielectric/cavity interfaces were exposed. The morphology of both top and bottom interfaces (see Figure 5.1) were investigated using optic microscope and SEM (scanning electron microscope). PD byproducts could be observed at the interfaces of the specimens having ageing times longer than 70 h. The composition of the byproducts was analyzed using EDAX (energy-dispersive X-ray spectroscopy) and confocal Raman microprobe spectroscopy. Subsequently, the byproducts were removed from the interface and the morphology of the polymer surface was studied using optic microscope and AFM (atomic force microscope).

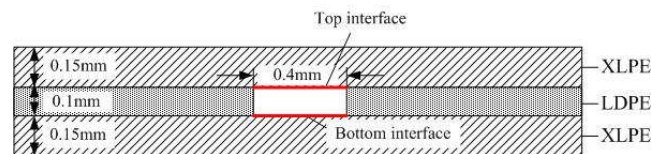
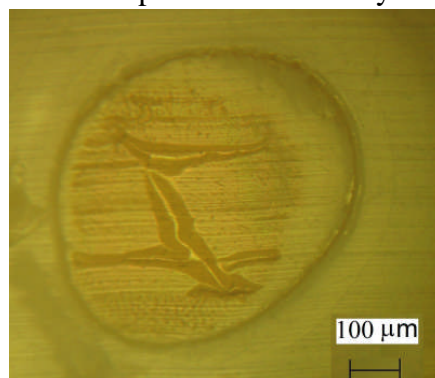


Figure 5.1 Sketch of the PE-layered specimens for microscope observation.

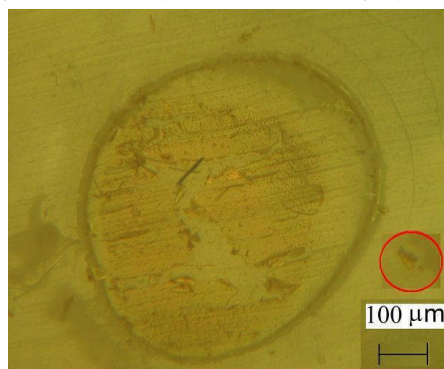
### 5.2 Morphology and Composition of the PD Byproducts

#### 5.2.1 Morphology of the PD byproducts

A layer of brownish solid byproducts was observed using optic microscope at both top and bottom interfaces of specimens having ageing times longer than 70 h. As an example, Figure 5.2a shows the morphology of the byproducts at the bottom interface of specimen NO.4 (ageing time = 100 h). The byproducts cover almost the entire area of the interface and are very fragile. Indeed, the byproduct layer broke into small pieces (tens of micron meters in diameter) when a thin stick of PE slid on it. Figure 5.2b shows the optic microscope photo of the cavity surface after the layer of byproduct broke. One of the broken pieces is marked by the red circle.



(a) Morphology of the cavity surface, covering by the PD byproducts



(b) After the byproduct layer broke into pieces

**Figure 5.2** Optic microscope photos of the PD byproducts covering the bottom interface of specimen NO.4 (ageing time 100h), before (a) and after (b) the byproduct layer breaks.

SEM observation was performed on the top and bottom interfaces of specimens NO.1, NO.2, NO.3 and NO.5, respectively. Their SEM photos, ageing times and ageing stages (see Figures 3.4 and 3.5) are reported in Figure 5.3. For each specimen, the top interface shows similar image to the bottom one. Therefore, for the sake of brevity, only the SEM photos of the bottom interfaces were reported.

The cavity area of specimen NO.1 (ageing time = 40 h, at ageing stage 3) is marked by the black circle in Figure 5.3a. As can be seen, no byproduct can be observed inside the circle. So, it is conceivable that byproducts start to accumulate during stage 4. A thin layer of byproducts can be observed at the bottom interface of specimen NO.2 (ageing time = 70 h, at ageing stage 4), as shown in Figure 5.3b. The byproduct layer broke into small pieces, as indicated by the arrows in the figure. From Figure 5.3b, 5.3c and 5.3d, we can speculate that the amount of the byproducts increases rising the ageing time.

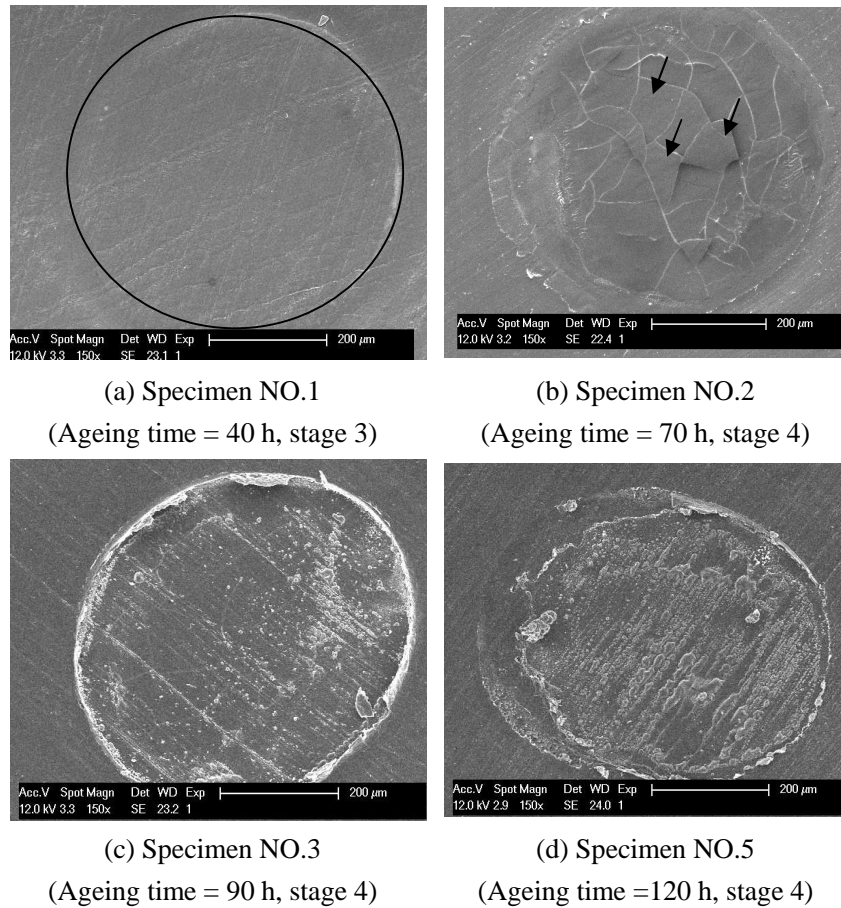
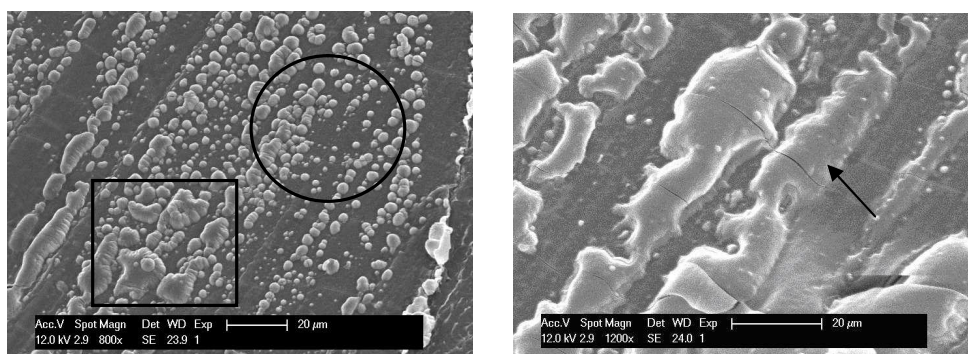


**Figure 5.3** SEM photos of the bottom interfaces of specimens NO.1, NO.2, NO.3 and NO.5, respectively.

Figure 5.4 shows the SEM photos with larger magnification of the bottom interface of specimen NO.5 (ageing time = 120 h, at ageing stage 4). The morphology of the byproducts can be clearly observed. Spherical particles having diameters less than 10  $\mu\text{m}$  can be found on the cavity surface (see the area marked by the black circle in Figure 5.4 a). It is arguable that, in the course of time, these particles gradually merge together to form elongated structures, as the one indicated by the arrow in Figure 5.4 b. Particle-merging is supported also by the observation of the area marked by the rectangle in Figure 5.4 a. Therefore, it can be speculated that the byproducts were liquid or gelatinous when they were originally generated at the interface. Then, oxidation along with reticulation processes allowed forming inter- and intra-molecular bonds, turning the byproducts into fragile solid substance. Similar spherical and elongated structures of the PD byproducts were observed at the dielectric/cavity interface of other specimens having ageing times longer than 100 h.



(a) Particle-shape byproducts

(b) Bar-shape byproducts

**Figure 5.4** SEM photos of the byproducts at the bottom interface of specimen NO.5

## 5.2.2 Composition of the PD byproducts

The composition of the PD byproducts deployed at the interfaces was analyzed using EDAX and confocal Raman microprobe spectroscopy. The EDAX result, reported in Figure 5.5, suggests that the byproducts mainly consist of carbon (C) and oxygen (O). The gold component (Au) reported in the figure is introduced by the surface metallization process before the SEM analysis.

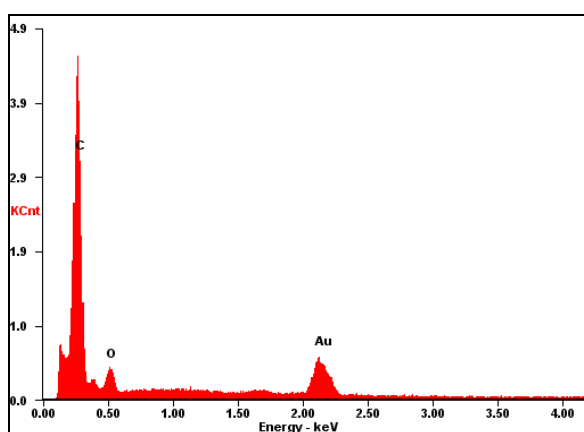


**Figure 5.5** EDAX analysis result on the PD byproducts at the interface.

The bottom interface of specimen NO.5 was investigated using confocal Raman microprobe spectroscopy. The laser beam was focused at three random spots (labeled as spots A, B and C) at the interface. Figure 5.6 reports the Raman spectra obtained at the three spots. Curves A, B, and C correspond to spots A, B and C, respectively. Oxygen containing moieties can be identified by the peaks wavenumber =  $500\text{ cm}^{-1}$  in the curves. These findings are in accordance with what found by Morshuis, Bartnikas and Hudon in [1-3]. They found the oxygen containing moieties to be a mixture of organic acids, like formic, acetic and carboxylic acids.

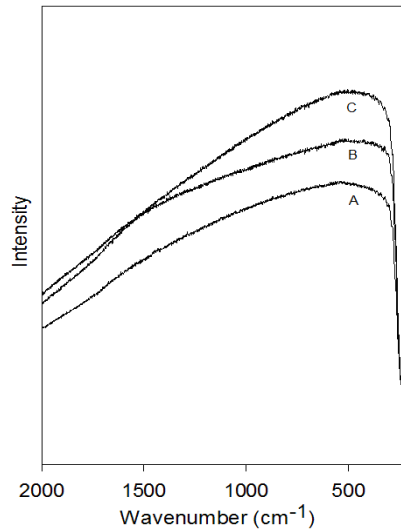
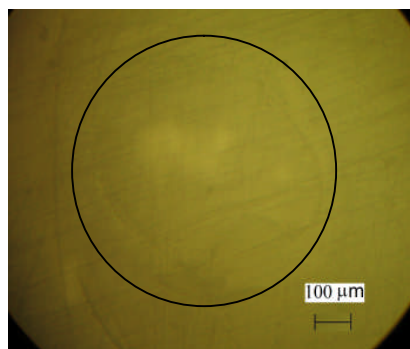


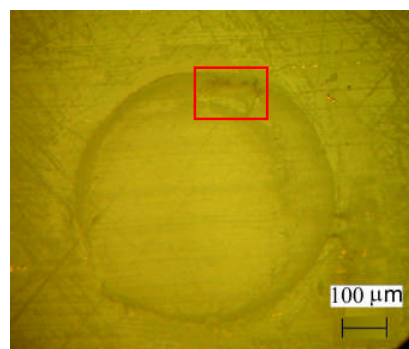
**Figure 5.6** Raman spectra of the byproduct deployed at the bottom interface of specimen NO.5. Curves A, B and C correspond to spots A, B and C, respectively

### 5.3 Degradation of the Polymer Surface

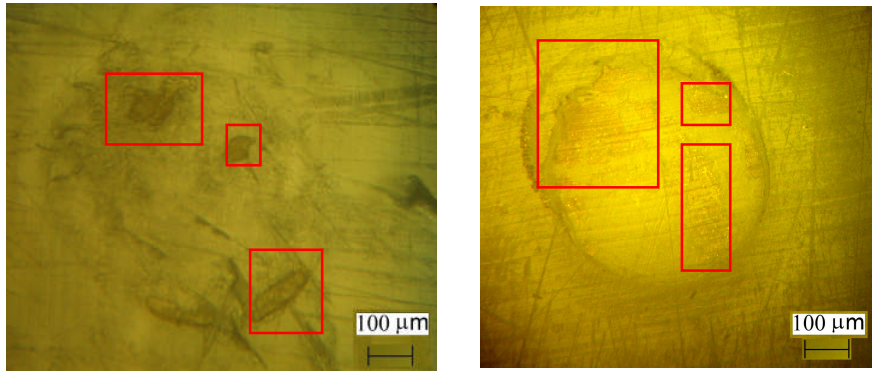
Degradation pits were observed after the PD byproducts were wiped off from the polymer surface. The optic microscope photos of the bottom interfaces for specimens NO.1, NO.2, NO.3 and NO.5 are shown in Figure 5.7. For specimen NO.1, no significant changes can be observed at the polymer surface (see the area marked by the black circle in Figure 5.7a). Degradation pits were found on the polymer surface of the specimens having ageing times longer than 70 h, as marked by the red rectangles in Figure 5.7b, 5.7c and 5.7d. It seems that the degradation pits were initially formed near the cavity edge (see Figure 5.7b). It could be explained by the stronger electric field near the edge of the cavity than near the cavity center (see Figure 5.8). The damaged area enlarged with ageing time, as can be seen from Figure 5.7b, 5.7c and 5.7d. The formation of these degradation pits on the PE surface can be attributed to bombardment of the avalanche electrons and/or chemical etching due to acidic PD byproduct (e.g. carboxylic groups, see [2, 3]).



(a) Specimen NO.1  
(Ageing time = 40 h, stage 3)



(b) Specimen NO.2  
(Ageing time = 70 h, stage 4)



(c) Specimen NO.3

(Ageing time = 90 h, stage 4)

(d) Specimen NO.5

(Ageing time = 120 h, stage 4)

**Figure 5.7** Optic microscope photos of the polymer surface after the byproducts were wiped off

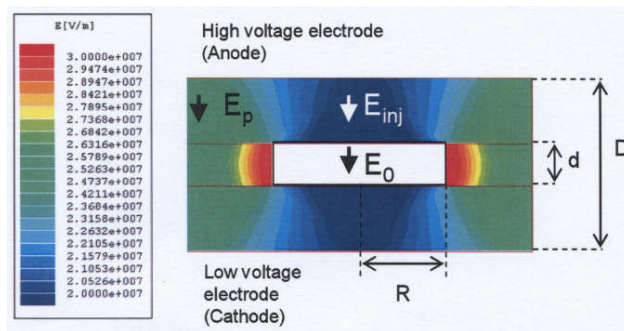
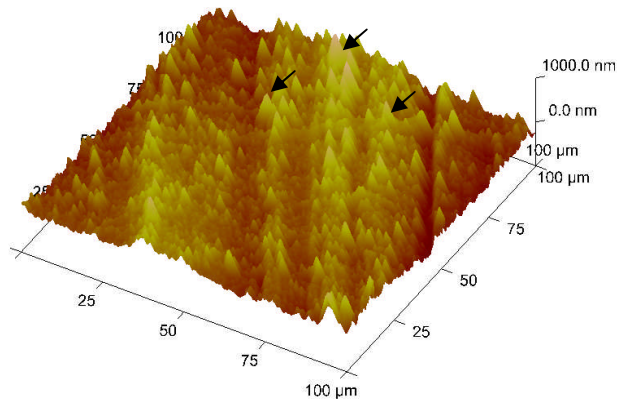
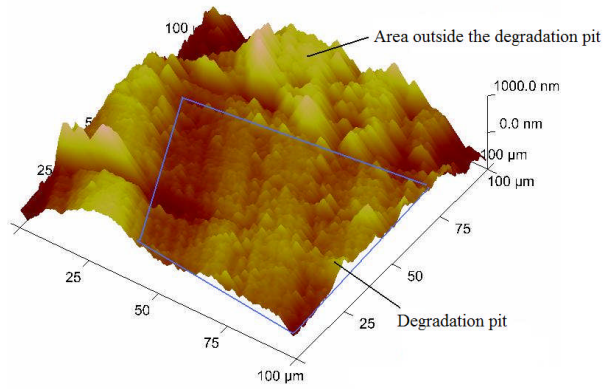


**Figure 5.8** Electric field distribution near the cavity (after [4])

Figures 5.9a and 5.9b show the AFM images of the XLPE surface before and after the ageing tests. Figure 5.9a was obtained by performing AFM analysis on the unaged XLPE surface. A large number of small tips can be observed on the surface, as indicated by the black arrows in Figure 5.9a. The formation of these tips can be attributed to the manufacturing of the XLPE sheet (i.e. peeling from power cable insulation). Figure 5.9b was obtained by performing AFM analysis on the bottom interface of specimen NO.5 after the PD byproducts were removed. Degradation pit (i.e. the area inside the blue quadrangle) can be observed at the XLPE surface.



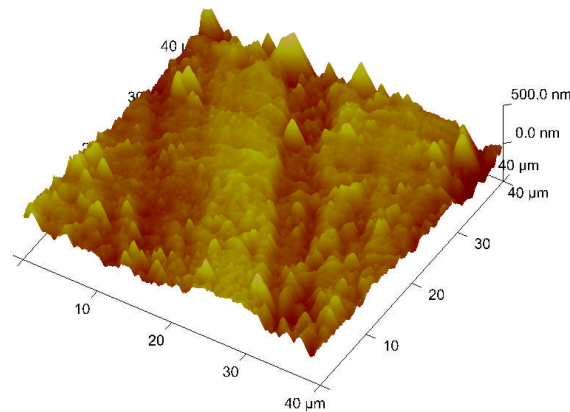
(a) AFM image of unaged XLPE surface



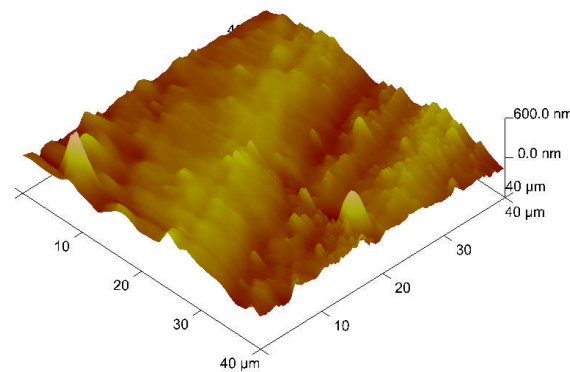
(b) AFM image of the bottom interface of specimen NO.5

**Figure 5.9** 100 $\mu\text{m}$  $\times$ 100 $\mu\text{m}$  $\times$ 1000nm AFM images of the XLPE surface before (a) and after (b) ageing

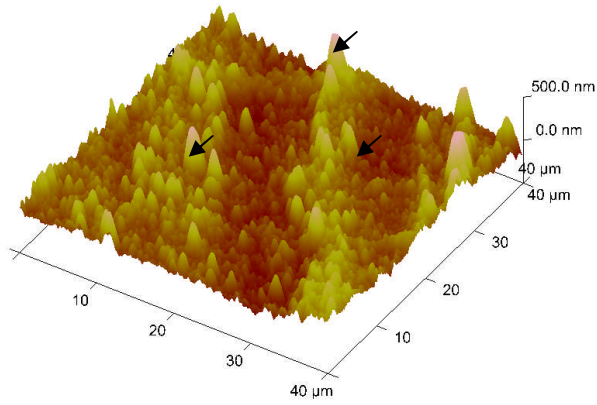
Figures 5.10a and 5.10b are AFM images obtained from the bottom interface of specimen NO.5. Figures 5.10a reports the image of the degradation pit. Figure 5.10b reports the image of the area outside the pit (see Figure 5.9b). Figure 5.10c reports the morphology of the XLPE surface outside the cavity region (unaged area). As can be seen, the sharp tips (marked by the black arrows in Figure 5.10c) disappeared in the cavity surface region. The XLPE surface inside the cavity region (shown in Figures 5.10a and 5.10b) is smoother than the surface outside the cavity region (shown in Figure 5.10c). The disappearance of the sharp tips could also be due to the electronic bombardment and chemical (acidic) etching.



(a) AFM image of the degradation pit area (see Figure 5.9b)



(b) AFM image of the area outside the degradation pit (see Figure 5.9b)



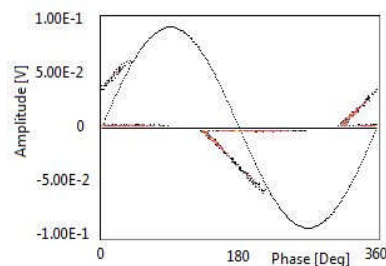
(c) AFM image of the area outside the cavity region

**Figure 5.10** 40μm×40μm×500nm AFM images of degradation pit area (a), the area outside the degradation pit (b) and the area outside the cavity region (c), obtained from the bottom interface of specimen NO.5.

## 5.4 Correlation between PD Patterns and Interface Conditions

PRPD patterns and PD parameters (i.e.  $N_w$  and  $Q_{alfa}$ ) were recorded for specimens NO.1, NO.2, NO.3 and NO.5 immediately before they were removed from ageing, as reported in Figure 5.11. The pattern of specimen NO.1 shows the rabbit-like shape, whereas the patterns of specimens NO.3 and NO.4 show the turtle-like shape. The pattern of specimen NO.2 seems to be undergoing the transition from rabbit-like to turtle-like, which can be inferred from the discharges appearing in the red circles in Figure 5.11.

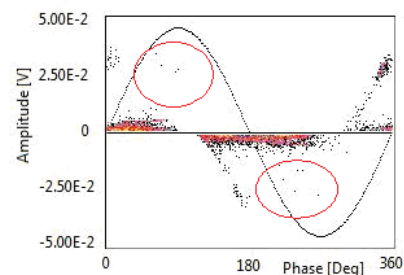
By comparing Figure 5.3 and Figure 5.11, we can speculate the correlation between the shape of the PRPD patterns and the conditions of the dielectric/cavity interface. The specimens having no significant PD byproduct at the interface show rabbit-like patterns (see Figures 5.3a and 5.11a), whereas those having large amount of byproducts show turtle-like patterns (see Figures 5.3c, 5.3d, 5.11c and 5.11d). At the early stage of byproduct accumulation, as in the case of specimen NO.2 (see Figure 5.3b), the patterns experience a transition period from rabbit-like shape to turtle-like shape (see Figure 5.11b).



$$N_w = 2.7, Q_{alfa} = 1.0 \times 10^{-2} \text{ V}$$

(a) Specimen NO.1

(Ageing time = 40 h, stage 3)



$$N_w = 28.7, Q_{alfa} = 5.0 \times 10^{-3} \text{ V}$$

(b) Specimen NO.2,

(Ageing time = 70 h, stage 4)

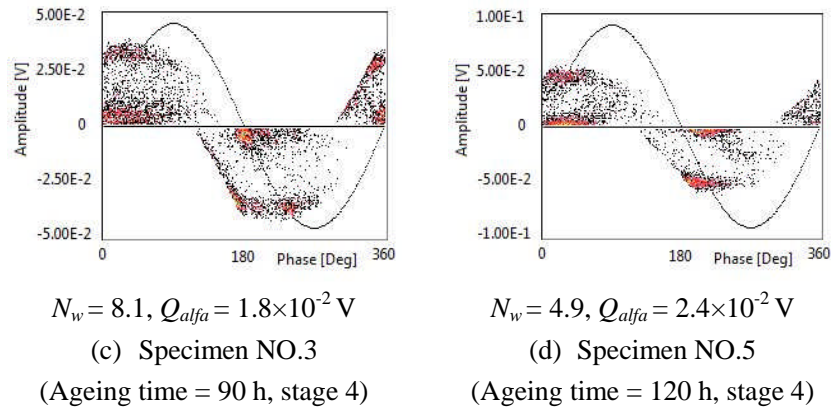


**Figure 5.11**  $N_w$  and  $Q_{alfa}$  values and PRPD patterns for specimens NO.1, NO.2, NO.3 and NO.5 immediately before they were removed from ageing.

## 5.5 Summary

The conditions of the dielectric/cavity interface at various ageing times were studied and reported. Morphology of the interface was investigated using optic microscope, SEM and AFM. A layer of brownish solid byproducts was observed, covering almost the entire area of the cavity surface. It can be speculated that the byproducts start to accumulate at the cavity surface from stage 4 and their amount increases rising the ageing time. EDAX and Raman spectroscopy analysis provided evidence of the formation of oxygen containing moieties (most likely acidic compounds) in the PD byproducts. Under optic microscope, degradation pits can be observed at the XLPE surface after the byproducts were removed. The formation of the pits can be due to electronic bombardment and/or acidic etching. AFM images show that the cavity surface inside the pit region is smoother than the unaged XLPE surface.

Correlation between the PRPD pattern shape and the interface conditions can be inferred. The transition of the pattern shape from rabbit-like to turtle-like, as reported in Chapter 3, could be related to the accumulation of the PD byproduct at the interface.

## CHAPTER 6

### NUMERICAL SIMULATION OF THE PD PATTERNS

In order to understand better the inherent correlation between the time behavior of the PD activity and the modification of physical/chemical properties of the dielectric/cavity interface, we studied the evolution of the charge injection parameters (i.e. work function,  $U_0$ , charge relaxation time constant,  $\tau$ , and the field enhancement coefficient,  $K$ ) by numerical simulation. In Section 2.3, the main features of the algorithm are introduced to simulate the PD phenomenon in a gas filled cavity subjected to AC electric field. According to the algorithm, we developed the numerical simulation program. The input parameters of the program are physical quantities of the insulation system (e.g. cavity dimensions, charge injection parameters of the interface and gas pressure in the cavity, etc.) and the applied voltage. The output results are PRPD patterns, discharge repetition rate and amplitude. By setting proper values to the input parameters, the PD phenomenon at different ageing times can be well reproduced. In this way, the evolution of the charge injection parameters and thus, the physical/chemical properties of the interface can be estimated.

#### 6.1 Algorithm of the simulation

In the numerical simulation, attention is focused on simulating the PD activity after the first discharge occurs. The time interval for the occurrence of the first starting electron is not considered (typical time durations of this time interval were given in [1, 2]). The mathematical treatment to simulate the main features of the PD activity is based on the following two hypotheses:

1. the avalanche process is considered to be instantaneous. (The duration of the discharge is of the order of tens of nanoseconds, much shorter than the time interval between adjacent discharges. Therefore, this hypothesis is reasonable.)
2. the charge generated by the partial discharges is assumed to be uniformly distributed at the dielectric/cavity interface at the end of the discharge.

##### 6.1.1 PD inception probability

The initiation of an electron avalanche in the cavity is considered as a stochastic process. The PD inception field,  $E_{inc}$ , is described by equation (2-26). The probability,  $p$ , of having a starting electron during a time interval,  $dt$ , is described by equations (2-27), (2-28), and (2-29). For the reader's convenience, these equations are rewritten below:

$$p = 1 - e^{-h \cdot dt} \quad (6-1)$$

$$h = h_{bg} + \lambda \quad (6-2)$$

$$\lambda = \frac{dN_{dt}}{dt} = N_{dt} \cdot v_0 \cdot e^{-\frac{U_0 - \sqrt{\frac{q_e^3 \cdot K \cdot E_i}{4\pi\epsilon_0}}}{kT}} \quad (6-3)$$

For cavities having the same size as those used in the ageing tests (surface radius  $R = 0.2$  mm; height  $d = 0.1$  mm),  $h_{bg}$  (the contributions to the starting electron availability that do not depend on the discharge activity) is negligible [1]. The fundamental phonon frequency,  $\nu_0$ , is constant, about  $10^{14}$  Hz for polyethylene.

The number of electrons available for being injected,  $N_{dt}$ , is evaluated considering the balance of two antagonistic processes:

1. PD-generated electrons accumulate at the dielectric/cavity interface, increasing the number of electrons available for being injected;
2. electrons decay through processes such as neutralization due to conductivity on cavity surface and diffusion into the dielectric bulk, decreasing the number of electrons for being injected.

The first process is expressed by the following expression:

$$N_{dt}(t_{PD}^+) = N_{dt}(t_{PD}^-) + |N_{PD}(t_{PD})| \quad (6-4)$$

where  $N_{PD}(t_{PD})$  is the number of detrappable electrons generated by the PD occurring at time  $t_{PD}$ . The reason for using the absolute value is that the number of detrappable electrons must be positive. Both positive and negative discharges are assumed to increase the number. However, equation (6-4) is not applicable to the first discharge after polarity inversion, in which case the discharge decreases the number of the detrappable electrons.  $N_{dt}(t_{PD}^-)$  is the number of detrappable electrons on the surface immediate prior to  $t_{PD}$ .  $N_{dt}(t_{PD}^+)$  is the number of available electrons immediately after  $t_{PD}$ . The number of electrons available for being detrapped is assumed to be the same for both surfaces. The second process is accounted for by the exponential law, with the same time constant,  $\tau$ , as that used to describe the relaxation of the space charge  $q_{SC}$ , as follows:

$$N_{dt} = N_{dt0} \cdot e^{-\Delta t/\tau} \quad (6-5)$$

where  $N_{dt0}$  is the number of detrappable electrons after the previous PD occurs;  $\Delta t$  is the time elapsed since the last PD occurred;  $N_{dt}$  is the detrappable electron number after the relaxation.

The electric field in the cavity,  $E_i$ , is discussed in detail in subsection 2.3.1. The coefficient  $K$  is introduced in order to simulate the ‘‘rabbit ear’’ structure in the PRPD patterns.  $K$  accounts for the enhancement of electric field at the interface caused by the accumulation of PD-induced space charges (see the discussion in subsection 2.3.3).

In fact, since the space charges on the cavity surface are subjected to the relaxation processes, a detailed description would require the expression of  $K$  to be a function of the amount of hetero-charge accumulated on cavity surface and of the time (since the accumulated charge is subjected to the relaxation process). In our simulations, a constant  $K$  value is used (see subsection 2.3.3) in order to show that the introduction of this coefficient can account properly for the “rabbit ear” feature of the PD patterns.

In the simulations, a random variable  $R_a \in [0, 1]$  is generated in each time interval,  $dt$ . The occurrence of the starting electron availability is evaluated as follows: If  $R_a \leq p$ , the starting electron is generated; otherwise, the starting electron is not generated.

### 6.1.2 Discharge amplitude

The number of electrons arriving at the cavity surface (i.e., discharge magnitude) is controlled by a multiplication factor based on the average number of impact ionizations per unit length. The electron multiplication is accounted for by the Townsend law, using the electric field dependant first Townsend coefficient. In the numeric simulation, the amount of charge ( $q_{PD}$ ) generated by the PD is evaluated by a cubic spline data interpolation,  $q_{PD} = f(E_i)$ , in which  $E_i = E_0 + E_q$ . The expression of  $E_q$  is described by equations (2-3) and (2-4). The function  $f(E_i)$  is obtained using simulations where the effective ionization coefficient was adjusted by trial and error [3].

### 6.2 Evolution of the injection parameters

The PD model under AC field reported in Section 2.3 is a physical ageing model based on physical quantities of the insulation system. The physical/chemical properties of the gas in the cavity and the dielectric/cavity interface are quantified as the input parameters in the simulation program. These parameters (referred to as simulation parameters in the following) are:

- 1)  $U_0$  - work function of the dielectric/cavity interface (eV);
- 2)  $\tau$  - charge relaxation time constant at the interface (ms);
- 3)  $K$  - electric field enhancement factor;
- 4)  $P$  - gas pressure in the cavity (kPa);
- 5)  $T$  - absolute temperature in the cavity (K).

By setting proper values to these parameters, we can reproduce the PRPD patterns, discharge repetition rate and amplitude at various ageing periods. Figure 6.1 reports the simulated PRPD patterns,  $N_w$  and the 98% percentile of the discharge amplitude distribution ( $Q_{max}(98\%)$ ) of the unaged specimen at 10kV, in comparison with the measured results. The dimensions of the cavity and the specimen are chosen according to the values reported in Figure 3.1. The gas pressure in the cavity,  $P = 40\text{kPa}$ , was calculated by equation (2-26), in which the PD inception field  $E_{inc}$  for the unaged specimen is 9.1 kV/mm. The values of the simulation parameters are reported

in Figure 6.1. The simulated PD pattern and parameters fit very well the measurement results.

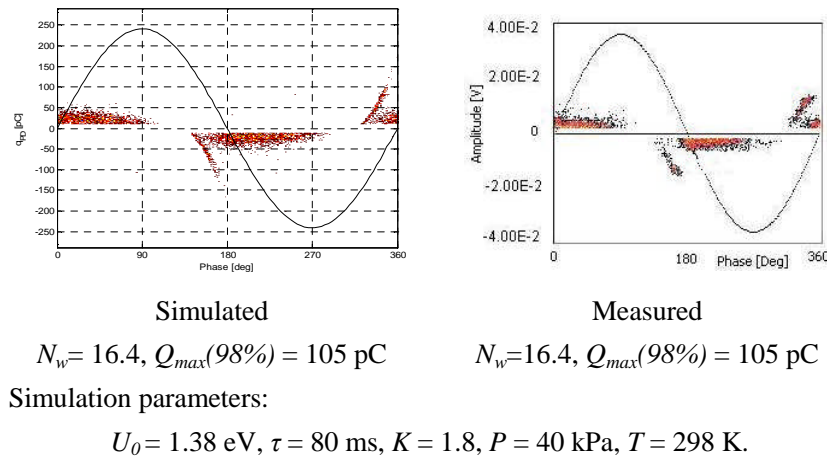


**Figure 6.1** Simulated and measured PD patterns and parameters for unaged specimen at 10kV

Figure 6.2 displays the simulated patterns of the unaged specimens at 10 kV with the gas pressure values set to 10 kPa and 100 kPa, respectively.  $U_0, \tau, K$  and  $T$  have the same values as those used in Figure 6.1. As can be seen, the patterns show the same shape characteristics. Slight difference can be found only in the  $N_w$  values. By modifying the gas pressure values, therefore, it is hard to observe significant modification of PD repetition rate and amplitude as those observed experimentally (see Figures 3.4, 3.5 and 3.6). This result agrees with what we have concluded in Chapter 4, i.e. the variation of gas pressure in the cavity has little influence on the PD phenomenon. Therefore, it can be speculated that the variation of the gas pressure is not sufficient by itself to fully explain the evolution of the PD activity. To describe properly the time evolution of the PD, other parameters (i.e.  $U_0, K, \tau$ ) should be varied.

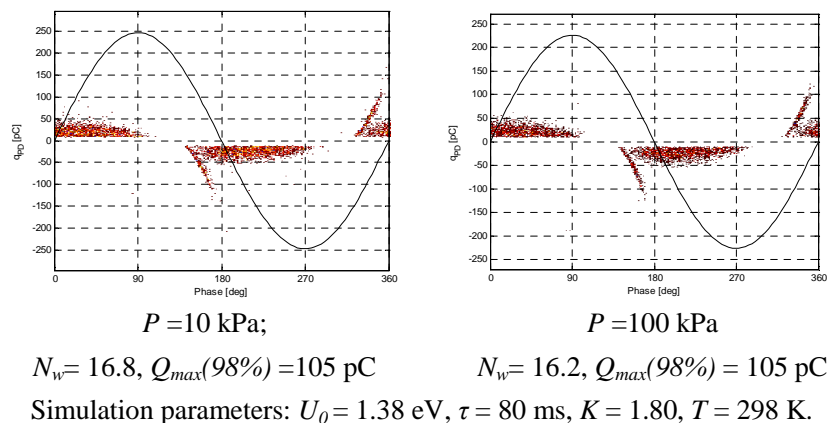
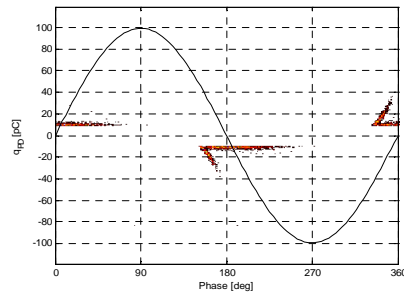


**Figure 6.2** Simulated patterns for unaged specimen at 10kV with gas pressure values set to 10 kPa and 100 kPa, respectively.

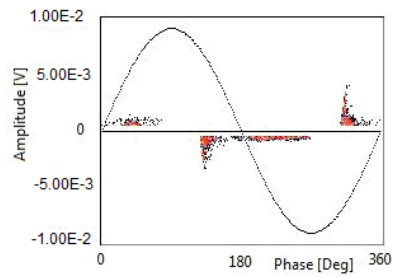
The simulated and measured PD patterns, as well as the  $N_w$  and  $Q_{max}(98\%)$  values, at stages 2, 3 and 4 (see Figures 3.4 and 3.5) are reported in Figure 6.3, in which the

gas pressure values are taken from Figure 4.8 and the temperature in the cavity is considered to be constant ( $T = 298$  K).



Simulated

$$N_w = 3.4, Q_{max}(98\%) = 30 \text{ pC}$$



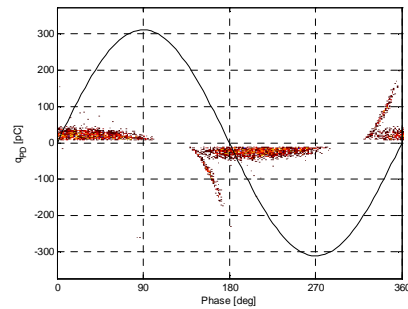
Measured

$$N_w = 3.3, Q_{max}(98\%) = 29 \text{ pC}$$

Simulation parameters:

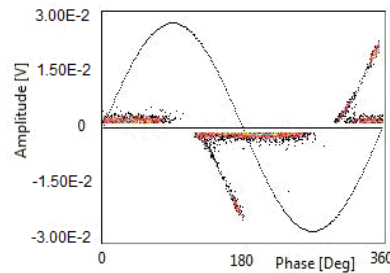
$$U_0 = 1.39 \text{ eV}, \tau = 130 \text{ ms}, P = 30 \text{ kPa}, K = 1.90, T = 298 \text{ K.}$$

(a) Stage 2: 10% of failure time



Simulated

$$N_w = 20.5, Q_{max}(98\%) = 170 \text{ pC}$$



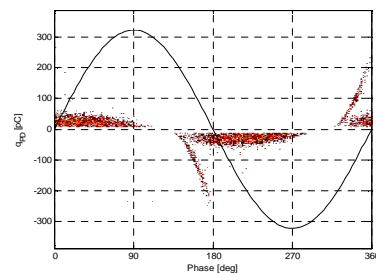
Measured

$$N_w = 20.4, Q_{max}(98\%) = 170 \text{ pC}$$

Simulation parameters:

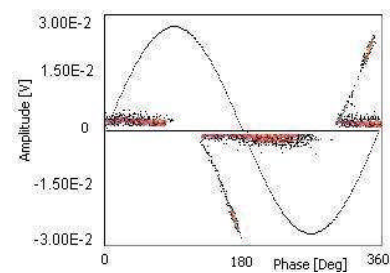
$$U_0 = 1.40 \text{ eV}, \tau = 150 \text{ ms}, P = 33 \text{ kPa}, K = 2.34, T = 298 \text{ K.}$$

(b) Boundary of stage 3 and stage 4: 25% of failure time



Simulated

$$N_w = 17.9, Q_{max}(98\%) = 200 \text{ pC}$$



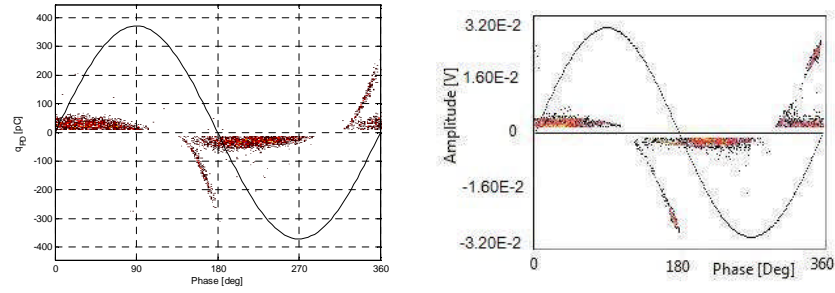
Measured

$$N_w = 18.0, Q_{max}(98\%) = 202 \text{ pC}$$

Simulation parameters:

$$U_0 = 1.42 \text{ eV}, \tau = 180 \text{ ms}, P = 28 \text{ kPa}, K = 2.39; T = 298 \text{ K.}$$

(c) Stage 4: 60% of failure time



Simulated
Measured

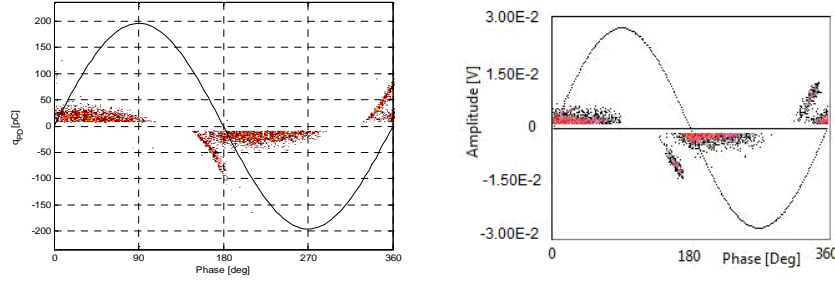
$N_w = 15.5, Q_{max}(98\%) = 220 \text{ pC}$ 
 $N_w = 15.4, Q_{max}(98\%) = 219 \text{ pC}$

Simulation parameters:  
 $U_0 = 1.43 \text{ eV}, \tau = 220\text{ms}, P = 24 \text{ kPa}, K = 2.41; T = 298 \text{ K}.$

(d) Stage 4: 100% of failure time (prior to breakdown)

**Figure 6.3** Simulated and measured PD patterns and parameters at 10 kV during ageing stages 2, 3 and 4.

In order to verify the validity of the simulation, we performed a cross-check procedure: during the ageing tests at 10 kV, the ageing voltage was shortly decreased to 8kV at 18 h, 45 h, 110 h and 175 h, corresponding to 10%, 25%, 60% and 98% of the scale parameter ( $\alpha = 178 \text{ h}$ ) of the failure time Weibull distribution (see Figure 3.3). The PD patterns and parameters were recorded by the PD detector at 8 kV. By adopting the simulation parameters at corresponding ageing times reported in Figure 6.3, the PD patterns, as well as  $N_w$  and  $Q_{max}(98\%)$  can be reproduced successfully at 8kV, suggesting that the simulation parameters can reflect the physical/chemical properties of interface at corresponding ageing times.

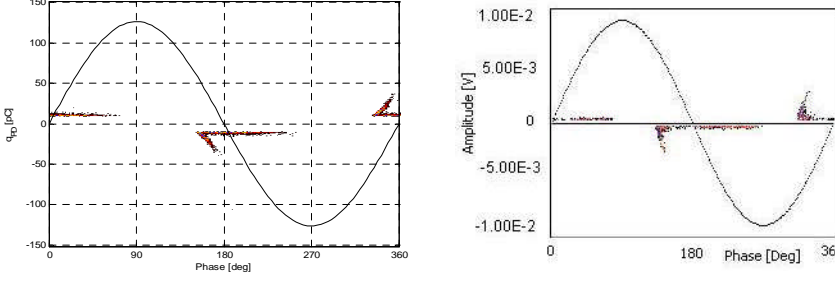


Simulated
Measured

$N_w = 12.2, Q_{max}(98\%) = 95 \text{ pC}$ 
 $N_w = 12.5, Q_{max}(98\%) = 97 \text{ pC}$

Simulation parameters:  
 $U_0 = 1.38 \text{ eV}, \tau = 80 \text{ ms}, K = 1.80, P = 40 \text{ kPa}, T = 298 \text{ K}.$

(a) Stage 1 (unaged specimen)



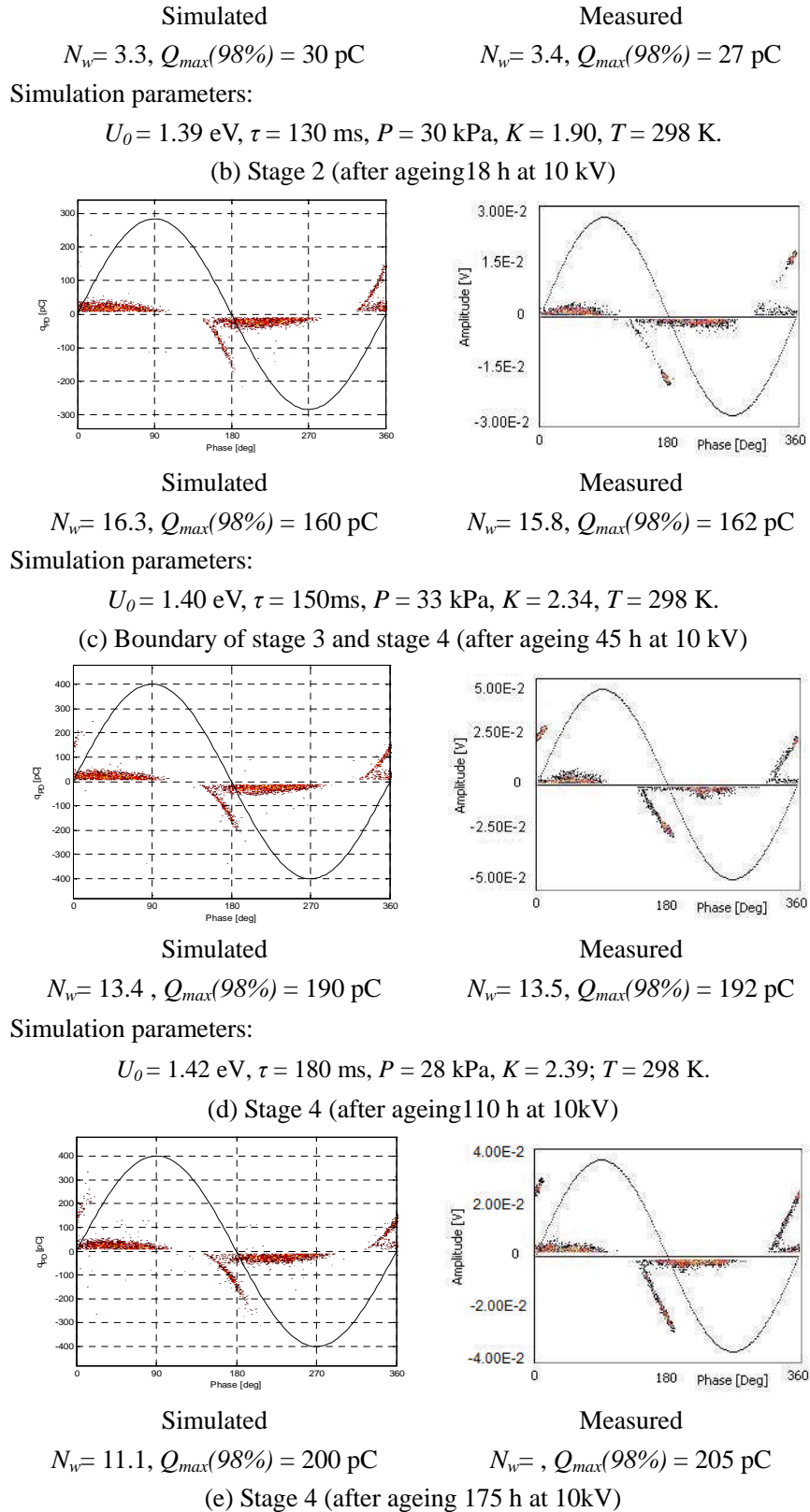


**Figure 6.4** Cross-check results: simulated and measured PD patterns and parameters at 8 kV after ageing 0 h, 18 h, 45 h, 110 h and 175 h at 10 kV.

It can be observed from Figure 6.3 and 6.4 that  $U_0$ ,  $\tau$ , and  $K$  values increase monotonously from  $U_0 = 1.38 \text{ eV}$ ,  $\tau = 80 \text{ ms}$ ,  $K = 1.80$  to  $U_0 = 1.43 \text{ eV}$ ,  $\tau = 220 \text{ ms}$ ,  $K$

= 2.41, respectively. The curves of the values  $U_0(t)/U_0(0)$ ,  $\tau(t)/\tau(0)$ , and  $K(t)/K(0)$  are reported in Figure 6.5 as a function of normalized ageing time (100% corresponds to the failure time). The cause for the change of  $U_0$ ,  $\tau$ , and  $K$  has not been properly understood and can only be speculate at present. The increase of  $U_0$  could be due to the formation of chemical traps (free radicals) in the byproduct layer (see Figure 5.3). A large density of deep traps can explain also the increase of the relaxation time constant,  $\tau$ , which turn into lower charge carrier mobility. Also, the slower movement of the space charge at the dielectric/cavity interface can result in a larger enhancement of the electric field and, thus, higher  $K$  value.

On the other hand, the PD byproducts were proved to be mainly organic acids [5, 6], which may increase surface conductivity [7-9] and thus, decrease the charge relaxation time constant,  $\tau$ . Therefore, there may be a balance between the contributions to increase  $\tau$  and those to decrease it. In our case, the contributions to increase it may predominate in the balance.

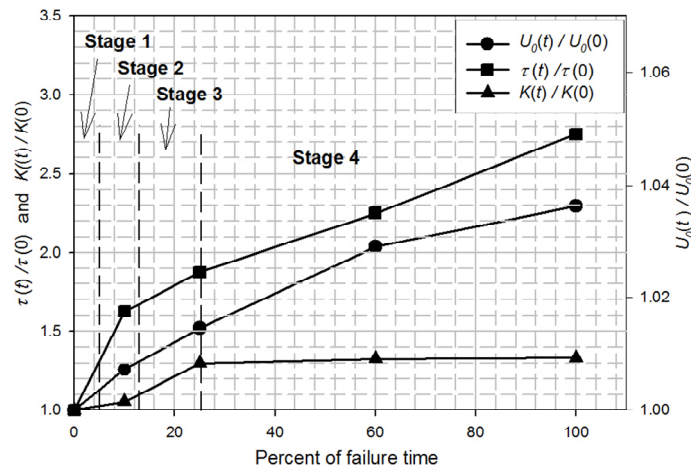


**Figure 6.5** Time behavior curves of  $U_0(t)/U_0(0)$ ,  $\tau(t)/\tau(0)$ , and  $K(t)/K(0)$

### 6.3 Summary

In order to study the correlation between PD and the physical/chemical conditions of the surrounding dielectrics, we developed the numerical simulation program and reproduced the PD patterns and parameters at each ageing stage. The evolution of the electron injection parameters (i.e.  $U_0$ ,  $\tau$ , and  $K$ ) was obtained by fitting the simulated patterns to the measured ones. The simulation results show that the modification of the dielectric/cavity interface tends to increase  $U_0$ ,  $\tau$ , and  $K$ . It is also confirmed by the simulation that the gas pressure in the cavity has very slight influence on the PD activity.

## CONCLUSIONS

In the framework of developing a physical aging model for damage inception and growth from micro-cavities subjected to PD under AC field, we studied the behavior of the PD activity in artificial cylindrical cavities embedded in three-layer PE-based specimens. Four ageing stages could be singled out according to the characteristics of PD statistical parameters, i.e. discharge repetition rate,  $N_w$ , and amplitude,  $Q_{alfa}$ . Two different types of pattern shape (i.e. “rabbit-like” and “turtle-like”) could be observed in the last ageing stage for specimens having long and short failure times, respectively. The product  $N_w \cdot Q_{alfa}$  was proposed in this thesis as a parameter to evaluate the PD-induced damage growth rate at the dielectric/cavity interface. The time behavior of  $N_w \cdot Q_{alfa}$  suggests that the last ageing stage contributes mostly to the failure of the specimen.

Modification of the gas in the cavity may be one of the key factors that cause the evolution of the PD patterns and parameters. Similar time behavior of  $N_w$  and  $Q_{alfa}$  was observed in the PD measurements under constant gas volume (CGV) and constant gas pressure (CGP) conditions, suggesting that the gas pressure variation has very slight influence on the PD activity. The modification of gas composition may play a fundamental role in the PD evolution.

The condition of the dielectric/cavity interface can also largely affect the PD behavior. Brownish PD byproducts, consisting of oxygen containing moieties (most likely organic acids), were observed at the dielectric/cavity interface. The formation of free radicals in the byproduct layer may create chemical traps at the interface, leading to the increase of the work function ( $U_0$ ) and the charge relaxation time constant ( $\tau$ ). The byproduct accumulation may also be related to the transition of the pattern shape from rabbit-like to turtle-like.

To sum up, the typical changing characteristics of the patterns and parameters of PD in the micro-cavities embedded in PE-based material under AC field are reported in this thesis. In order to understand the formation of the PD behaviour, we studied the evolution of the gas pressure in the cavity and the morphology modification of the dielectric/cavity interface. The correlation between PD and the surrounding dielectrics (i.e. gas filling the cavity and dielectric/cavity interface) is inferred. These results provide experimental basis for the modelling of the PD phenomenon in micro-cavities and, thus for evaluating the PD-induced ageing rate under AC field.

# REFERENCES

## Chapter 1

- [1] IEC 505, "Evaluation and identification of electrical insulation systems. Part 1: general Principles and Guide to Application", 1975; IEC TC 63 (Sec.) 75, 1992. IEEE 1064, IEEE Guide for Multifactor Stress Functional Testing of Electrical Insulation Systems, 1991.
- [2] G. C. Montanari and L. Simoni, "Ageing phenomenology and modeling", IEEE Trans. Dielectr. Electr. Insul., Vol. 28, NO.5, October, pp. 755-776, 1993.
- [3] P. K. David, "Correlation of Arrhenius parameters: the Electrotechnical aging compensation effect", IEEE Trans. Electr. Insul, Vol. 22, pp. 229-236, June 1987.
- [4] P. K. David and G. C. Montanari, "Compensation effect in thermal aging investigated according to Eyring and Arrhenius models", ETEP, Vol. 2, No. 3, pp. 187-194, June 1992.
- [5] G. C. Montanari and F. J. Lebok, "The thermal degradation of electrical insulating materials and the thermokinetic background. Theoretical basis. Experimental data", IEEE Trans. Electr. Insul, Vol. 25, pp. 1029-1045, 1990.
- [6] J. P. Crine, J. L. Parpal and G. Lessard, "A model of aging of dielectric extruded cables", IEEE ICSD, Trondheim, Norway, pp. 347-351, 1989.
- [7] S. N. Zhurkov, "Kinetic concept of the strength of solids", Int. Journ. Fract. Mech., Vol. 1, pp. 311-323, 1965.
- [8] L. A. Dissado and J. C. Fothergill, "Electrical degradation and breakdown in polymers", P. Peregrinus, London, 1992.
- [9] W. T. Starr, H. S. Endicott, "Progressive stress: a new accelerated approach to voltage endurance", IEEE Trans. Power. App. Syst., pp. 515-522, 1961.
- [10] G. C. Montanari and G. Mazzanti, "From thermodynamic to phenomenological multistress models for insulating materials without or with evidence of threshold", J. Phys. D: Appl. Phys., Vol. 27, pp.1691- 1702, 1994.
- [11] S. A. Boggs, "Theory of defect-tolerant dielectric systems", IEEE Trans. Electr. Insul, Vol. 28, pp. 365-371, 1993.
- [12] G. Jiang, J. Kuang, S. Boggs, "Critical parameters for electrical tree formation in XLPE", IEEE Trans. Power. Del., Vol. 13, pp. 292 - 296, 1998.
- [13] A. See, L.A. Dissado, J.C. Fothergill, "Electric field criteria for charge packet formation and movement in XLPE", IEEE Trans. Dielectr. Electr. Insul, Vol. 8, pp. 859-866, 2001.
- [14] K. Wu, L.A. Dissado and T. Okamoto, "Percolation model for electrical breakdown in insulating polymers", Appl. Phys. Lett., Vol. 85, pp. 4454-4456, 2004.
- [15] L. A. Dissado, G. Mazzanti and G. C. Montanari, "The incorporation of space charge degradation in the life model for electrical insulating materials", IEEE Trans. Dielectr. Electr. Insul, Vol. 2, , pp. 1147-1158, 1995.
- [16] G. Mazzanti, G. C. Montanari and L.A. Dissado, "A space-charge life model for AC electrical aging of polymers", IEEE Trans. Dielectr. Electr. Insul, Vol. 6, pp. 864-875, 1999.
- [17] G. Mazzanti, G. C. Montanari and L.A. Dissado, "Life modeling of AC cable insulation based on space-charge inference", Proceedings of the 5th International Conference on Insulated Power Cables, pp. 707-712, Versailles, France, 1999.

- [18] L. A. Dissado, G. Mazzanti and G. C. Montanari, "Elemental strain and trapped space charge in thermoelectrical aging of insulating materials. Part 1: elemental strain under thermo-electrical-mechanical stress", *IEEE Trans. Dielectr. Electr. Insul.*, Vol. 8, pp. 959-965, 2001.
- [19] L. A. Dissado, G. Mazzanti and G. C. Montanari, "Elemental strain and trapped space charge in thermoelectrical aging of insulating materials. Part 2: Life modeling", *IEEE Trans. Dielectr. Electr. Insul.*, Vol. 8, pp. 966-971, 2001.
- [20] T. J. Lewis, "Polyethylene under electrical stress", *IEEE Trans. Dielectr. Electr. Insul.*, Vol. 9, pp. 717-729, 2002.
- [21] J. P. Crine, "A molecular way to evaluate the impact of ageing on space charges in polymer dielectrics", *IEEE Trans. Dielectr. Electr. Insul.*, Vol. 4, pp. 487-496, 1997.

## Chapter 2

- [1] S. Serra, G. C. Montanari and G. Mazzanti, "Theory of inception mechanism and growth of defect-induced damage in polyethylene cable insulation", *J. Appl. Phys.*, Vol. 98, pp. 034102.1-034102.15, 2005.
- [2] G. Mazzanti, G. C. Montanari and F. Civenni, "Model of inception and growth of damage from Microcavities in polyethylene-based materials for HVDC cables Part 1: Theoretical approach", *IEEE Trans. Dielectr. Electr. Insul.*, Vol. 14, NO.5, October, pp. 1242-1354, 2007.
- [3] G. C. Montanari, G. Mazzanti and S. Serra, "Theoretical study of inception mechanism and growth of defect-induced damages in cable polymeric insulation", *IEEE Conf. Electr. Insul. Dielectr. Phenomena (CEIDP)*, Kitchener, Canada, pp. 644-647, 2001.
- [4] G. Mazzanti, G. C. Montanari and S. Serra, "Aging model of polyethylene-based materials for HV cables founded on damage inception and growth from air-filled cavities", *IEEE ICSD*, Toulouse, France, pp. 525-529, 2004.
- [5] A. Cavallini, F. Ciani, G. Mazzanti and G. C. Montanari, "Firs electron availability and partial discharge generation in insulation cavities: effect of light irradiation", *IEEE Trans. Dielectr. Electr. Insul.*, Vol. 12, NO.2, April, pp. 387-394, 2005.
- [6] Choong-sik Kim, T. Kondo and T. Mizutani, "Change in PD pattern with ageing" *IEEE Trans. Dielectr. Electr. Insul.*, Vol.11, NO.1, pp.13-18, February 2004.
- [7] G. Mazzanti, G. C. Montanari and L. Dissado, "Electrical aging and life models: the role of space charge", *IEEE Trans. Dielectr. Electr. Insul.*, Vol. 12, No.5, pp. 876-890, 2005.
- [8] C. M. Righi, S. Serra, E. Tosatti, S. Scandolo, G. Santoro, "Surface states and negative electron affinities in polyethylene", *Phys. Rev. Lett.*, Vol. 87,076802,2001.
- [9] L. A. Dissado, C. Laurent, G. C. Montanari and P. H. F. Morshuis, "Demonstrating a threshold for trapped space charge accumulation in solid dielectrics under DC field", *IEEE Trans. Dielectr. Electr. Insul.*, Vol. 12, NO.3, pp. 612-620, 2005.
- [10] L. Testa, "Physical model of damage inception and growth in polymeric insulation materials subjected to partial discharges under DC and AC voltage", PhD thesis, University of Palermo, 2009.
- [11] G. C. Montanari, "Bring an insulation to failure: the role of space charge", *IEEE International Conference on Electrical Insulation and Dielectric Phenomenon (CEIDP)*, Whitehead memorial lecture, Westlafayette, USA, 2010.

- [12] L. Testa, G. C. Montanari, A. Cavallini, S. Serra, L. A. Dissado, "Model of ageing inception and growth from micro-voids in polyethylene-based materials under AC voltage", IEEE CEIDP, pp. 29-32, Quebec City, Canada, October, 2008.
- [13] L. Testa, S. Serra, and G. C. Montanari, "Advanced modeling of electron avalanche process in polymeric dielectric voids: Simulations and experimental validation", J. Appl. Phys., Vol. 108, pp.034110.1- 034110.2, 2010.
- [14] G. C. Montanari, G. Mazzanti and L. Simoni, "Progress in electrothermal life modeling of electrical insulation over the last decades", IEEE Trans. Dielectr. Electr. Insul., Vol.9, pp. 730-745, 2002.
- [15] S. A. Boggs, "Theory of a defect-tolerant dielectric system", IEEE Trans. Electr. Insul., Vol. 28, NO.3, pp. 365-371, 1993.
- [16] L. Sanche, "Nanoscopic aspects of electronic aging in dielectrics", IEEE Trans. Dielectr. Electr. Insul., Vol. 4, pp.507-543, 1997.
- [17] G. Jiang, J. Kuang and S. Boggs, "Critical parameters for electrical tree formation in XLPE", IEEE Trans. Pow. Del., Vol. 13, NO.2, pp. 292-306, 1998.
- [18] Z. Zheng and S. Boggs, "Defect tolerance of solid dielectrics transmission class cable", IEEE Electr. Insul. Magazine, Vol. 21, NO.1, pp. 34-41, 2005.
- [19] G. Bahder, T. Garrity, M. Sosnowski, R. Eaton and C. Katz, "Physical model of electric aging and breakdown of extruded polymeric insulated power cables", IEEE Trans. Pow. App. Sys., Vol. 101, NO.6, pp. 1378-1388, 1982.
- [20] L. Niemyer "A generalized approach to partial discharge modeling", IEEE Trans. Dielectr. Electr. Insul., Vol. 2, NO. 4, pp. 685-699. August, 1995.
- [21] F. Gutlefish and L. Niemyer "Measurement and simulation of PD in epoxy voids", IEEE Trans. Dielectr. Electr. Insul., Vol. 2, NO. 5, pp. 729-743, October, 1995.
- [22] A. Cavallini, G. C. Montanari, "Effect of supply voltage frequency on testing of insulation system", IEEE Trans. Dielectr. Electr. Insul., Volume 13, No.1, pp. 111-121, February 2006.
- [23] K. Wu, Y. Suzuoki, L. A. Dissado, "The contribution of discharge area variation to partial discharge patterns in disc-voids", J. Phys. D: Appl. Phys. 37, pp.1815-1823, 2004.
- [24] K. Wu, T. Okamoto, Y. Suzuoki, "Effects of Discharge Area and Surface Conductivity on Partial Discharge Behavior in Voids under Square Voltages", IEEE Trans. Dielectr. Electr. Insul., Vol. 14, No. 2, April 2007, pp. 461-470.
- [25] D. Fabiani, G. C. Montanari, "Polymeric HVDC cable design and space charge accumulation. Part 1: insulation/semicon interface", IEEE Trans. Electr. Insul., Vol. 23, NO.6, pp. 11-19, 2007.
- [26] P. H. F. Morshuis and F. H. Kreuger, "Transition from streamer to Townsend mechanisms in dielectric voids", J. Phys. D: Appl. Phys., Vol. 23, pp. 1562 - 1568, 1990.
- [27] C. Hudon, R. Bartnikas and M.R. Wertheimer, "Surface conductivity of epoxy specimens subjected to partial discharges", IEEE Intern. Sympos. Electr. Insul. Cat. No. 90 CH27276, pp. 153-155, 1990.
- [28] P. H. F. Morshuis, "Parital Discharge Mechanisms", PhD thesis, Delft University of Technology, ISBN 90-6275-931-9, 1993.
- [29] K. Temmen, "Evaluation of surface charges in flat cavities due to ageing by means of phase-angle resolved partial discharge measurement", J.Phys. D. Appl. Phys., Vol.33, pp. 603 –

608, 2000.

- [30] Y. Sekii and K. Yamauchi, "Analysis of Deterioration by Partial Discharge of XLPE using GCMS and FTIR", Proceedings of 2008 International Conference on Condition Monitoring and Diagnosis, Beijing, China, April, 2008.
- [31] Y. Sekii, H. Oguma, T. Hagiwara and K. Yamauchi "GC-MS and FTIR analysis of LDPE and XLPE deteriorated by partial discharge" IEEE Conference on Electrical Insulation and Dielectric Phenomenon (CEIDP), pp.237-240, 2005.
- [32] M. Gamez Garcia, R. Bartnikas and M. R. Wertheimer, "Synthesis reactions involving XLPE subjected to partial discharges", IEEE Trans. Electr. Insul., Vol. 22, pp. 199-205, 1987.
- [33] C. Hudon, R. Bartnikas and M.R. Wertheimer, "Analysis of Degradation Products on Epoxy Surfaces subjected to pulse and glow type discharges", IEEE Electr. Insul. Dielectr. Phenom. (CEIDP), pp. 237 - 243, 1991.
- [34] C. Hudon, R. Bartnikas, M. R. Wertheimer "Effect of physico-chemical degradation of epoxy resin on partial discharge behavior", IEEE Trans. Electr. Insul., Vol. 2, pp. 1083-1094, 1987.
- [35] Y. Sekii, T. Fukuyama, K. Kikuchi, "Deterioration by partial discharges of polyethylene in oxygen containing gas atmosphere", Proceedings of International Conference on Properties and Applications of Dielectric Materials (ICPADM), pp.479-482, Xi'an China, 2000.

### **Chapter 3**

- [1] L. Testa, "Physical model of damage inception and growth in polymeric insulation materials subjected to partial discharges under DC and AC voltage", PhD thesis, University of Palermo, 2009.

### **Chapter 4**

- [1] A.C. Gjaerde, "A Phenomenological Ageing Model for Combined Thermal and Electrical Stress", IEEE Trans. Dielectr. Electr. Insul., Vol.4, NO.6, pp.674-680, December 1997.
- [2] A.C. Gjaerde, "Measurement of Void Gas Pressure during Combined Thermal and Partial Discharge Ageing of Epoxy", IEE Proceedings Science, Measurement and Technology, Vol. 142, NO.1, January 1995.
- [3] A.C. Gjaerde and J Sletbak, "Influence of partial discharges on void gas pressure", Proceedings of International Conference on Partial Discharge (ICPD), pp.119-120, Canterbury, August, 2002.
- [4] C. Kim, T. Kondo and T. Mizutani, "Change in PD Pattern with Ageing", IEEE Trans. Dielectr. Electr. Insul., Vol.11, NO.1, pp.13-18, February 2004.
- [5] E. Larsen, C. Bak Petersen and M.Henriksen, "Determination of Gas Pressure in Voids in Epoxy Casting Using an Ultrasonic Measuring Technique", IEEE International Symposium on Electrical Insulation (ISEI), June, 1990.
- [6] F. Gutfleisch and L. Niemeyer, "Measurement and Simulation of PD in Epoxy Cavities", IEEE Trans. Dielectr. Electr. Insul., Vol. 2, NO.5, October, pp. 729-743, 1995.

- [7] P.H.F. Morshuis, "Parital discharge mechanisms", PhD thesis, Delft University of Technology, ISBN 90-6275-931-9, 1993.
- [8] M.Hikita, K.Yamada, A.Nakamura, T.Mizutani, A.Oohasi, and M.Ieda, "Measurement of partial discharges by computer and analysis of partial discharge distribution by the Monte Carlo Method", IEEE Trans. Dielectr. Electr. Insul., Vol.25, NO.3, pp.453-48, December 1995.
- [9] Yasuo Sekii and Kazuki Yamauchi, "Analysis of Deterioration by Partial Discharge of XLPE using GCMS and FTIR", Proceedings of 2008 International Conference on Condition Monitoring and Diagnosis (ICCMD), Beijing, China, April, 2008.
- [10] Yasuo Sekii, Hidenori Oguma, Takeo Hagiwara and Kazuki Yamauchi "GC-MS and FTIR analysis of LDPE and XLPE deteriorated by partial discharge" IEEE Conference on Electrical Insulation and Dielectric Phenomenon (CEIDP), pp.237-240, Nashville, USA 2005.
- [11] Y. Sekii, T. Fukuyama and K. Kikuchi, "Deterioration by Partial Discharges of Polyethylene in Oxygen containing Gas Atmosphere," Proceedings of 6th International Conference on Properties and Applications of Dielectric Materials (ICPADM), pp.479-482, Xi'an, China, 2000.
- [12] R.J.Van Brunt, "Physics and chemistry of partial discharge and corona", IEEE Trans. Dielectr. Electr. Insul., Vol.1, NO.5, pp.761-784 October 1994.
- [13] T.Tanaka, "Internal partial discharge and material degradation", IEEE Trans. Dielectr. Electr. Insul., Vol.EI-21, NO.6, December, 1986.
- [14] K.Temmen, "Evaluation of Surface Changes in Flat Cavities due to Ageing by Means of Phase-angle Resolved Partial Discharge Measurement", J.Phys. D: Appl. Phys. 33, pp.603-608, 2000.
- [15] Peter H.F. Morshuis, "Degradation of Solid Dielectrics due to Internal Partial Discharge: Some thoughts on progress made and where to go now", IEEE Trans. Dielectr. Electr. Insul., Vol.12, NO.5, October, 2005.

## **Chapter 5**

- [1] P. H. F. Morshuis, "Parital Discharge Mechanisms", PhD thesis, Delft University of Technology, ISBN 90-6275-931-9, 1993.
- [2] M. Gamez Garcia, R. Bartnikas and M. R. Wertheimer, "Synthesis reactions involving XLPE subjected to partial discharges", IEEE Trans. Electr. Insul., Vol. 22, pp. 199-205, 1987.
- [3] C. Hudon, R. Bartnikas and M.R. Wertheimer, "Analysis of Degradation Products on Epoxy Surfaces subjected to pulse and glow type discharges", IEEE Electr. Insul. Dielectr. Phenom. (CEIDP), pp. 237 - 243, 1991.
- [4] L. Testa, "Physical model of damage inception and growth in polymeric insulation materials subjected to partial discharges under DC and AC voltage", PhD thesis, University of Palermo, 2009.

## **Chapter 6**

- [1] A. Cavallini, G.C. Montanari, "Effect of supply voltage frequency on testing of insulation

- system”, IEEE Trans. Dielectr. Electr. Insul., Volume 13, No.1, pp. 111-121, February, 2006.
- [2] G. C. Montanari, M. Conti, F. Ciani, A. Cavallini, G. Mazzanti, S. Serra, “First electron availability and PD generation in insulation cavities”, IEEE CEIDP, Albuquerque, NM, USA, pp. 576-580, 2003.
- [3] L. Testa, “Physical model of damage inception and growth in polymeric insulation materials subjected to partial discharges under DC and AC voltage”, PhD thesis, University of Palermo, 2009.
- [4] F. Gutlefish and L. Niemyer “Measurement and simulation of PD in epoxy voids”, IEEE Trans. Dielectr. Electr. Insul., Vol. 2, NO. 5, pp. 729-743, October, 1995.
- [5] M. Gamez Garcia, R. Bartnikas and M.R. Wertheimer, “Synthesis reactions involving XLPE subjected to partial discharges”, IEEE Trans. Electr. Insul., Vol. 22, pp. 199-205, 1987.
- [6] C. Hudon, R. Bartnikas and M.R. Wertheimer, “Analysis of Degradation Products on Epoxy Surfaces subjected to pulse and glow type discharges”, IEEE Electr. Insul. Dielectr. Phenom. (CEIDP), pp. 237 - 243, 1991.
- [7] P.H.F. Morshuis, “Parital discharge mechanisms”, PhD thesis, Delft University of Technology, ISBN 90-6275-931-9, 1993.
- [8] K.Temmen, “Evaluation of surface changes in flat cavities due to ageing by means of phase-angle resolved partial discharge measurement”, J.Phys. D: Appl. Phys. 33, pp.603-608, 2000.
- [9] T. Tanaka and Y. Ikeda, “Internal discharges in polyethylene with an artificial cavity”, IEEE Trans. Electr. Insul., Vol. PAS-90, pp. 2692-2702, 1971.